



Cenozoic basin evolution of the central Tibetan plateau as constrained by U-Pb detrital zircon geochronology, sandstone petrology, and fission-track thermochronology

Michael W. McRivette^{a,*}, An Yin^{b,c}, Xuanhua Chen^d, George E. Gehrels^e

^a Department of Geological Sciences, Albion College, Albion, MI 49224, USA

^b Department of Earth, Planetary, and Space Sciences, University of California, Los Angeles, CA 90095-1567, USA

^c Structural Geology Group, School of Earth Sciences and Resources, China University of Geosciences (Beijing), Beijing 10083, China

^d Institute of Geomechanics, Chinese Academy of Geological Sciences, Beijing 100081, China

^e Department of Geosciences, University of Arizona, Tucson, AZ 85721, USA

ARTICLE INFO

Keywords:

Hoh Xil Basin
Qaidam Basin
Kunlun Range
Tibetan plateau
U-Pb zircon geochronology

ABSTRACT

We conduct sandstone-composition analysis, U-Pb detrital-zircon dating, and apatite fission-track thermochronology to determine how basin development was associated with the Cenozoic deformation across central Tibet. Our results are consistent with a two-stage basin development model: first a single fluvial-lacustrine system formed (i.e., Paleo-Qaidam basin) in between two thrust belts (i.e., the Fenghuoshan and Qilian Shan thrust belts) in the Paleogene, which was later partitioned into two sub-basins in the Neogene by the Kunlun transpressional system and its associated uplift. The southern sub-basin (i.e., Hoh Xil basin) strata have detrital-zircon age populations at 210–300 Ma and 390–480 Ma for the Eocene strata and at 220–310 Ma and 400–500 Ma for the early Miocene strata; petrologic analysis indicates that the late Cretaceous-Eocene strata were recycled from the underlying Jurassic rocks. The northern sub-basin (i.e., Qaidam basin) strata yield detrital-zircon age clusters at 210–290 Ma and 370–480 Ma in the Eocene, 220–280 Ma and 350–500 Ma in the Oligocene, 250–290 Ma and 395–510 Ma in the Miocene, and 225–290 Ma and 375–480 Ma in the Pliocene. Proterozoic ages of the detrital zircon are most useful for determining provenance: the pre-Neogene Hoh Xil and Qaidam strata all contain the distinctive age peaks of ~1800 Ma and ~2500 Ma from the Songpan-Ganzi terrane south of the Kunlun fault, whereas detrital zircon of this age is absent in the Neogene Qaidam strata suggesting the emergence of a topographic barrier between the two basins. This inference is consistent with our fission-track thermochronological data from the Eastern Kunlun Range that suggest rapid cooling within the range did not start until after 30–20 Ma. Our new data support the Paleo-Qaidam hypothesis that requires the Hoh Xil and Qaidam basins were parts of a single Paleogene basin bounded by the Qilian Shan and Fenghuoshan thrust belts.

1. Introduction

Despite being the largest elevated landmass on Earth, the Tibetan plateau was the locus of thick (> 5 km) and extensive (> 400,000 km²) sedimentation during the Cenozoic Indo-Asian collision as expressed by the development of the late Cretaceous-Miocene Hoh Xil basin and the Paleocene-Quaternary Qaidam basin (Fig. 1) (Yin and Harrison, 2000; Pan et al., 2004; Yin et al., 2008a, 2008b; Yin, 2010). Because the combined area of the two basins occupies nearly one-third of the Tibetan plateau (Fig. 1), understanding how these basins were developed during the Indo-Asian collision is fundamental to deciphering the growth mechanism of the plateau (Yin et al., 2002, 2007a, 2008a,

2008b). In the past three decades, researchers have focused on the Cenozoic evolution of each basin individually (e.g. Bally et al., 1986; Leeder et al., 1988; Burchfiel et al., 1989a; Song and Wang, 1993; Huang et al., 1996; Métivier et al., 1998; Liu and Wang, 2001; Yin et al., 2002; Wang et al., 2002, 2006, 2008a; Bush et al., 2016; Cheng et al., 2014, 2016a; Zhu et al., 2017) with little consideration given to the relationship between them and the role of recycling in affecting Cenozoic provenance analysis (cf., Yu et al., 2017a). Yet this information is key to testing two end-member models for the development of the Tibetan plateau: (1) the plateau grew sequentially from south to north in association with northward initiation of new basins (i.e., the *independent* basin model) (Métivier et al., 1998; Tapponnier et al., 2001),

* Corresponding author.

E-mail addresses: mmcrivette@albion.edu (M.W. McRivette), ayin54@gmail.com (A. Yin).

<https://doi.org/10.1016/j.tecto.2018.12.015>

Received 13 March 2018; Received in revised form 3 December 2018; Accepted 13 December 2018

Available online 21 December 2018

0040-1951/ © 2019 Elsevier B.V. All rights reserved.

Harrison et al., 2000). The southern boundary of the Xigaze forearc basin is the Indus-Tsangpo suture (Fig. 1). Post-collision volcanism and dike intrusion occurred widely across the Lhasa terrane between 26 and 10 Ma (Coulon et al., 1986; Yin et al., 1994; Miller et al., 1999; Williams et al., 2001; Mo et al., 2006, 2007; Hou et al., 2012; Xu et al., 2017; Chen et al., 2018a).

The Qiangtang terrane exposes a 600-km long and 300-km wide east-plunging anticlinorium defined by metamorphic rocks and late Paleozoic strata in the core and Jurassic to Cretaceous strata across the limbs (Yin and Harrison, 2000; Kapp et al., 2000, 2003) (Fig. 1). The metamorphic rocks, consisting of blueschist-facies metapelites, metabasite and nearly ultrahigh-pressure eclogites (Kapp et al., 2000; Zhang et al., 2006a) are all exposed in the footwalls of latest Triassic-early Jurassic low-angle normal faults overlain by middle and late Jurassic red beds (Kapp et al., 2000, 2003). The southern margin of the Qiangtang terrane is defined by the Bangong-Nujiang suture, along which the Lhasa and Qiangtang blocks converged during the Jurassic and early Cretaceous, closing the Meso-Tethys Ocean (e.g., Dewey et al., 1988; Murphy et al., 1997; Kapp et al., 2005a, 2007a; Guynn et al., 2006). The Jinsha suture, demarcating the northern margin of the Qiangtang terrane, formed when southward subduction of the Paleo-Tethys ended in the Triassic (Yin and Harrison, 2000). Igneous rocks with late Paleozoic and Mesozoic ages are common in the Qiangtang terrane (e.g., Kapp et al., 2000, 2003; Roger et al., 2003, 2004; Wallis et al., 2003; Guynn et al., 2006; Pullen et al., 2011; Li et al., 2013a, 2014, 2015a, 2017a; Fan et al., 2015; Hao et al., 2016; Liu et al., 2017a; Lu et al., 2017; Wang et al., 2018a). Early Paleozoic igneous rocks are also present, including Cambrian-Ordovician plutonic rocks that have been documented in the exhumed high-grade metamorphic rocks (Kapp et al., 2005a; Hu et al., 2015; Liu et al., 2016). U-Pb zircon dating also reveals the presence of Eocene granitoids in the region (e.g., Roger et al., 2000; Spurlin et al., 2005; Jiang et al., 2006; Yang et al., 2014; Ou et al., 2017). Post-collisional volcanic rocks (< 45 Ma), mostly dated by K-Ar and Ar-Ar methods, are widely scattered across the Qiangtang terrane and the western Songpan-Ganzi terrane to the north (Burchfiel et al., 1989b; Turner et al., 1993, 1996; Chung et al., 1998, 2005; Hacker et al., 2000; Roger et al., 2000; Jolivet et al., 2003; Ding et al., 2003, 2007; Guo et al., 2006; Jiang et al., 2008a; Wang et al., 2005a, 2008b; Long et al., 2015; Chen et al., 2018a). Ages for detrital zircons from the Paleozoic strata exposed in central Qiangtang are dominantly 500–1000 Ma, with smaller populations centered at ca. 350 Ma, ca. 1850 Ma, and ca. 2500 Ma (e.g., Kapp et al., 2003; Yang and Li, 2006; Pullen et al., 2008, 2011; Dong et al., 2011; Gehrels et al., 2011; Peng et al., 2014). Detrital zircons from Mesozoic strata exhibit a similar distribution in addition to a prominent ca. 250 Ma peak (e.g., Gehrels et al., 2011; Pullen et al., 2011; Ding et al., 2013).

The Songpan-Ganzi terrane is comprised mainly of a middle to late Triassic flysch complex deposited during the closure of the Paleo-Tethys Ocean and sourced from the nearby arcs and collisional belts (Huang and Chen, 1987; Gu, 1994; Yin and Nie, 1993; Nie et al., 1994; Zhou and Graham, 1996; Yin and Harrison, 2000; She et al., 2006; Weislogel et al., 2006, 2010; Enkelmann et al., 2007; Ding et al., 2013; Tang et al., 2018) (Fig. 1). The flysch sequence overlies rarely exposed Paleozoic sequences that rest on the Precambrian basement of both the North and South China cratons (Huang and Chen, 1987; Ingersoll et al., 1995; Burchfiel et al., 1995; Zhou and Graham, 1996; Bruguier et al., 1997; Burchfiel and Chen, 2012; Ding et al., 2013). The flysch complex is overlain by non-marine Jurassic strata; Cretaceous strata are generally absent (e.g., Liu et al., 2001; Pan et al., 2004; Ding et al., 2013). The Songpan-Ganzi terrane is intruded by post-orogenic granites with ages ranging from 150 Ma to 230 Ma (e.g., Roger et al., 2004; Zhang et al., 2014a; Jolivet et al., 2015; Chen et al., 2017). Detrital zircon ages determined for the Triassic strata have a main population of 200–500 Ma corresponding to the plutonic ages of the Eastern Kunlun Range and smaller age peaks at ~750–900 Ma, ~1750–2000 Ma, and ~2350–2550 Ma (Bruguier et al., 1997; Weislogel et al., 2006, 2010;

Enkelmann et al., 2007; Pullen et al., 2011; Ding et al., 2013; Wu et al., 2016; Tang et al., 2018), reflecting complex derivation from the adjacent source regions (Weislogel, 2008; Robinson et al., 2012; Ding et al., 2013).

The Kunlun-Qaidam terrane includes the Eastern Kunlun Range and Qaidam basin. Basement exposed along and underlying the northern Qaidam basin consists of Paleoproterozoic-Mesoproterozoic metamorphic rocks (e.g., Lu et al., 2008; Chen et al., 2012; Gong et al., 2012; Yu et al., 2017b, 2017c). Paleoproterozoic-early Neoproterozoic basement units are also recognized within the Eastern Kunlun Range along the southern margin of the terrane (Chen et al., 2006; Wang et al., 2007a; He et al., 2016a, 2016b), where they are intruded by Ordovician to early Devonian and late Carboniferous to late Triassic arc sequences comprising the prominent Kunlun batholith (e.g., Liu, 1988; Harris et al., 1988; Mock et al., 1999; Cowgill et al., 2003; Roger et al., 2003; Bian et al., 2005; Zhu et al., 2006a; Dai et al., 2013; Wu et al., 2016) (Fig. 1). U-Pb zircon ages of plutonic rocks across the terrane comprise two prominent groups at ~195–285 Ma and ~360–485 Ma (Harris et al., 1988; Roger et al., 2003; Chen et al., 2001, 2002; Arnaud et al., 2003; Cowgill et al., 2003; Liu et al., 2004; Pullen et al., 2008). The Permian-Triassic ages comprise a distinctive age population centered at ~245 Ma that is unique within the major terranes of central and northern Tibet. Late Devonian to early Carboniferous shallow marine strata may have been deposited during back-arc extension between the arc events (Yin and Harrison, 2000). A small number of magmatic and metamorphic ages ranging from ~730 Ma to ~1080 Ma have also been reported (e.g., He et al., 2016a, 2016b). Detrital zircons ages from the Eastern Kunlun Range units define two prominent peaks corresponding to the two arc events, and minor populations ~750–1000 Ma, and ~2350–2550 Ma (e.g., Wang et al., 2004a; Lu et al., 2009; Jin et al., 2015; He et al., 2016a; Wu et al., 2016; Pei et al., 2017). The Triassic Yidun arc in eastern Tibet is bound by the Qiangtang terrane to the southwest and the Songpan-Ganzi terrane to the northeast. It is characterized by primarily Triassic-age (~195–245 Ma) intermediate-felsic intrusive rocks locally intruded by late Cretaceous (~75–105 Ma) granitoids (e.g., Reid et al., 2007; Chen et al., 2014; Cao et al., 2016; Yang et al., 2016; Wu et al., 2017a). The Yidun arc has been interpreted as an eastern extension of the Kunlun batholith that was rifted away from the Kunlun terrane in the middle-Triassic and accreted to the northeastern margin of the Qiangtang terrane in the late Triassic (Pullen et al., 2008). Scattered Jurassic to Cenozoic continental strata overlie the highly folded Triassic strata across the Eastern Kunlun Range (Pan et al., 2004). At the western end of the Eastern Kunlun Range, a Cretaceous pluton has also been documented (Robinson et al., 2003).

The Qilian terrane exposes early Paleozoic flysch sequences, arc complexes, and low- to high-grade metamorphic rocks north of the Qaidam basin (Li et al., 1978; Liu, 1988; Gansu BGMR (Bureau of Geology and Mineral Resources), 1989; Qinghai BGMR (Bureau of Geology and Mineral Resources), 1991; Yin and Nie, 1996; Song et al., 2014; also see Wu et al., 2016 for a review) (Fig. 1). The terrane consists of three belts: a Proterozoic passive-continental-margin sequence in the central part is bounded to the north and south by subduction mélange zones (Yang et al., 2002; Gehrels et al., 2003a, 2003b; Song et al., 2005, 2006; Zhang et al., 2005). Three main phases of magmatism occurred in the Qilian terrane (Cowgill et al., 2003; Gehrels et al., 2003a, 2003b, 2011; Wu et al., 2016; Zusa and Yin, 2017; Zusa et al., 2018): (1) at ~890–1050 Ma as small and isolated plutons that intrude into Proterozoic passive continental margin sequences along the southern edge of the North China craton, and as arc-related plutons presently exposed within the North Qaidam ultrahigh-pressure (UHP) belt and as part of the Quanji massif on the northern margin of Qaidam basin, (2) at 520–400 Ma as arc-related plutons and volcanic complexes coeval with the North Qaidam UHP metamorphic event (e.g., Yin et al., 2007b), and (3) at ~240–270 Ma as isolated plutons of the Permian Kunlun arc. Relatively rare Paleoproterozoic metamorphic and

magmatic protolith ages are also documented (e.g., Lu et al., 2008; Chen et al., 2009, 2013; Gong et al., 2012; Yu et al., 2017b). The Altyn Tagh Range bounding Qaidam basin to the northwest represents the western extension of the Qilian terrane offset ~400 km to the southwest by the Cenozoic Altyn Tagh fault and is characterized by a similar magmatic and metamorphic history (e.g., Yin and Harrison, 2000; Zuza and Yin, 2017). Detrital zircons from Proterozoic and Paleozoic units in the Qilian terrane and Altyn Tagh are similar with ca. 475 Ma and ca. 920 Ma peaks, though minor Paleoproterozoic detrital zircon populations are present in the Qilian terrane at ~1600–1900 Ma and ~2350–2500 Ma while the Altyn Tagh has a more prominent peak centered at ca. 1900 Ma (e.g., Gehrels et al., 2003b, 2011; Yang et al., 2009; Chen et al., 2012, 2018b; Zhang et al., 2012b, 2014b, 2017; Wang et al., 2013b; Yu et al., 2013a, 2013b; Wu et al., 2017b; Zuza et al., 2018).

3. Sedimentary basins in central Tibet

3.1. Jurassic-Early Cretaceous basins

Jurassic sediments are present across much of central and northern Tibet. In Qaidam basin, Jurassic strata are exposed along the north-eastern and western basin margins; they are important potential hydrocarbon source units described in detail elsewhere (e.g., Ritts et al., 1999; Yang et al., 2003; Wang et al., 2005b; Yu et al., 2017a). Detrital zircon geochronology indicates that Jurassic strata in Qaidam basin were derived from the Kunlun batholith (Cheng et al., 2015; Yu et al., 2017a). In the Songpan-Ganzi terrane, Jurassic rocks are restricted to local occurrences of coal-bearing deltaic deposits (Weislogel, 2008).

Further south, Jurassic sediments of the Yanshiping Group are widely exposed in the Qiangtang terrane (Figs. 1 and 2; Leeder et al., 1988; Pan et al., 2004). This thick Jurassic sequence overlies middle to late Triassic shallow marine strata that were likely deposited in sub-basins marginal to the closing Songpan-Ganzi remnant ocean basin (Yin et al., 1988; Yin and Harrison, 2000; Zhang et al., 2006b). In the vicinity of the Golmud-Lhasa highway, the Jurassic exposures define the nose of the east-plunging metamorphic-cored Qiangtang anticlinorium (e.g., Yin and Harrison, 2000).

The Yanshiping Group consists of ~5000 m of both marine and non-marine deposits (Leeder et al., 1988; Yin et al., 1988). The non-marine clastic strata exhibit stacked fluvial channel geometries with sandstone and conglomerate lenses intercalated with variegated mudstone. Conglomerate clasts are dominantly derived from adjacent sandstone and mudstone units. Mudstone beds are typically laterally-extensive over 10s to 100s of meters and are interpreted as floodplain deposits with variable degrees of paleosol development. Individual marine limestone intervals are generally white to dark gray in color, locally highly fossiliferous, and are up to ~200 m thick. Paleocurrent directions obtained from channel sandstones and cross-stratification in Yanshiping Group sediments are generally to the south (Leeder et al., 1988). Fossils collected from both marine limestone and non-marine fluvial deposits, mainly bivalves, have been interpreted to indicate a middle to late Jurassic age for the Yanshiping Group (Leeder et al., 1988; Sha et al., 2002). However, a Jurassic age assignment for the entirety of the Yanshiping Group has been questioned on the basis of palynomorph assemblages that suggest an early Cretaceous age for the uppermost portion of the sequence (Li and Batten, 2004). Along the northern margin of Qaidam basin, Lower Cretaceous alluvial conglomerates and

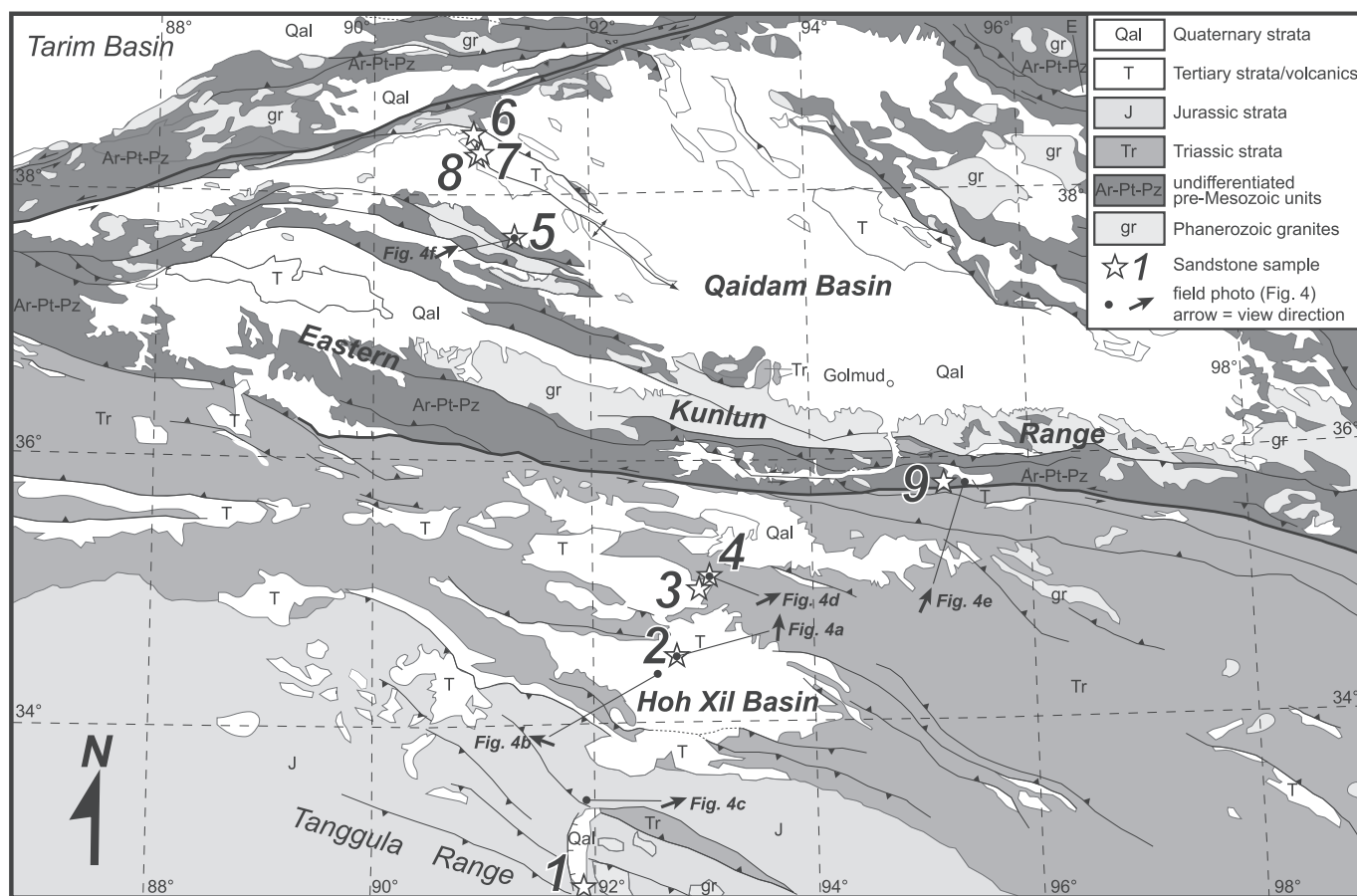


Fig. 2. Generalized geologic map of the central and northern Tibetan plateau, including the Qaidam and Hoh Xil basins and the Eastern Kunlun Range. Locations of sandstone samples 1 through 9 collected for petrographic analysis and U-Pb detrital zircon geochronology are indicated by the white stars. Black dots show the locations of field photographs in Fig. 4, with the view direction indicated by the black arrows.

fluvial sandstones and mudstones of the Quanyagou Formation are locally exposed and are interpreted to be proximally sourced from the southern Qilian Shan (Wu et al., 2011). Elsewhere, possible Lower Cretaceous strata are restricted to the southern and far-western Qiangtang terrane (e.g., Zhang et al., 2006b).

Northern derivation of detritus suggests that the marine depositional environment in the Jurassic was located near the southern margin of the Qiangtang terrane, consistent with an increase in marine limestone occurrence towards the south (Leeder et al., 1988). Provenance studies on Jurassic turbiditic sequences along the Bangong-Nujiang suture between the Lhasa and Qiangtang terranes suggest derivation from the north (Leier et al., 2007; Li et al., 2017b, 2017c). This marine environment was likely composite in nature, consisting of an epeiric seaway covering portions of the southern Qiangtang crustal block and the actively-closing Meso-Tethys ocean basin between the Lhasa and Qiangtang terranes, which closed completely by the early Cretaceous (e.g., Dewey et al., 1988; Murphy et al., 1997; Kapp et al., 2005a, 2007a; Guynn et al., 2006). This interpretation is consistent with the evolution of the Yanshiping Group sequence proposed by Leeder et al. (1988): fluvial deposition in the middle Jurassic gave way to sedimentation in coastal plain and marginal marine environments, based on a higher proportion of marine limestone units upsection within the sequence, followed by a return to fluvial conditions near the end of the Jurassic.

3.2. Late Cretaceous-Cenozoic basins

3.2.1. Hoh Xil basin

The late Cretaceous-Cenozoic Hoh Xil basin lies across the Songpan-Ganzi and northern Qiangtang terranes, bounded by the Eastern Kunlun and Tanggula ranges to the north and south, respectively (Fig. 2). In the east, the basin stratigraphy is comprised of the basal Fenghuoshan Group with a Cretaceous to Eocene depositional age, the overlying late Eocene Yaxicuo Group, and the capping Miocene Wudaoliang Group (also known as the Chabaoma Group) (Liu and Wang, 2001; Staisch et al., 2014) (Fig. 3). In the western Hoh Xil basin, the Kangtuo and Suonahu Formations have been correlated with the Fenghuoshan and Yaxicuo Groups, respectively, based on stratigraphic, provenance, and stable isotope analyses (Dai et al., 2012; Li et al., 2018a). The maximum total thickness of Hoh Xil basin strata exceeds 5800 m (Liu and Wang, 2001) overlying older Mesozoic sedimentary units (Fig. 2). An early study interpreted a prominent contact between the Fenghuoshan Group and the underlying strata along the Golmud-Lhasa Highway in the central portion of the basin as a Tertiary thrust placing Fenghuoshan Group strata over a sequence of interbedded light-red fine-grained sandstone and siltstone with an inferred Neogene age (Leeder et al., 1988). However, evidence of faulting along the length of the contact between the units has never been established in the field. We observed this contact in the field to be clearly depositional as indicated by the presence of wide (10s of meters in width) channels of the Fenghuoshan Group incised into the underlying strata that we infer to be of early Cretaceous age (Fig. 4A). Clast components of the basal conglomerate of the Fenghuoshan Group at this outcrop are dominantly recycled fine-grained sandstones and siltstones derived from the underlying unit. A few kilometers to the southwest, the underlying early Cretaceous(?) strata are in normal-fault contact with Triassic flysch deposits (Fig. 4B). The late Cretaceous-Oligocene Fenghuoshan and Yaxicuo Groups and the underlying Jurassic and inferred early Cretaceous (?) strata are all folded in association with complex thrusting in the Cenozoic Fenghuoshan-Nangqian thrust belt (Fig. 4C) (also see Leeder et al., 1988; Liu and Wang, 2001). The concordant style of deformation of the Jurassic to Cenozoic strata suggests that the Jurassic sequences were deformed mainly by Cenozoic contraction. In contrast to the intense contractional deformation observed in the Fenghuoshan and Yaxicuo Group strata, the overlying Miocene Wudaoliang Group is broadly folded over a long wavelength (Fig. 4D) (Wu et al., 2008).

The depositional age of the Fenghuoshan Group has been the subject of considerable debate. Early magnetostratigraphic studies suggested depositional ages for the Fenghuoshan and Yaxicuo Groups of 51–31 Ma (early Eocene-early Oligocene) and ~31–30 Ma (early Oligocene), respectively (Liu et al., 2003). However, more recent biostratigraphic and magnetostratigraphic studies incorporating isotopic dating of interbedded tuffs have revised the depositional age of the Fenghuoshan Group to late Cretaceous to early Eocene, ending at 51 Ma (Staisch et al., 2014; Jin et al., 2018). These results are consistent with existing Cretaceous-Eocene palynological and fossil assemblage dates determined for the Fenghuoshan Group (e.g., Smith and Xu, 1988; Zhang and Zheng, 1994; Li et al., 2015b). The age of the Yaxicuo Group has similarly been revised to late Eocene (Miao et al., 2016). The flat-lying to gently warped Wudaoliang Group unconformably overlies the extensively folded and thrust-faulted Fenghuoshan and Yaxicuo Groups and other Mesozoic units (Coward et al., 1988; Yin et al., 1988; Wang et al., 2002; Staisch et al., 2016). Climatostratigraphic analysis suggests that the Wudaoliang Group was deposited between ca. 24.1 Ma and 14.5 Ma (Wu et al., 2009), consistent with fossil and pollen assemblages indicating a Miocene age (Yin et al., 1988; Zhang and Zheng, 1994; Wu et al., 2008). The significant deformation of the late Cretaceous-Eocene Fenghuoshan and Yaxicuo Group strata relative to the overlying Miocene Wudaoliang Group (e.g., Staisch et al., 2016) and the extensive erosional surface upon which the latter was deposited require that a depositional hiatus must have occurred across the vast majority of Hoh Xil basin in the Oligocene (e.g., Wang et al., 2002; Wu et al., 2008). The cessation of deposition of the Wudaoliang Group is further constrained by whole rock K-Ar dating of unconformably overlying lavas at ca. 13.5 Ma in the western Hoh Xil basin (Li et al., 2004) and late Miocene-Pliocene sporopollen assemblages identified in localized overlying sediments in the eastern Hoh Xil basin (Wu et al., 2008).

The average thickness of the Fenghuoshan Group is about 4.8 km (Liu and Wang, 2001; Li et al., 2018a). The strata consist of a basal conglomerate overlain by interbedded quartzose sandstone and mudstone, with minor conglomerate, gypsum, and limestone beds (Leeder et al., 1988; Yin et al., 1988; Liu and Wang, 2001), indicating a fluvial environment with significant incursions of lacustrine and alluvial fan-delta settings (Liu and Wang, 2001; Cyr et al., 2005). Paleocurrent directions for the Fenghuoshan Group are dominantly to the north and northeast (Leeder et al., 1988; Liu and Wang, 2001; Wang et al., 2002, 2008a; Cyr et al., 2005; Liu et al., 2005a; Yi et al., 2008; Li et al., 2012). North to northeast paleocurrent directions have also been documented for the equivalent Kangtuo Formation in the western part of the basin (Dai et al., 2012). Petrologic analyses of Fenghuoshan Group sandstones indicate that they were derived primarily from recycled orogen sources (Wang et al., 2002).

The Yaxicuo Group is 670–2000 m thick and consists of alternating sandstone and mudstone with gypsum and occasional conglomerate, marl, and silty limestone beds (Liu et al., 2001, 2005a; Liu and Wang, 2001). They are interpreted to have been deposited in fluvial and lacustrine environments evident from the observed channel, overbank, lakeshore, shallow lacustrine, and saline lacustrine facies (Liu and Wang, 2001). Like the Fenghuoshan Group, paleocurrent directions are typically to the north and northeast, becoming more easterly higher in the section (Liu and Wang, 2001; Wang et al., 2002, 2008a; Liu et al., 2005a; Yi et al., 2008). A change to southward flow in the upper Yaxicuo Group has been documented in exposures along the southern Hoh Xil basin margin (Li et al., 2012). Analysis of sandstone petrology suggests that the Yaxicuo Group sediments were derived primarily from a weathered sedimentary-rock source (Wang et al., 2002).

The Wudaoliang Group consists of dolostone, micritic limestone, marl, sandy limestone, mudstone, and sandstone, with a total thickness from < 100 m to ~800 m (Liu and Wang, 2001; Liu et al., 2005a; Zhu et al., 2006b; Zhou et al., 2007; Wu et al., 2008). The strata were deposited in a series of lakes across much of the present-day Hoh Xil basin, with an area > 10⁵ km² (Wu et al., 2008). The proportion of coarse

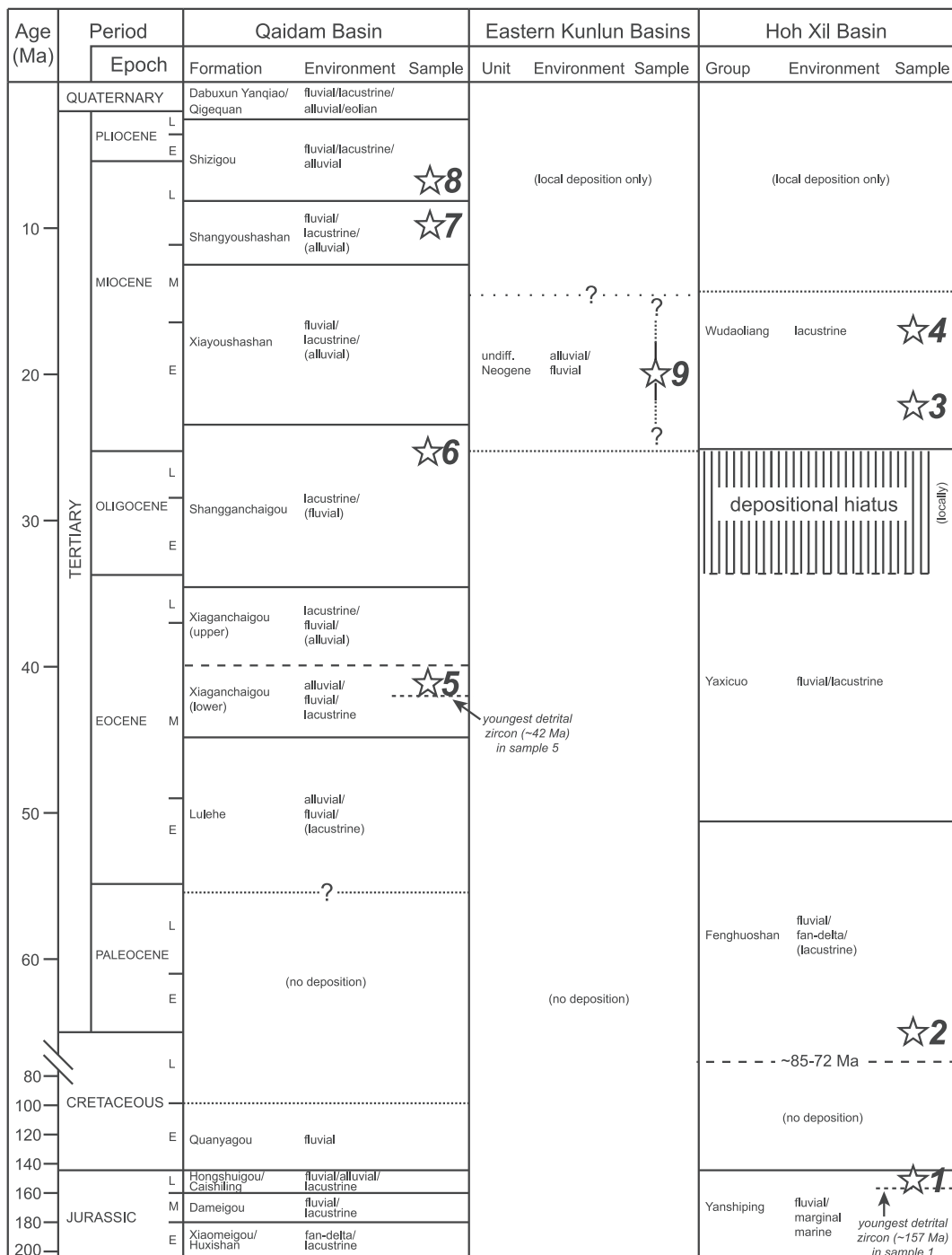


Fig. 3. Cenozoic stratigraphy of the central and northern Tibetan plateau, including lithologic unit names and interpreted depositional environments (see text for references). Stratigraphic positions of sandstone samples 1 through 9 collected for petrographic analysis and U-Pb detrital zircon geochronology are indicated by the white stars.

clastic materials relative to carbonates increases towards the northern and southern margins of the basin (Wu et al., 2008). Younger Neogene and Quaternary fluvial and alluvial units locally overlie the Wudaoliang Group strata along basin margins (Wu et al., 2008). Due to the dominantly lacustrine nature of the Wudaoliang Group strata, paleocurrent data are sparse, though southward flow has been documented near the base of the unit (Liu et al., 2005a).

3.2.2. Qaidam basin

Qaidam basin, bounded to the north by the Altyn Tagh and southern Qilian Shan ranges and to the south by the Eastern Kunlun Range

(Fig. 2), is the largest topographic depression within the Tibetan plateau and preserves a complete record of Cenozoic sedimentation since at least the early Eocene. Along the western portion of the northern margin of the basin, the south-directed North Qaidam thrust system juxtaposes Jurassic and older rocks over the Cenozoic strata (Yin et al., 2008a). Farther east, north-directed thrusts are more prominent (Yu et al., 2017d). In the south, the Cenozoic basin strata overlap Paleozoic and older rocks of the Eastern Kunlun Range in a depositional contact (Yin et al., 2007a). This contact is well-exposed along the southwestern margin of Qaidam basin and the contact surface can be traced via seismic reflection profiles as a north-dipping basement reflector below

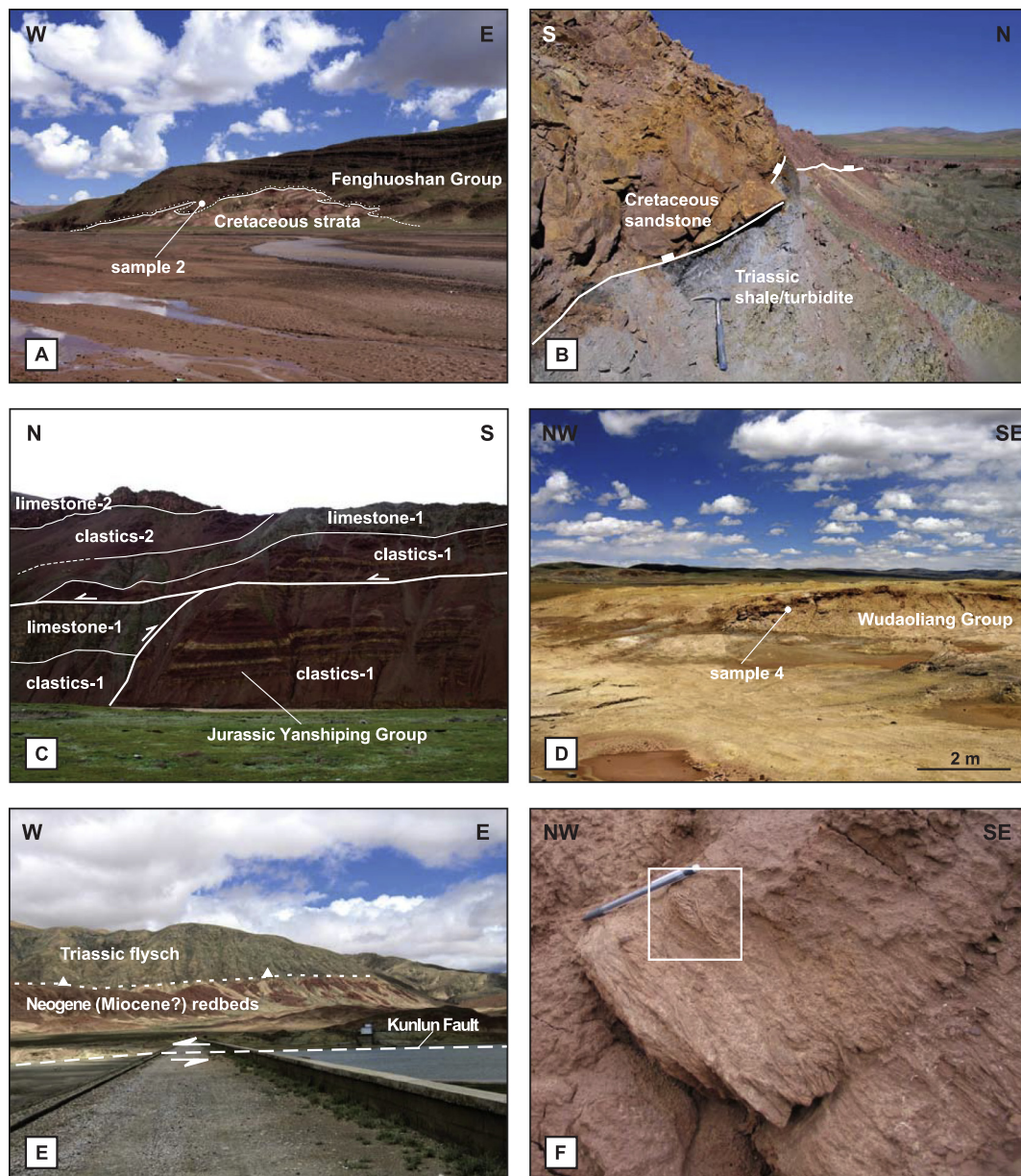


Fig. 4. Field photographs. See Fig. 2 for photo locations and view directions (A) Unconformity between the Fenghuoshan Group of Hoh Xil basin and underlying strata of inferred early Cretaceous age. The erosional/depositional character of this contact is clearly shown by the incised paleo-channels on the left and right sides of the outcrop. The location of sandstone sample 2 from the Fenghuoshan Group is indicated. (B) Normal fault juxtaposing Cretaceous strata in the hanging-wall and Triassic flysch in the footwall. (C) Complex thrusting in the Jurassic Yanshiping Group. (D) Outcrop of Wudaoliang Group strata in the central Hoh Xil basin. The location of sandstone sample 4 is indicated. (E) Exposure of Neogene (inferred Miocene) strata adjacent to the Kunlun fault in the interior of the Eastern Kunlun Range. The strata are in the footwall of an active north-dipping thrust fault. (F) Rare trough cross-stratification in the Xiaganchaigou Formation near the location of sandstone sample 5. White box highlights best exposure.

the basin fill (Yin et al., 2007a). The overall structure of the Cenozoic basin is a broad synclinorium bounded by an active duplex system in the north initiated at ca. 50 Ma and an active south-directed thrust system in the Eastern Kunlun Range in the south that started to develop at 30–20 Ma (Yin et al., 2008b).

Eight Cenozoic lithostratigraphic formations are recognized in Qaidam basin: the Paleocene-lower Eocene Lulehe Formation (> 52–44.2 Ma), upper Eocene Xiaganchaigou Formation (44.2–34.2 Ma), Oligocene Shangganchaigou Formation (34.2–23 Ma), lower-middle Miocene Xiayoushashan Formation (23–12.44 Ma), upper Miocene Shangyoushashan Formation (12.44–8.1 Ma), upper Miocene-Pliocene Shizigou Formation (8.1–2.5 Ma), Pleistocene Qigequan Formation (< 2.5 Ma), and Holocene Dabuxun Yanqiao Formation

(Fig. 3). Lithostratigraphic units have been correlated across the basin using a dense network of seismic reflection profiles and drill-hole data (Huo, 1990; Qinghai BGMR (Bureau of Geology and Mineral Resources), 1991; Yang et al., 1992; Song and Wang, 1993; Huang et al., 1996; Xia et al., 2001; Qiu, 2002; Sun et al., 2005; Rieser et al., 2006a, 2006b; Yin et al., 2008b). Extensive biostratigraphic, magnetostratigraphic, and detrital low-temperature thermochronologic studies have been conducted on Qaidam strata (e.g., Yang, 1988; Yang et al., 1992, 1997; Rieser et al., 2006a; Sun et al., 1999, 2005; Fang et al., 2007; Wang et al., 2007b, 2017b; Lu and Xiong, 2009; Chang et al., 2015; Ji et al., 2017); however, the establishment of a definitive chronology of the Cenozoic stratigraphy has remained elusive. Most magnetostratigraphic results from Qaidam basin are restricted to a

subset of the complete stratigraphic sequence, but two recent studies examined sections spanning the Lulehe to Shizigou Formations located ~10 km apart along the northern margin of the basin (Ji et al., 2017; Wang et al., 2017b). Despite the close proximity and similar stratigraphic extents, the initiation age of deposition of the Lulehe Formation determined by these studies varied from > 52 Ma (Ji et al., 2017) to ~25.5 Ma (Wang et al., 2017b). Herein, we largely adopt the chronology established by Ji et al. (2017) because it was established for a nearly complete section of Cenozoic Qaidam strata and is more consistent with the majority of other magnetostratigraphic and biostratigraphic results (also see discussion in Song et al., in press). Age assignments for the Xiayoushashan Formation are adopted from a magnetostratigraphic analysis in western Qaidam basin (Chang et al., 2015) due to the close proximity of the examined section to our sample locations.

The maximum total thickness of Cenozoic strata in Qaidam basin exceeds 16 km in the west-central part of the basin and progressively thins eastward along its central axis to < 2 km in the east (Huang et al., 1996; Yin et al., 2008b). The Lulehe Formation is a few hundred to 2600 m thick (Lee, 1984; Huang et al., 1996; Qiu, 2002; Wang et al., 2006) and lies unconformably over Proterozoic-Paleozoic metamorphic units, Paleozoic plutons, and Mesozoic strata (Xu, 1985; Huo, 1990; Yang et al., 1992; Yin et al., 2002; Wang et al., 2006; Ji et al., 2017). The unit consists dominantly of conglomerate interbedded with sandstone and mudstone deposited in alluvial, fluvial, delta plain, and shallow lacustrine environments (Lee, 1984; Wang and Coward, 1990; Song and Wang, 1993; Métivier et al., 1998; Hanson et al., 2001; Xia et al., 2001; Yin et al., 2002; Pang et al., 2004; Wang et al., 2006, 2017b; Zhu et al., 2006b; Fang et al., 2007; Bush et al., 2016; Ji et al., 2017).

The Xiaganchaigou Formation is a few hundred to 2800 m thick and consists of sandstone and mudstone interbedded with marl, thinly bedded micritic limestone and gypsum beds (Lee, 1984; Hanson et al., 2001; Pang et al., 2004; Sun et al., 2005; Wang et al., 2006, 2017b; Zhu et al., 2006b; Fang et al., 2007; Bush et al., 2016; Ji et al., 2017). The fine-grained character of the strata and the increasing presence of carbonates and evaporites in the upper sequence of the formation clearly suggest a transition to a more lacustrine depositional environment with alluvial/fluvial environments near the basin margins (Hanson et al., 2001; Yin et al., 2002; Wang et al., 2006; Fang et al., 2007). The Shangganchaigou Formation above the Xiaganchaigou Formation consists of up to 2000 m of sandstone, mudstone, and minor calcareous shale, limestone, and conglomerate, indicating continued in a dominantly lacustrine and deltaic environment (Lee, 1984; Song and Wang, 1993; Huang et al., 1996; Pang et al., 2004; Sun et al., 2005; Wang et al., 2006, 2017b; Fang et al., 2007; Zhuang et al., 2011; Chang et al., 2015; Ji et al., 2017).

The Xiayoushashan Formation consists of up to 2600 m of mudstone, sandstone, local limestone, and fine-grained conglomerate (Lee, 1984; Xu, 1985; Huang et al., 1996; Qiu, 2002; Pang et al., 2004; Wang et al., 2006, 2017b; Fang et al., 2007; Bush et al., 2016; Ji et al., 2017). Conglomerate units are more common in the Xiayoushashan Formation than in the underlying lacustrine-dominated strata. The coarsening-upward trend has been interpreted as indicating deposition in a shallowing lacustrine environment and a transition to a more fluvial/alluvial-dominated depositional environment (Rieser et al., 2005, 2006a; Chang et al., 2015; Bush et al., 2016). The conformably overlying Shangyoushashan Formation (Sun et al., 1999; Fang et al., 2007; Wang et al., 2007b; Chang et al., 2015), with a maximum thickness of 2600 m, is generally lithologically similar to the Xiayoushashan Formation and suggests a fluvial-dominated environment (Lee, 1984; Xu, 1985; Huang et al., 1996; Qiu, 2002; Pang et al., 2004; Wang et al., 2006, 2017b; Zhou et al., 2006; Bush et al., 2016; Ji et al., 2017). Occurrences of intercalated mudstone and gypsum suggest periods of arid lacustrine conditions existed in Qaidam basin during this time (Chen and Bowler, 1986; Wang et al., 2006; Ji et al., 2017).

The Shizigou Formation has a maximum thickness of ~2000 m and consists of alluvial sandstone and conglomerate near the basin margins and lacustrine mudstone and evaporite units near the basin center (Lee, 1984; Xu, 1985; Song and Wang, 1993; Hanson et al., 2001; Wang et al., 2006, 2017b; Zhu et al., 2006b; Fang et al., 2007; Bush et al., 2016; Ji et al., 2017). The overlying Qigequan Formation has a maximum thickness of ~3000 m (Lee, 1984; Qiu, 2002; Wang et al., 2006) and exhibits a basinward transition from alluvial/fluvial to deltaic to lacustrine depositional environments with an eolian component (Chen and Bowler, 1986; Xia et al., 2001). The identification of paleo-shoreline features and the presence of extensive evaporites in late Pliocene and Pleistocene strata have been interpreted to reflect the establishment and fluctuating persistence of large lakes in Qaidam basin extending into the Holocene (e.g., Chen and Bowler, 1986; Lehmkühl and Haselein, 2000; Mischke et al., 2006a, 2006b). The Holocene Dabuxun Yanqiao Formation consists of mixed fluvial, alluvial, eolian, and lacustrine clastic and evaporitic sediments, in places exceeding 300 m in thickness (Lee, 1984; Xu, 1985; Hanson et al., 2001).

3.3. Cenozoic basins in the Eastern Kunlun Range

Intermontane basins of Cenozoic age exposed within the Eastern Kunlun Range are typically associated with active south-directed thrusts (Zhong et al., 2004; Yin et al., 2007a) (Fig. 4E). Basin development in the western segment of the Eastern Kunlun Range started in the Eocene and Oligocene in a lacustrine setting (Zhong et al., 2004), which is interpreted to be part of a larger Paleogene Paleo-Qaidam basin prior to the uplift of the Eastern Kunlun Range at the start of the Neogene (Yin et al., 2007a). In the central and eastern segments of the Eastern Kunlun Range, Cenozoic basins may have started to develop in the Neogene in alluvial fan settings (Wu et al., 2008). These basins have been interpreted to be the northern proximal facies of a large Miocene lake present in the Hoh Xil region during the deposition of the Wudaoliang Group (Wu et al., 2008). Despite the above interpretations, it should be noted that age constraints and detailed sedimentologic studies on the Cenozoic basins in the Eastern Kunlun Range are generally lacking. As a result, the tectonic settings of the basins within the range and their relationships to the nearby Qaidam and Hoh Xil basins remain poorly understood.

4. Sandstone petrology

4.1. Methods

We collected seven Cenozoic sandstone samples from Hoh Xil and Qaidam basins for petrographic analysis. As Jurassic units dominate the southern margin of the Hoh Xil basin, we analyzed one Jurassic sample to determine their contribution to the clastic composition of the Hoh Xil Cenozoic strata. Sample locations are shown in Fig. 2. The lithostratigraphic assignments of samples were determined based on observed field relationships and published geologic maps (Qinghai BGMR (Bureau of Geology and Mineral Resources), 1991; Staisch et al., 2014; Chang et al., 2015) and are indicated schematically in Fig. 3. For petrographic analysis, standard thin sections were prepared and stained for identification of potassium feldspar. Modal compositions were determined by employing the modified Gazzi-Dickinson point-counting method of Ingersoll et al. (1984). We use the following abbreviations to facilitate description of our petrological results: F for feldspar, L for non-quartzose lithic grains, Lt for total lithic grains including quartzose grains, Qm for monocrystalline quartz, and Qt for total quartz. Raw point-counting data is summarized in Supplementary Table 1 and recalculated modal abundances are plotted on the ternary diagrams of Dickinson et al. (1983) and shown in Fig. 5.

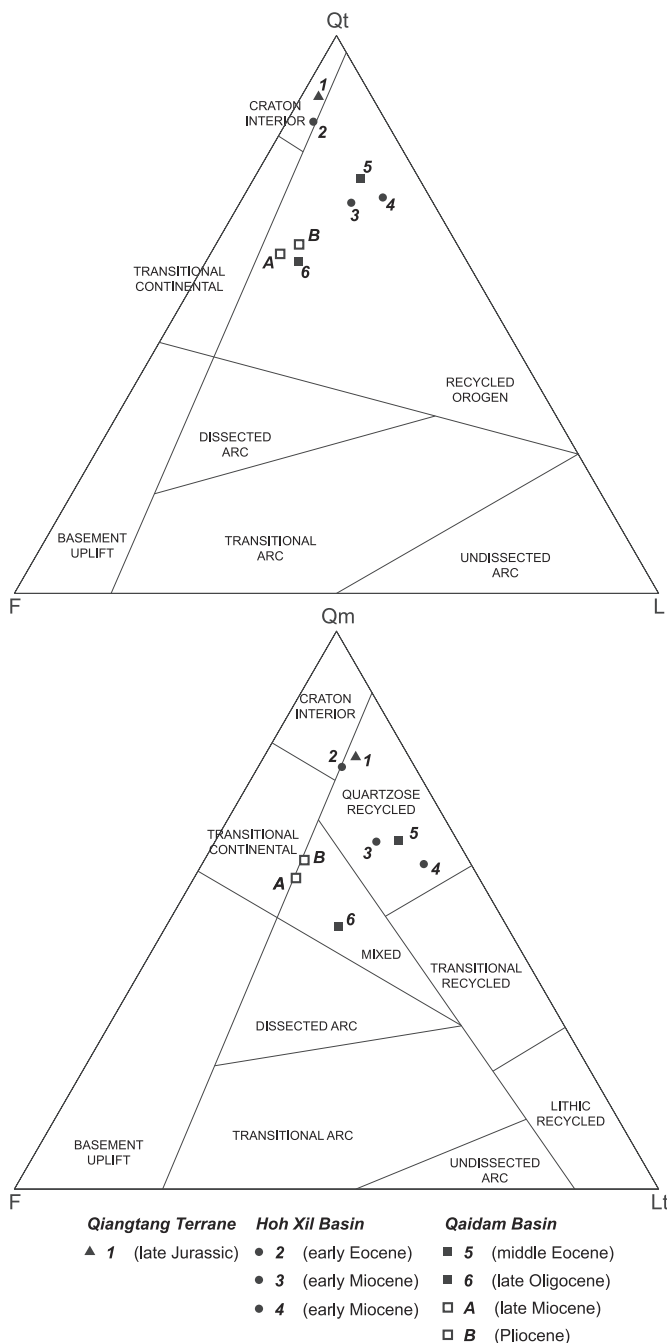


Fig. 5. Ternary diagrams (QtFL and QmFLt) indicating modal abundances recalculated from raw-point counting data (Table 1) for sandstone samples 1 through 6. The provenance fields of Dickinson et al. (1983) are shown to aid in potential source interpretation. Mean results for the Shangyoushashan and Shizigou Formations of Qaidam basin from Rieser et al. (2005) are also shown (samples A and B). The Jurassic sample from the Qiangtang terrane and the Eocene sample from Hoh Xil basin (samples 1 and 2) plot near the boundary between the craton interior and recycled fields in both diagrams, whereas younger samples from Hoh Xil basin and all samples from Qaidam basin plot in the recycled and mixed fields, suggesting a two-phase history for the evolution of Hoh Xil basin.

4.2. Results from Jurassic sample of the Qiangtang terrane

Jurassic strata are present at the surface across much of the Qiangtang terrane in central Tibet, with the northernmost exposures stratigraphically between the underlying Triassic Songpan-Ganzi flysch sequence and the overlying Tertiary strata of the Hoh Xil basin (Fig. 2).

Sample 1 was collected from a light gray, massive medium- to coarse-grained sandstone of late Jurassic age exposed in the Tanggula Range on the southern margin of the Hoh Xil basin (Figs. 2 and 3). In thin section, the sample exhibits partially interlocking quartz grains indicating a low degree of recrystallization and contains very little cement or matrix material. Its modal composition is Qt:F:L = 89:8:3 and Qm:F:Lt = 78:8:14, plotting in the “craton interior” and “quartzose recycled” provenance fields, respectively (Fig. 5).

4.3. Results from Cenozoic samples of the Hoh Xil basin

Sample 2 was collected in the central Hoh Xil basin from a late Cretaceous fine- to medium-grained red sandstone unit directly above the unconformity between the Fenghuoshan Group and underlying early Cretaceous(?) strata (Figs. 2, 3, and 4A). Sample 2 is characterized by subangular to subrounded grains and interstitial calcite cement. The modal compositions are Qt:F:L = 85:11:4 and Qm:F:Lt = 76:11:13, plotting near the boundary between the “craton interior” and “recycled” fields in both ternary diagrams (Fig. 5). These results are similar to those obtained by Wang et al. (2002) for Fenghuoshan Group sandstones.

Sample 3 was collected from the base of the early Miocene Wudaoliang Group in the northern Hoh Xil basin (Fig. 3). It is from a light red-brown, fine-grained sandstone that is part of an interbedded sequence of lenticular sandstones and sandy siltstones. Calcite cementation is pervasively developed between moderately well-sorted subangular to subrounded grains and secondary hematite is common. Sample 4, a fine-grained white sandstone, was collected from a stratigraphically higher position within the Wudaoliang Group (Figs. 2, 3, and 4D). Grains in sample 4 exhibit a higher degree of roundedness than those in sample 3, and the cement is both calcitic and siliceous. Modal compositions for sample 3 are Qt:F:L = 70:13:17 and Qm:F:Lt = 62:13:25. Modal compositions for sample 4 are Qt:F:L = 71:7:22 and Qm:F:Lt = 58:7:35. Results for both samples plot in the “recycled orogen” field in the QtFL diagram and in the “quartzose recycled” field in the QmFLt diagram (Fig. 5).

4.4. Results from Cenozoic samples of Qaidam basin

Sample 5 was collected from a red-brown, very fine-grained sandstone within a sequence of interbedded mudstone and fine-grained sandstone mapped as the upper Eocene Xiaganchaigou Formation exposed locally along the southern margin of Qaidam basin (Qinghai BGMR (Bureau of Geology and Mineral Resources), 1991; Figs. 2 and 3). The sandstone is moderately well-sorted with rounded to subrounded framework grains, calcite cement, and secondary hematite. Detrital modes are Qt:F:L = 74:9:17 and Qm:F:Lt = 63:9:28, plotting in the “recycled orogen” and “quartzose recycled” fields (Fig. 5). These results indicate a slightly more quartzose composition than those reported by Rieser et al. (2005) for the same unit along the northern margin of the Qaidam basin (Qt:F:L = 65:22:13; Qm:F:Lt = 61:22:17), possibly suggesting different source regions for the northern and southern margins of the Qaidam basin during the late Eocene. This interpretation is further supported by variations in detrital heavy mineral compositions within samples of the Xiaganchaigou Formation collected from areas adjacent to the Altyn Tagh Fault and the Qimen Tagh (Li et al., 2018b).

Sample 6 was collected from strata of the Oligocene Shangganhaigou Formation exposed near the core of the Youshashan anticline in the western Qaidam basin (Figs. 2 and 3). The sample is a poorly-sorted, very fine- to medium-grained massive sandstone from a succession of interbedded sandstone and pebble conglomerate with common granitoid, sandstone, and quartzite clasts. Calcite cement and clay matrix material are common in the interstices between subrounded framework grains. The modal composition of the sample is Qt:F:L = 60:26:14 and Qm:F:Lt = 47:26:27, plotting in the “recycled

orogen” and “mixed” fields on the ternary diagrams (Fig. 5). These results are also good agreement with those reported previously for the Shangganhaigou Formation (Rieser et al., 2005; Qt:F:L = 60:27:13; Qm:F:Lt = 58:26:16).

Samples 7 and 8 were collected from the late Miocene Shangyoushashan Formation and the Pliocene Shizigou Formation, respectively, exposed along the southwest limb of the Youshashan anticline (Fig. 2). They are the youngest samples we collected from Qaidam basin. Sample 7 is poorly-sorted, fine- to coarse-grained subangular to subrounded sand while sample 8 is poorly-sorted, fine-grained subangular to subrounded sand. Both samples were from interbedded sequences of sandstones and pebble conglomerates. Accurate point counting was not possible for the two samples due to the difficulty of preparing coherent thin sections of the poorly lithified samples. However, a visual examination of the detrital composition suggests that they share a similar modal composition to sample 6 from the Shangganhaigou Formation. Rieser et al. (2005) also performed petrologic analysis of sandstone samples from the same units near the locations of our samples 7 and 8. Their results show that the modal composition for the late Miocene Shangyoushashan Formation is Qt:F:L = 61:28:11 and Qm:F:Lt = 56:29:15 and the modal composition for the Pliocene Shizigou Formation is Qt:F:L = 62:25:13 and Qm:F:Lt = 59:26:15. The above modal abundances plot in the “recycled orogen” and “mixed” fields on the ternary diagrams (Fig. 5).

4.5. Cenozoic sample from an Eastern Kunlun Intermontane basin

Many of the fault-controlled intermontane basins within the Eastern Kunlun Range are active, and in some cases, basin fill is locally exposed along the margins of these basins in both the footwalls and hanging-walls of late Cenozoic thrust faults. Sample 9 was collected from the northern, faulted margin of a narrow basin within which the left-slip Kunlun fault is located (Figs. 2, 3, and 4F). At the sample locality, the Neogene sequence is overturned and exposed in the footwall of a south-directed thrust. Hanging-wall lithologies include low-grade Triassic metasedimentary units and a small, undeformed granodiorite body of inferred late Triassic age. Based on the structural setting of this exposure, our proposed late Oligocene-early Miocene age for the initiation of widespread uplift of the Eastern Kunlun Range, and the occurrence of other small exposures of strata assigned a Neogene age at nearby locations adjacent to the Kunlun fault (Qinghai BGMR (Bureau of Geology and Mineral Resources), 1991), we tentatively assign these strata an early Miocene age. Sample 9 is a medium-grained, red arkosic sandstone exhibiting moderate sorting, sub-angular clasts, and abundant feldspar. These observations suggest that the Eastern Kunlun intermontane basin Neogene strata consist of generally immature sediment, as expected based on the proximity of the basins to their probable sedimentary sources in the adjacent mountains.

5. U-Pb Detrital Zircon Geochronology

5.1. Sampling and analytical method

We performed U-Pb dating of detrital zircons from samples 1–9 described in the previous section. Sandstone samples of ~10 kg were collected in the field and were processed by standard mineral separation techniques, including crushing and density and magnetic separation. Approximately 500 grains of the resulting zircon separates were split *en masse* to provide a random selection of the total zircon population for analysis. Separated zircons were mounted in 1-inch diameter epoxy plugs, which were subsequently polished to approximately one-half mean grain thickness to expose the interiors of the detrital zircon grains. Approximately 100 detrital zircon grains from each sample were randomly selected for analysis from the separated grains. Zircon grains with cracks or inclusions were excluded from the analysis to avoid complication in age determination.

Laser ablation-multicollector-inductively coupled plasma mass spectrometry (LA-MC-ICPMS) U-Pb dating of detrital zircons was performed using the Arizona LaserChron Center's GVI Isoprobe. Zircon grains were ablated with a New Wave/Lambda Physik DUV193 Excimer laser ($\lambda = 193$ nm, spot diameter = ~35 μm) and ablated material was transported via helium gas to the plasma source of the GVI Isoprobe. U and Pb isotopes were measured simultaneously in static mode using Faraday collectors for ^{238}U , ^{232}Th , ^{208}Pb , ^{207}Pb , and ^{206}Pb , and an ion-counting channel for ^{204}Pb . For each analysis, background levels were checked via one 20-s integration on peaks with the laser off, followed by 12 or 20 one-second integrations measuring ablated material. Individual analyses were separated by 30 s to purge the previous sample and allow peak signal intensities to return to background levels. Corrections for common Pb and Hg contribution to the measured ^{204}Pb were carried out by assuming an initial Pb composition from Stacey and Kramers (1975) and subtraction of peak-centered background values, respectively. Measured isotopic ratios were corrected for fractionation by comparison with a zircon standard with a known age of 564 ± 4 Ma (2σ error), fragments of which were measured after every fifth detrital zircon grain. The ages presented are $^{206}\text{Pb}/^{238}\text{U}$ ages for grains less than ~800–1050 Ma and $^{206}\text{Pb}/^{207}\text{Pb}$ ages for grains greater than ~800–1050 Ma; the specific threshold age used for each sample is given with the full analytical results in Supplementary Table 2. Reported uncertainties for age determination of individual grains are at the 1 σ level and reflect measurement errors only. Individual analyses with > 10% uncertainty, > 20% discordance, or > 5% reverse discordance are not included in our interpretations of the analytical results.

Detrital zircon ages for all samples are shown on concordia diagrams (Fig. 6) and as histograms with relative probability plots generated using Isoplot 3.75 Ludwig (2012) and kernel density estimate (KDE) plots produced using the Provenance package for R (Vermeesch et al., 2016) (Fig. 7A). Measured Th/U ratios for over 98% of all zircon grains (880/895) are > 0.1, suggesting the detrital zircons in our samples are dominantly of magmatic origin (e.g., Rubatto, 2002). Dating results for individual samples are described below. Characterizations of age spectra are based on KDE plots unless noted. Minor populations refer to those accounting for < 10% of the zircon ages of the respective sample.

5.2. Detrital zircon ages from Jurassic sample of the Qiangtang Terrane

Analyses of zircon grains from the Jurassic sandstone (sample 1 in Figs. 2 and 3) provided 98 usable ages. The youngest ages constrain the maximum depositional age of the sample to ~157 Ma ($n = 3$), consistent with the late Jurassic age previously assigned to these strata (Leeder et al., 1988). Zircon ages at 230–290 Ma and 430–470 Ma are common and define two prominent peaks at ~275 Ma and ~445 Ma, respectively (combined 24% of zircon ages). The highest peak is in the early Proterozoic between 1750 Ma and 2000 Ma, centered at ~1850 Ma (32% of zircon ages). A low broad peak at ~1020 Ma defined by 970–1220 Ma ages (16% of zircon ages) and a minor population at 2350–2550 Ma are also present.

5.3. Detrital zircon ages from Late Cretaceous-Cenozoic samples of the Hoh Xil basin

Analyses of zircon grains from the Fenghuoshan Group sandstone (sample 2 in Figs. 2, 3, and 4A) provided 103 usable ages. The dominant age population is at 210–300 Ma (32% of zircon ages) with a peak at ~270 Ma. Age populations of 390–475 Ma (21% of zircon ages) and 1600–2100 Ma (21% of zircon ages) have peaks of ~435 Ma and ~1875 Ma, respectively. Minor age populations of 750–840 Ma and 2400–2500 Ma are also present.

Analyses of zircon grains from lower and upper sections of the early Miocene Wudaoliang Group (samples 3 and 4 in Figs. 2, 3, and 4D) provided a total of 106 and 101 usable ages, respectively. Three

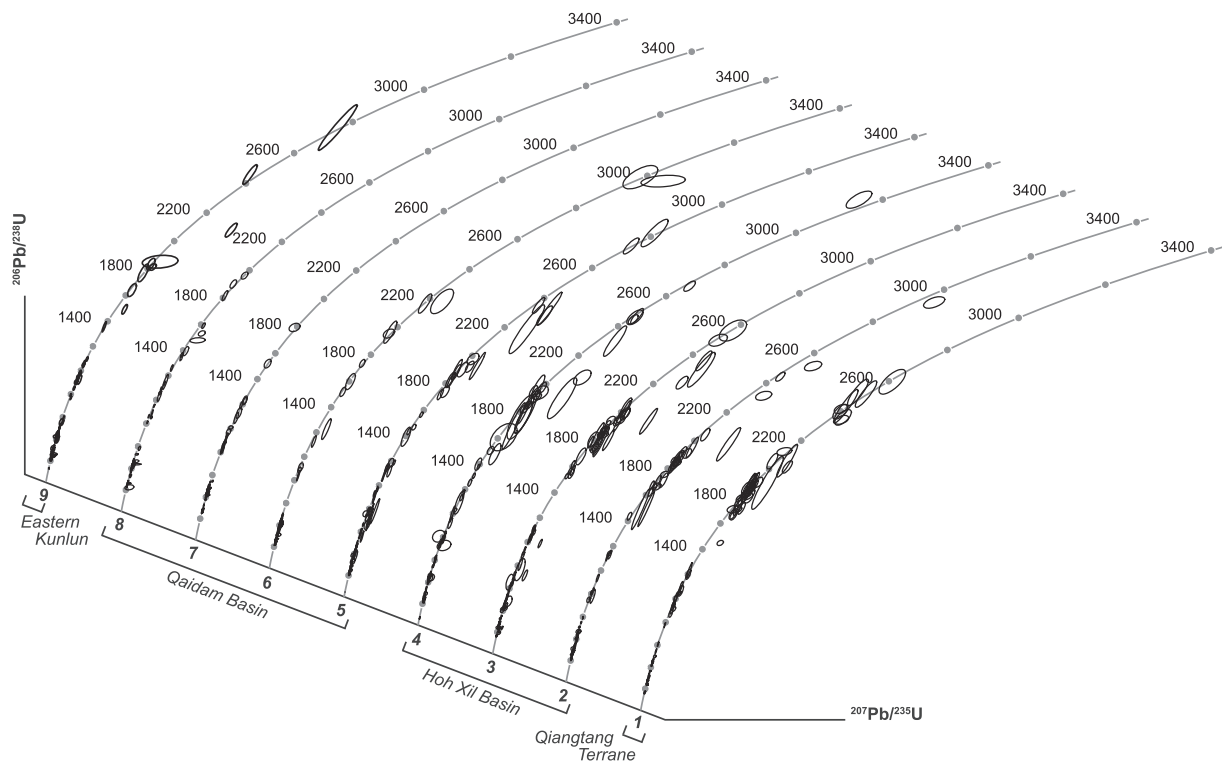


Fig. 6. U-Pb detrital zircon geochronology concordia diagrams of sandstone samples 1 through 9. Ages are in Ma and error ellipses show 2σ errors. See text for description of criteria employed to accept results.

prominent age populations are evident for both samples: 220–310 Ma (20% of combined zircon ages) with a peak at ~ 250 Ma, 400–500 Ma (19% of combined zircon ages) with a peak at ~ 450 Ma, and 1800–2050 Ma (18% of combined zircon ages) with a peak at ~ 1900 Ma. Minor age populations of 2450–2550 Ma are also present in both samples. Sample 3 additionally exhibits two minor peaks at ~ 1100 Ma and ~ 1620 Ma. In sample 4, 720–850 Ma ages (10% of zircon ages) define a peak at ~ 770 Ma, and a spread of ages from 1060 to 1390 Ma (8% of zircon ages) define a low broad peak.

5.4. Detrital zircon ages from Cenozoic samples of the Qaidam basin

We obtained 104 usable zircon ages from the late Eocene Xiaganchaigou Formation sandstone (sample 5 in Figs. 2 and 3). As the KDE plots fails to discriminate the two age maxima evident in the histogram for zircon ages < 500 Ma, identification of age populations and peaks for this sample is based on the relative probability plot. The < 500 Ma zircons can be separated into groups at 210–290 Ma (20% of zircon ages) and 370–480 Ma (23% of zircon ages), with the peaks at ~ 255 Ma and ~ 430 Ma. A broad spread of ages from 500 to 1600 Ma exhibits apparent minor peaks at ~ 575 Ma, ~ 745 Ma, ~ 930 Ma, and ~ 1100 Ma. Important minor age populations of 1800–2050 Ma (9% of zircon ages) and 2390–2510 Ma (5% of zircon ages) define peaks of ~ 1870 Ma and ~ 2500 Ma, respectively. A single zircon yielded an age of 42 ± 1 Ma. Although this single date is not a robust measure of the maximum depositional age of the sample, it is nevertheless consistent with the middle Eocene-early Oligocene age assignment of the Lower Xiaganchaigou Formation.

Analyses of zircon grains from the late Oligocene Shangganhaigou Formation sandstone (sample 6 in Figs. 2 and 3) provided 96 usable ages. The majority of detrital zircon ages for this sample are < 500 Ma, comprising two major populations at 220–280 Ma (28% of zircon ages) and 350–500 Ma (50% of zircon ages) with corresponding peaks of ~ 265 Ma and ~ 415 Ma. Detrital zircon ages > 500 Ma have widely scattered Archean and Proterozoic ages and define no apparent peaks.

Analyses of zircon grains from the late Miocene Shangyoushashan Formation sandstone (sample 7 in Figs. 2 and 3) provided 92 usable ages. Similar to sample 6, most zircons in sample 7 are of Paleozoic and Mesozoic ages, comprising two age populations of 255–290 Ma (14% of zircon ages) and 395–510 Ma (63% of zircon ages). Corresponding peaks are at ~ 275 Ma and ~ 450 Ma. Zircons ranging from 825 to 1240 Ma account for the majority of the remaining ages (78% of Proterozoic zircon ages). Analyses of zircon grains from the Pliocene Shizigou Formation sandstone (sample 8 in Figs. 2 and 3) provided 95 usable ages. Detrital zircon ages from this sample are also primarily < 500 Ma. Main age populations of 225–290 Ma (26% of zircon ages) and 370–480 Ma (48% of zircon ages) define peaks at ~ 265 Ma and ~ 430 Ma. Older zircon ages are scattered throughout the Proterozoic.

5.5. Detrital zircon ages from Neogene sample of an Eastern Kunlun Intermontane basin

We obtained 100 usable zircon ages from the inferred Miocene-age sandstone collected from an intermontane basin within the Eastern Kunlun Range (sample 9 in Figs. 2 and 3). The majority of zircons comprise two main age populations: 210–290 Ma (32% of zircon ages) with a peak at ~ 245 Ma and 375–470 Ma (30% of zircon ages) with a peak at ~ 430 Ma. A smaller middle Proterozoic age population of 900–1090 Ma (13% of zircon ages) has an apparent peak at ~ 950 Ma.

6. Apatite and zircon fission-track thermochronology

6.1. Method

Fission-track thermochronology is based on crystal-lattice damage manifested as linear tracks resulting from the constant-rate spontaneous fission of trace levels of ^{238}U in zircon and apatite grains. Above $\sim 240^\circ\text{C}$, the spontaneous tracks in produced in zircon grains are completely annealed (Bernet and Garver, 2005), and we use this value

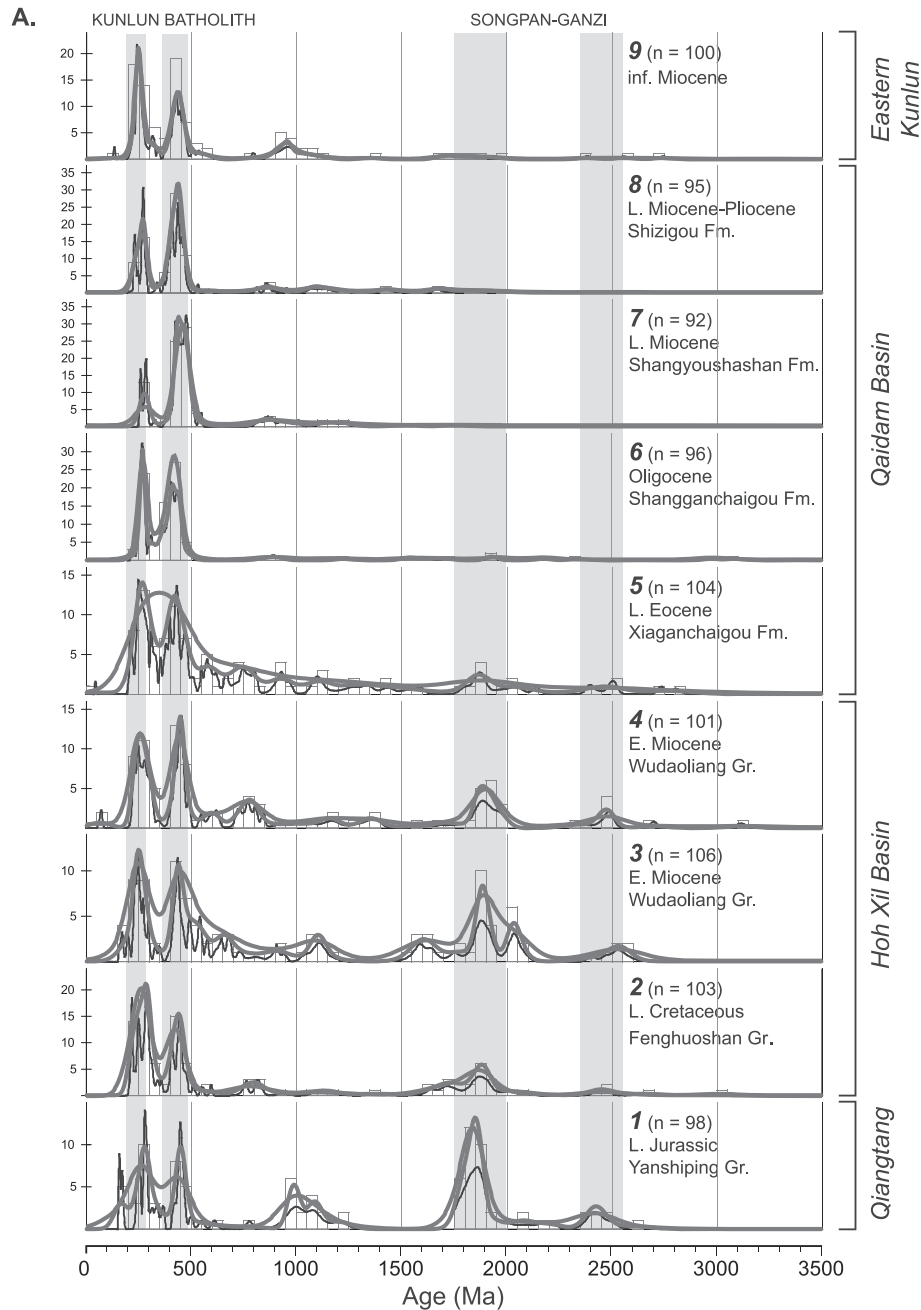


Fig. 7. (A) Histograms (bin size = 50 Ma), relative probability plots (black curves), and kernel density estimates (bold gray curves) for U-Pb detrital zircon geochronologic results for sandstone samples 1 through 9. Characteristic age signatures of the Eastern Kunlun Range and the Triassic Songpan-Ganzi flysch sequence (see below) are shown as vertical bars on the plots for comparative purposes. (B–F) Compilations of published U-Pb zircon ages from potential source regions in central and northern Tibet. Histograms (bin size = 50 Ma) show igneous crystallization ages. Black curves are kernel density estimates of concordant to slightly discordant (discordance < ~20%) detrital zircon ages from Proterozoic to Mesozoic units in each source region. (G) Kernel density estimate of U-Pb detrital zircon ages from mid-Mesozoic strata in basins along the Bangong-Nujiang suture zone between the Lhasa and Qiangtang terranes. Kernel density estimates for compiled data were generated using the Provenance package for R (Vermeesch et al., 2016). See Supplementary Information for a complete list of references for age compilations in B–G.

as an effective closure temperature for fission track retention and accumulation. For apatite, total annealing occurs above ~110 °C, but complete retention requires temperatures below ~60 °C (e.g., Ketcham, 2005). The range ~60–110 °C is termed the apatite partial annealing zone (PAZ), within which fission tracks are incompletely annealed. The decrease in temperature of a sample through the PAZ as a function of time is reflected by the distribution of lengths for the partially-annealed tracks. We use the above properties of apatite fission-track thermochronology to determine the low-temperature thermal history of the central segment of the Eastern Kunlun Range and combine the results

with zircon fission-track cooling ages to extend cooling paths to ~240 °C. This information in turn permits us to infer the onset age for the uplift of the Eastern Kunlun Range.

We collected nine samples for apatite fission-track (AFT) analyses from two traverses west and east of the Golmud-Lhasa Highway; zircon fission-track (ZFT) analyses were obtained for eight of these samples, as well as for two additional samples (Fig. 8). Fission track ages were measured using the external detector method (Gleadow, 1981) and calculated using the zeta calibration method (Hurford and Green, 1983). Grains of Durango apatite (31.4 ± 0.5 Ma) were used as the

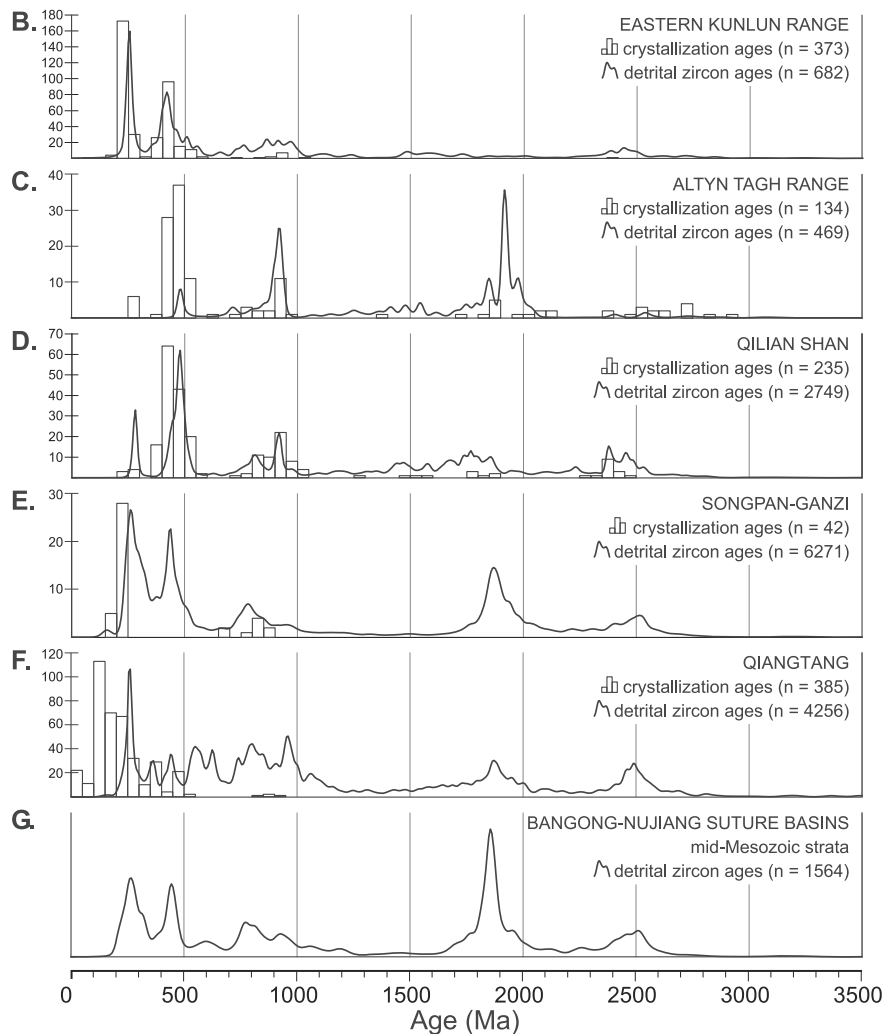


Fig. 7. (continued)

age-calibration standard for AFT analyses, and grains of Fish Canyon tuff zircon (27.9 ± 0.7 Ma) were used as the age-calibration standard for ZFT analyses. Apatite and zircon grains were separated from ~ 5 -kg samples using standard mineral separation techniques. Polished grain mounts were prepared and etched to reveal spontaneous fission tracks. Apatite grain mounts were etched in 7% HNO_3 at 20°C for 40 s; zircon grain mounts were etched in a 96% NaOH :82% KOH :98% LiOH solution at $210 \pm 10^\circ\text{C}$ for 4.5 h. All samples were irradiated at the China Institute of Atomic Energy reactor facility. Neutron fluences during irradiation were measured using NIST trace element glass SRM612 as a dosimeter. Low-U muscovite external detectors covering apatite grain mounts were etched in 40% HF at 20°C for 20 min to reveal induced fission tracks. Fission tracks were counted using an Olympus microscope at $1000\times$ magnification. Ages were calculated using the following zeta values: $\zeta_{\text{apatite}} = 352.4 \pm 29$ and $\zeta_{\text{zircon}} = 354.6 \pm 16$ (J.L. Wan).

6.2. Age results

Sample locations, AFT pooled ages, and ZFT central ages are summarized in Table 1 and shown on Fig. 8. AFT ages for all analyzed samples except sample S-21 are in the range between 0.9 ± 0.3 Ma and 16.3 ± 1.7 Ma (1σ), while sample S-21 has a significantly older AFT age of 52.9 ± 3.4 Ma (1σ). ZFT results define three distinct age groups. Samples S-22, S-23, and S-24 comprise the oldest group with early Jurassic ages between 175.6 ± 11.2 Ma and 188.3 ± 10.1 Ma (1σ).

Samples S-25, S-72, and S-75 yield late Jurassic to early Cretaceous ages between 139.3 ± 10.4 Ma and 156.9 ± 10.4 Ma (1σ). Samples S-21, S-26, S-73, and S-76 yield early to middle Cretaceous ZFT ages between 95.6 ± 5.8 Ma and 112.1 ± 6.8 Ma (1σ).

6.3. Cooling histories

Because fission track systematics in apatite are characterized by a PAZ between ~ 60 – 110°C , AFT ages and measured fission track length distributions can be inverted to produce suites of compatible thermal histories. We performed inverse modeling of the AFT data using the HeFTy v. 1.9.3 software of Ketcham (2005) and the kinetic annealing model for apatite of Ketcham et al. (2007) to produce time-temperature pathway models. For each sample, modeling was constrained by the ZFT central age and 1σ uncertainty determined for the same sample, and a ZFT closure temperature approximated as $240 \pm 30^\circ\text{C}$. For sample S-74, which lacks ZFT data, a broader time constraint ranging from 90 to 200 Ma, corresponding to the range of ZFT central ages for the other samples, was used. All models were further constrained by a surface temperature of 10°C . Modeling of each sample was run until 500 randomly-generated thermal histories with “good” fits were identified, where “good” indicates that forward modeling of the path produces model ages and track lengths in good agreement with the actual measured data for the sample (see Ketcham, 2005 for additional details on the statistical assessment of goodness of fit implemented in HeFTy). Fig. 9 shows the results of the HeFTy thermal modeling, including time-

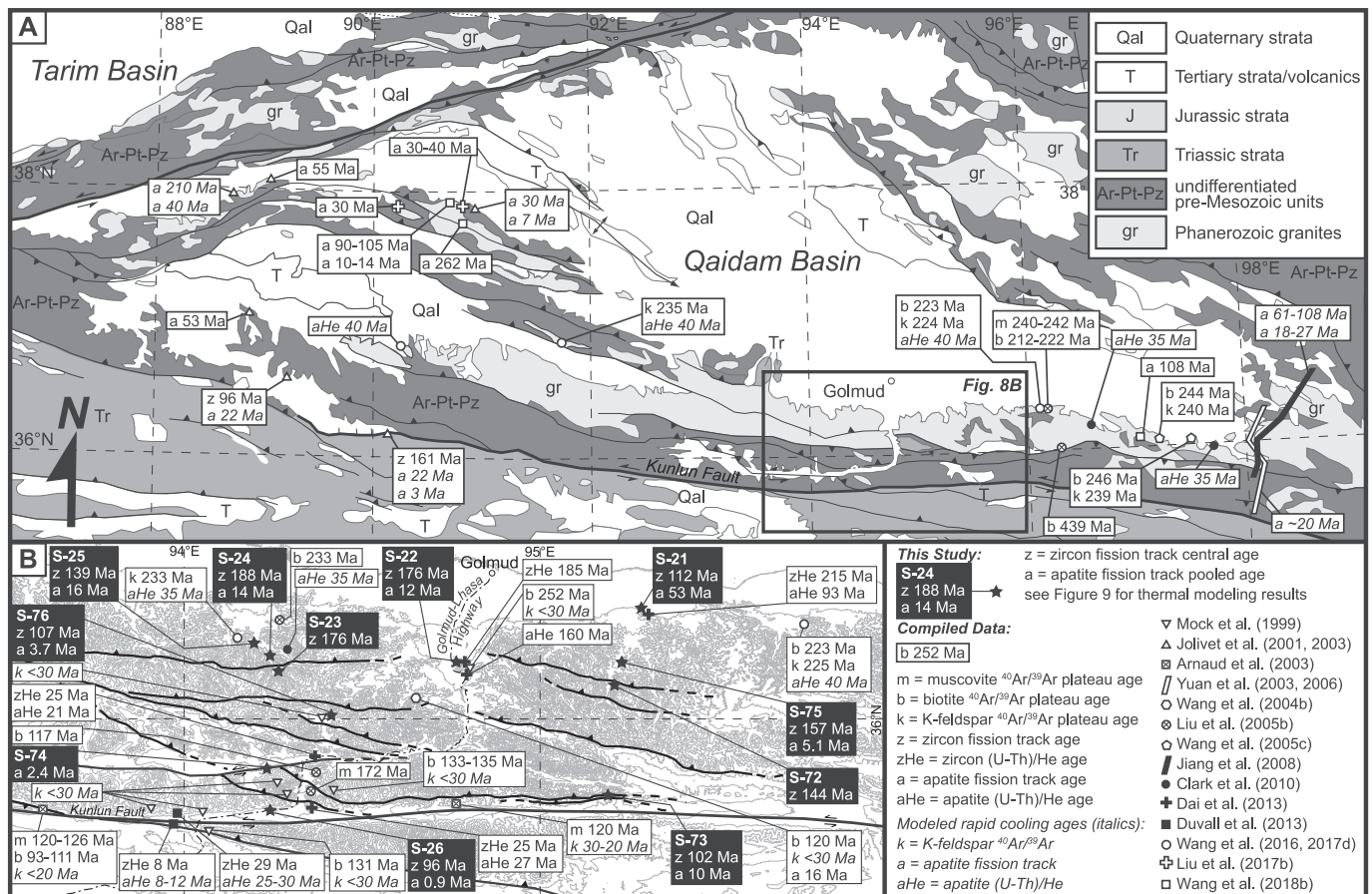


Fig. 8. (A) Geologic map of the Eastern Kunlun region indicating compiled thermochronologic results for the western and eastern ends of the Eastern Kunlun Range. (B) Detailed location map of the central section of the Eastern Kunlun Range showing the AFT/ZFT results from this study and compiled thermochronologic results.

temperature path envelopes for “good” and “acceptable” fits, the best-fit model for each sample, and a comparison of the observed and best-fit model track length distributions. The modeled thermal histories suggest that all samples except sample S-21 cooled rapidly through the apatite PAZ after 20 Ma, which is consistent with the pooled AFT ages reported above (Table 1). Sample S-21, collected from the northernmost margin of the Eastern Kunlun Range, cooled through the partial annealing temperature range at ~60–40 Ma.

The AFT age results can be used to investigate the timing of uplift of the Eastern Kunlun Range. West of the Golmud-Lhasa Highway, samples S-25, S-24, S-76, S-74, and S-26 display a southward-younging trend for the onset of rapid cooling (Figs. 8 and 9). The northernmost sample (S-25) began to cool rapidly at ~20 Ma, while the southernmost sample (S-26) did not start cooling rapidly until ~1 Ma. In contrast to the cooling trend described for the western traverse, samples collected east of the Golmud-Lhasa Highway indicate nearly coeval onset of rapid cooling at ~10–15 Ma for samples S-75 and S-73. Sample S-21 from the northernmost margin of the range shows the onset of rapid cooling at a much earlier time of ~45 Ma. One sample from the Golmud-Lhasa Highway (sample S-22) experienced rapid cooling at ~15 Ma.

7. Discussion

Our sandstone petrologic analyses suggest that the Jurassic strata in the Qiangtang terrane were sourced from a craton-interior provenance setting. Our work also suggests that the Hoh Xil basin received detritus of a similar provenance in the late Cretaceous-Eocene, but sedimentary material was derived from a recycled-orogen provenance setting in the early Miocene (Fig. 5). In contrast, the compositions of sediment deposited in the western Qaidam basin throughout the Cenozoic are

consistent with recycled-orogen sources, although more feldspathic compositions in the younger samples are suggestive of a shift towards a mixed provenance (Fig. 5). The results of our U-Pb detrital zircon geochronology indicate that Jurassic strata along the southern margin of the Hoh Xil basin comprise three main age populations at 230–290 Ma, 430–470 Ma, and 1750–2000 Ma (Fig. 7A). Strata of Hoh Xil basin have similar age populations at 210–300 Ma, 390–475 Ma, and 1600–2100 Ma in the late Cretaceous, and at 220–310 Ma, 400–500 Ma, and 1800–2050 Ma in the early Miocene (Fig. 7A). In Qaidam basin, Cenozoic strata have the following age populations: 210–290 Ma and 370–480 Ma in the early Eocene, 220–280 Ma and 350–500 Ma in the Oligocene, 255–290 Ma and 395–510 Ma in the Miocene, and 225–290 Ma and 375–480 Ma in the Pliocene. In addition to these general age characteristics, minor age populations, particularly those in the Proterozoic, are useful for determining provenance. Apatite fission-track thermochronology results from the Eastern Kunlun Range suggest that rapid cooling did not start across the interior of the range until ~30–20 Ma, and that an early cooling event may have been locally experienced along its northern margin at ~45 Ma, a result consistent with the knowledge of the region (e.g., Jiang et al., 2008b; Clark et al., 2010; Duvall et al., 2013; Liu et al., 2017b). Zircon fission-track thermochronology results from the range indicate that the region cooled below 240 °C between the early Jurassic and early Cretaceous, consistent with previous studies suggesting regionally-widespread Mesozoic cooling (e.g., Mock et al., 1999; Chen et al., 2003; Yuan et al., 2006; Dai et al., 2013; Wang et al., 2016, 2017d, 2018b). Below, we use our new data to address the question of how Hoh Xil basin, Qaidam basin, and the Eastern Kunlun Range have interacted with one another tectonically during development of the Tibetan plateau.

Table 1
Apatite and zircon fission-track analyses.

Sample	Lithology	Latitude (°N)	Longitude (°E)	Elevation (m)	Analysis	Grains	ρ_d (cm ⁻²)	N_d	ρ_s (cm ⁻²)	N_s	ρ_i (cm ⁻²)	N_i	U (ppm)	P (χ^2) (%)	Fission-track age ($\pm 1\sigma$ Ma)	Mean track length ($\pm 1\sigma$ μ m)	Std. dev. (μ m)
S-21	Granite	36.327	95.306	2950	AFT	17	1.044E + 06	2610	5.068E + 05	821	1.756E + 06	2844	20.7	98	52.9 \pm 3.4	14.04 \pm 0.13	1.27
					ZFT	21	2.786E + 05	696	1.332E + 07	5569	5.797E + 06	2423	255.9	0	112.1 \pm 6.8		
S-22	Biotite granite	36.173	94.774	3091	AFT	5	1.040E + 06	2599	7.030E + 04	26	1.078E + 06	399	12.8	87.6	11.9 \pm 2.5	14.20 \pm 0.19	1.01
					ZFT	30	2.778E + 05	694	1.526E + 06	9157	4.200E + 05	5219	185.9	0	176.2 \pm 11.4		
S-23	Granodiorite	36.136	94.266	3647	ZFT	30	2.770E + 05	693	1.527E + 06	9162	4.200E + 05	2521	186.6	0	175.6 \pm 11.2		
S-24	Biotite granite	36.194	94.252	3327	AFT	17	1.031E + 06	2578	8.440E + 04	151	1.088E + 06	1947	13	59.6	14.1 \pm 1.4	14.09 \pm 0.14	1.24
					ZFT	30	2.762E + 05	691	1.358E + 06	8149	3.470E + 05	2084	154.7	0	188.3 \pm 10.1		
S-25	Biotite granite	36.218	94.215	3245	AFT	16	1.027E + 06	2568	1.333E + 05	136	1.476E + 06	1506	17.7	99.8	16.3 \pm 1.7	13.84 \pm 0.17	1.35
					ZFT	11	2.755E + 05	689	1.449E + 06	3187	5.070E + 05	1116	226.5	0	139.3 \pm 10.4		
S-26	Mylonitic granite	35.739	94.26	4236	AFT	33	1.023E + 06	2557	4.500E + 03	13	8.910E + 05	2559	10.8	78.1	0.9 \pm 0.3	14.88 \pm 0.31	1.22
					ZFT	30	2.747E + 05	687	1.074E + 06	6441	5.410E + 05	3245	242.2	0	95.6 \pm 5.8		
S-72	Biotite granite	36.105	95.221	3837	ZFT	23	2.607E + 05	652	1.478E + 06	6797	4.580E + 05	2105	215.9	0	144.3 \pm 10.1		
S-73	Granodiorite	35.757	95.224	4088	AFT	11	1.037E + 06	2593	3.610E + 04	35	6.580E + 05	638	7.8	65.4	10.0 \pm 1.8	14.21 \pm 0.24	1.26
					ZFT	30	2.599E + 05	650	1.154E + 06	6925	4.980E + 05	2985	235.4	0	101.9 \pm 8.1		
S-74	Biotite granite	35.857	94.238	3796	AFT	24	1.037E + 06	2593	9.800E + 03	16	7.390E + 05	1204	8.8	15.2	2.4 \pm 0.6	14.33 \pm 0.31	1.42
S-75	Biotite granite	36.17	95.244	3477	AFT	8	1.037E + 06	2593	3.30E + 04	14	1.188E + 06	499	14.1	68.4	5.1 \pm 1.4	14.30 \pm 0.27	1.08
					ZFT	19	2.583E + 05	464	1.786E + 06	6785	5.050E + 05	1920	241	0	156.9 \pm 10.4		
S-76	Granite	36.006	94.431	4117	AFT	24	1.037E + 06	2593	2.030E + 04	24	1.002E + 06	1182	11.9	29.2	3.7 \pm 0.8	14.06 \pm 0.26	1.43
					ZFT	30	2.579E + 05	644	1.720E + 06	10,319	7.290E + 05	4374	347.7	0	106.5 \pm 5.4		

ρ_d = standard track density.

N_d = total number of fission tracks in standard.

ρ_s = spontaneous track density.

N_s = total number of spontaneous fission tracks.

ρ_i = induced track density.

N_i = total number of induced fission tracks.

P (χ^2) = chi-square test probability that all single-crystal ages represent a single population (> 5% passes; < 5% fails).

Fission-track age = pooled age for samples that pass χ^2 test; central age for samples that fail χ^2 test.

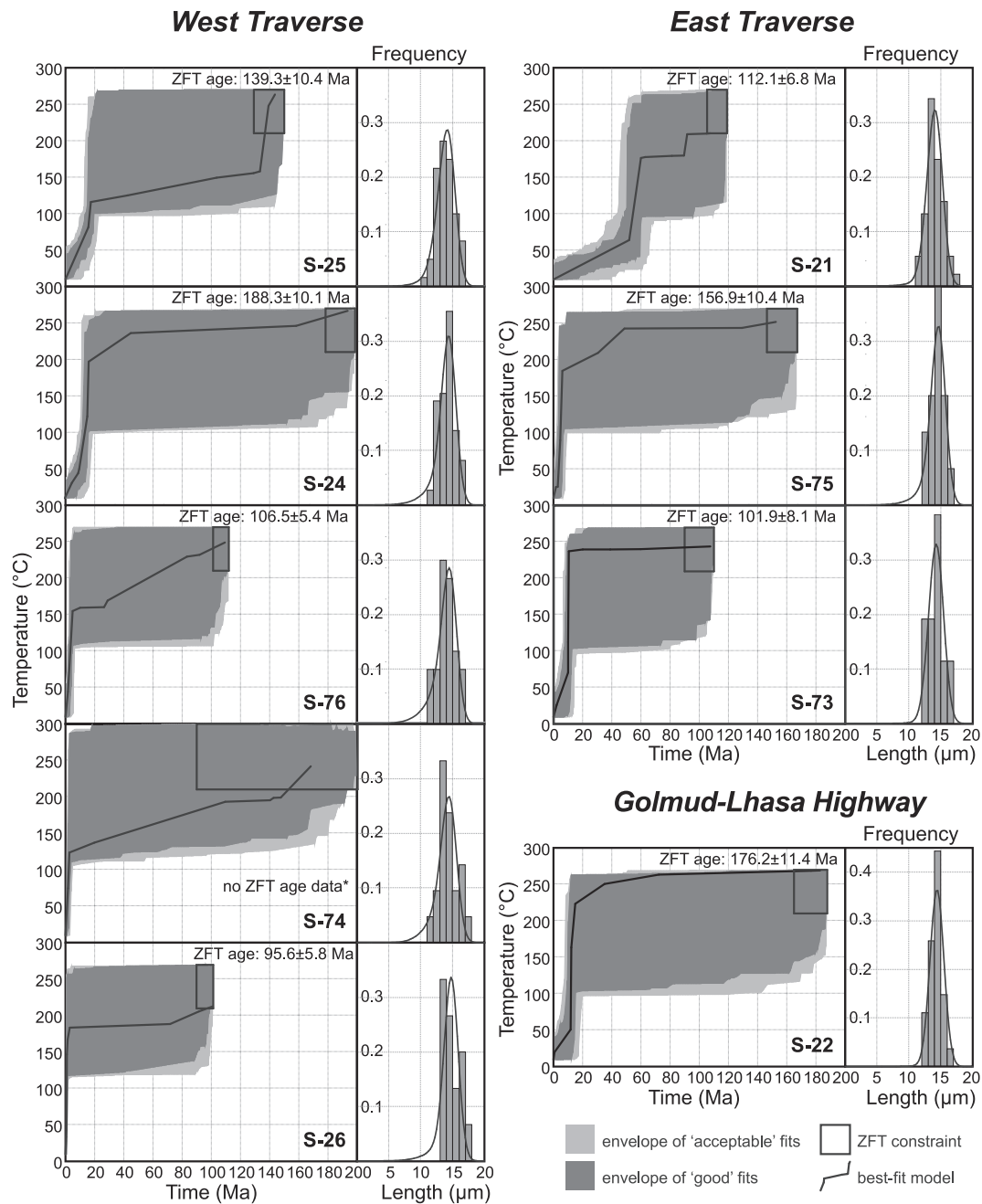


Fig. 9. Cooling histories for samples collected for fission-track dating produced using the HeFTy thermal modeling program (Ketcham, 2005). Low-temperature histories are derived from inverse modeling of AFT results, constrained by ZFT results when available. Dark and light gray areas represent “good” and “acceptable” fit envelopes. Black lines represent the best-fit model for each sample, and the corresponding modeled track length distributions are shown with histograms of the observed track lengths. See text for additional details about modeling parameters.

7.1. Provenance analysis

To facilitate our discussion on the provenances of our sandstone samples from central Tibet, we compiled published U-Pb zircon ages dating magmatic crystallization and detrital grains from the major terranes of central and northern Tibet (Figs. 7B–G). See the Supplementary Information for the complete list of references.

7.1.1. Jurassic strata

For the sample from middle-late Jurassic Yanshiping Group in the northern Qiangtang terrane (sample 1), the two prominent Phanerozoic populations with peaks at ~275 Ma and ~445 Ma correspond to the bimodal age distribution characteristic of the Kunlun batholith (Fig. 7A

and B). Similar Kunlun ages have also been noted in Yanshiping Group sandstones over 300 km to the west of our sample location (Ding et al., 2013). Southward paleocurrent indicators in Yanshiping Group strata (Leeder et al., 1988) are consistent with the Kunlun terrane acting as a source for these sediments.

Some of the Jurassic samples examined by Ding et al. (2013) also contain Paleoproterozoic zircons with ages of ~1800–2050 Ma and ~2450–2550 Ma, consistent with the results from our sample. Possible sources for these age populations are the Triassic strata of the Songpan-Ganzi terrane to the north (Fig. 7E) and Paleozoic strata exposed primarily in the central Qiangtang terrane to the south (Fig. 7F). We suggest that recycling of Songpan-Ganzi strata was a contributing process, as drainage systems transporting detritus from the Kunlun

terrane to Qiangtang would necessarily cross these units. A significant population of Songpan-Ganzi detrital zircons have ages between 500 Ma and 1000 Ma (Fig. 7E), which are largely absent from sample 1 (Fig. 7A). Detailed provenance studies of the Songpan-Ganzi turbidite sequences have suggested that subbasins within the terrane received detritus from surrounding source regions in varying proportions (e.g., Weislogel, 2008; Ding et al., 2013), thus the compilation of ages from across the entire Songpan-Ganzi terrane shown in Fig. 7E obscures the provenance variability exhibited by different regions within the terrane. Several source regions have been identified for the Songpan-Ganzi deposits: the Permian-Triassic Eastern Kunlun arc to the north, the Qinling orogenic belt and the North China block to the northeast, and the South China craton to the east (Weislogel, 2008). The North China block is the primary source of the Paleoproterozoic zircons (Weislogel et al., 2006) and mainly provided sediment to the northeastern Songpan-Ganzi subbasin (Weislogel, 2008). The South China craton is most responsible for the 500–1000 Ma detrital zircon ages (Weislogel et al., 2006), but the region only contributed detritus to the eastern portion of the flysch basin (Weislogel, 2008). Therefore, it is likely that the Jurassic sediments in the northern Qiangtang terrane were derived mostly from recycling of strata in the northwestern and northeastern portions of the Songpan-Ganzi terrane. These recycled zircons may have been transported as far south as the southern margin of the Qiangtang terrane as indicated by detrital zircon results for mid-Mesozoic sediments along the Bangong-Nujiang suture zone which have an age distribution strikingly similar to the Triassic flysch of the Songpan-Ganzi terrane (Leier et al., 2007; Li et al., 2017b; Fig. 7E and G).

In addition to the dominantly Proterozoic ages discussed above, the Triassic Songpan-Ganzi deposits also contain prominent Kunlun age peaks at ~260 Ma and ~440 Ma (Fig. 7E). Thus, the Kunlun batholith signature in sample 1 may potentially be explained simply by sourcing from Songpan-Ganzi strata alone. However, we suggest that the prominent Kunlun signature in Jurassic sandstones in northern Qiangtang is at least partly the result of erosion of the Kunlun arc and distant transport of detrital material to the south made possible by Jurassic unroofing of the Eastern Kunlun region. Such a hypothesis is similar to that proposed for other regions in northern Tibet adjacent to the Altyn Tagh fault (Ritts and Biffi, 2000, 2001; Sobel et al., 2001; Delville et al., 2001; Chen et al., 2003; Gehrels et al., 2003b), and may correspond to an early phase of a late Mesozoic cooling event in the Eastern Kunlun Range (e.g., Mock et al., 1999; Wang et al., 2018b). This model is also consistent with the generally mature nature of the Yanshiping Group sediments and their “craton interior” provenance (Leeder et al., 1988; this study). Detrital zircons with Permian-Triassic ages matching the younger Kunlun arc event are also prominent in Jurassic strata along the Altyn Tagh fault (Cheng et al., 2015), in northern Qaidam basin (Yu et al., 2017a), and within the Qilian terrane (Gehrels et al., 2011), further suggesting the Kunlun terrane was a source of sediment across broad portions of central and northern Tibet during this time.

Sample 1 also contains Jurassic ages between 155 Ma and 175 Ma and a relatively restricted population of Grenville ages between 970 Ma and 1220 Ma (Fig. 7A). These ages do not clearly match crystallization ages or prominent detrital zircon age populations reported from any potential source regions north of the Qiangtang terrane, though the older age group partially overlaps dominantly Neoproterozoic ages documented in the Kunlun, Altyn Tagh, and Qilian terranes (Fig. 7B–D). However, both Jurassic and Grenville ages are present in the Qiangtang terrane itself (Fig. 7F). Jurassic zircons are most likely derived from Mesozoic intrusions in southern Qiangtang associated with north-dipping subduction of oceanic crust prior to the collision of the Lhasa and Qiangtang terranes (e.g., Guynn et al., 2006; Pullen et al., 2011; Li et al., 2014; Liu et al., 2017a). Potential local or southern derivation of material is also suggested by the cluster of Grenville-age zircons, which are common in Paleozoic strata of the Tethyan Himalayan sequence (THS) exposed in the Himalaya (DeCelles et al., 2004). While these THS rocks were separated from the Qiangtang terrane by the Neo-Tethys

Ocean and the Lhasa terrane in the Jurassic and therefore cannot be considered as a direct source of detrital material, Paleozoic paleogeographic reconstructions suggest that the shallow marine environment in which the Tethyan Himalayan sequence was deposited extended across the Lhasa and Qiangtang terranes (Dewey et al., 1988; Leeder et al., 1988; Şengör and Natal'in, 1996). Detrital zircon studies of Paleozoic units in the Qiangtang terrane indicate that Grenville-age zircons are common in these rocks (Fig. 7F). Thus, recycling of marine Paleozoic units from the Lhasa and Qiangtang terranes may also have been a potential source of detritus to Jurassic depositional zones in the northern Qiangtang region. Local derivation has been suggested for lower-middle Jurassic sandstones in the northern Qiangtang terrane (Wang et al., 2017c).

7.1.2. Hoh Xil basin

The analyzed late Cretaceous sandstone of the Fenghuoshan Group (sample 2) exhibits two significant populations of 210–300 Ma and 390–475 Ma (Fig. 7A) corresponding to the characteristic ages of the Kunlun batholith (Fig. 7B). A third major age population spans the range 1600–2100 Ma (Fig. 7A). The presence of these Proterozoic zircons indicates that the Kunlun cannot be the sole source of sediment to Hoh Xil basin in the late Cretaceous. Similar to the results for sample 1, the three major age groups are consistent with significant contribution of detrital material from the Songpan-Ganzi strata upon which the Hoh Xil basin strata are superposed. However, this age distribution is also consistent with recycling of detritus from the thick Jurassic strata of the Qiangtang terrane to the south, as the results from sample 1 demonstrate, although Grenville-age zircons are rarer in sample 2 (Fig. 7A). A Qiangtang source is consistent with the dominantly northward paleocurrent directions obtained for strata of the Fenghuoshan and Yaxicuo Groups (Leeder et al., 1988; Liu and Wang, 2001; Wang et al., 2002, 2008a; Cyr et al., 2005; Liu et al., 2005a; Yi et al., 2008; Li et al., 2012). Petrologic analyses of Fenghuoshan and Yaxicuo sandstones point to a recycled-orogen provenance for the detrital material and a sedimentary lithology for the eroded source (Wang et al., 2002; this study). This is consistent with the interpretation of the southern Hoh Xil basin as a foreland basin controlled by the north-directed Tanggula thrust system (Li et al., 2012, 2018a). Field mapping indicates that this thrust system extensively deformed the Jurassic rocks along the northern margin of the Tanggula Range, making them a likely source for Hoh Xil basin strata (Li et al., 2012). Our results are generally consistent with other detrital zircon ages for the Fenghuoshan Group in the eastern Hoh Xil basin (Dai et al., 2012), except our sample has relatively few zircon ages from 500 to 1000 Ma which are most likely to have been derived from Paleozoic Qiangtang strata based on the northward paleocurrent direction. Zircons of these ages are variably present in Fenghuoshan Group and Yaxicuo Group strata across both the eastern and western parts of the Hoh Xil basin (Dai et al., 2012; Li et al., 2018a). In general, late Cretaceous-Eocene Hoh Xil basin strata with prominent Kunlun age peaks largely lack 500–1000 Ma zircons and vice versa (Dai et al., 2012; Li et al., 2018a; this study), suggesting that the relative contributions from recycled Paleozoic and Jurassic sedimentary sources to Hoh Xil basin varied spatially and temporally.

The two Miocene sandstones from the Wudaoliang Group (samples 3 and 4) exhibit age distributions similar to that for the Fenghuoshan Group (sample 2), with peaks at ~250 Ma, ~450 Ma, and ~1900 Ma, and minor populations at ~2500 Ma (Fig. 7A). The two youngest peaks again correspond to the characteristic ages of the Kunlun batholith; however, as with sample 2, exclusive sourcing from the Kunlun terrane cannot account for the Paleoproterozoic zircons in these samples. The overall distributions for both samples are consistent with derivation from recycled Triassic Songpan-Ganzi, Jurassic Qiangtang, or early Cenozoic Fenghuoshan Group strata, or a combination thereof. Both Miocene samples exhibit a significant number of detrital zircons with 500–1000 Ma ages (Fig. 7A). Potential sources for these zircons include the Songpan-Ganzi and central Qiangtang regions discussed previously.

However, we also recognize the late Cretaceous-Eocene Fenghuoshan and Yaxicuo Groups as possible sources of recycled zircons as a result of uplift associated with the Fenghuoshan thrusts in the Eocene-Oligocene (Staisch et al., 2016). In the southern Hoh Xil basin, limited paleocurrent data indicate southward flow for the coarse basal unit of the Wudaoliang Group (Liu et al., 2005a), further supporting the interpretation that partial late Paleogene inversion of the Hoh Xil basin in the Fenghuoshan region led to intrabasinal recycling of detrital zircons. In the northern Hoh Xil basin, isopach data for the Wudaoliang Group show pronounced thickening of the Miocene strata near the northern basin margin adjacent to the Eastern Kunlun Range (Zhu et al., 2006b). This pattern suggests that tectonic loading due to uplift of the range may have contributed to basin subsidence, and that the northern Hoh Xil basin likely received sediment from both the Fenghuoshan and Eastern Kunlun in the Miocene.

7.1.3. Qaidam basin

Samples 5–8 from the Xiaganchaigou, Shanganchaigou, Shanggou, and Shizigou Formations, respectively, have two prominent peaks corresponding to the characteristic Ordovician-early Devonian and late Carboniferous-Triassic magmatic phases of the Eastern Kunlun Range (Fig. 7A). However, sample 5 from the middle-late Eocene Xiaganchaigou Formation is clearly distinguished from the younger samples by a notable population of Archean-Proterozoic ages (48% of all zircon ages) defining a broad spread of ages from 550 to 1600 Ma and two groups with peaks at ~1870 Ma and ~2500 Ma (Fig. 7A) that are not common in the Eastern Kunlun Range (Fig. 7B). The age spectrum of sample 5 is similar to those of the Hoh Xil basin strata discussed above (samples 2–4) (Fig. 7A), which we interpret to result from recycling of material originally sourced from the Songpan-Ganzi and central and southern Qiangtang terranes. Sample 5 also gives a single zircon age of 42 ± 1 Ma. While a single grain is not a robust indicator of provenance, it is noteworthy that potential sources for zircons of this age are all located to the south of the Eastern Kunlun Range. These sources include scattered Cenozoic volcanics and small intrusions identified in central Tibet (e.g., Chung et al., 1998; Roger et al., 2000; Wang et al., 2001, 2008b; Ding et al., 2003; Spurlin et al., 2005; Yang et al., 2014; Ou et al., 2017; Chen et al., 2018a) and widely-exposed Paleogene igneous rocks in the Lhasa terrane (e.g., Harrison et al., 2000; Chung et al., 2003; Kapp et al., 2005b). Thus, the presence of this Eocene zircon in sample 5 may result from northward fluvial transport from south of the Kunlun terrane, but could also have been transported as wind-blown ash derived from these volcanic centers (cf. Cheng et al., 2016b).

Our interpretation of a southern source for sample 5 is further supported by rare trough cross-stratification observed in the sampled outcrop (Fig. 4F) giving a mean paleocurrent direction of 358° . Existing paleocurrent data for Paleogene Qaidam strata in the western part of the basin are reported from the northwestern margin of the basin adjacent to the Altyn Tagh fault and indicate a change from generally northward flow in the lower Xiaganchaigou Formation to southward flow in the upper Xiaganchaigou and Shanganchaigou Formations (Meng and Fang, 2008; Wu et al., 2012). The evolution of Cenozoic depositional systems along the northwestern margin of Qaidam is generally interpreted to be controlled by slip along the Altyn Tagh Fault (e.g., Yin et al., 2002), and the change in paleocurrent direction has been linked with an increase in sediment sourcing from the Altyn Tagh Range (e.g., Cheng et al., 2016b). Isopach data for Qaidam basin reveal a major Eocene depocenter in western Qaidam basin (Yin et al., 2008b). We therefore infer that generally northward paleoflow likely prevailed at the sample 5 location throughout the Eocene.

The Oligocene-Pliocene sandstones collected from western Qaidam basin (samples 6–8) all exhibit similar detrital zircon age distributions that are clearly distinct from that of sample 5 (Fig. 7A). All three samples are characterized by two prominent age peaks corresponding to intrusive rocks exposed in the Eastern Kunlun Range, while

populations of zircons with peaks at ~1850 Ma and ~2500 Ma, as identified in the other analyzed samples from central and northern Tibet, are not present. The absence of these ages precludes consideration of Songpan-Ganzi, Qiangtang, or Hoh Xil strata as direct or recycled sources for the Oligocene-Pliocene sediments. Rather, the age distributions strongly support the Eastern Kunlun Range as a major source of detritus to the western Qaidam basin over this time period. Close inspection of the relative significance of the early Paleozoic and late Paleozoic-early Mesozoic age populations in these samples reveals that sediment derivation was not uniform. For example, the proportion of all zircon ages < 500 Ma corresponding to the early Paleozoic age population increased from ~60% to ~80% from the late Oligocene (sample 6) to the Miocene (sample 7), while the proportion of all zircons with Archean-Proterozoic ages also increased from ~15% to ~20%. These shifts likely reflect increased contribution of detrital material from the Altyn Tagh (Fig. 7C), possibly as a result of continued left-lateral slip on the Altyn Tagh fault (e.g., Yin et al., 2002; Cheng et al., 2016b). The Qilian Shan contains a similar distribution of zircon ages (Fig. 7D) but is not considered a likely detrital source for our Qaidam samples as depocenters were located between the Qilian Shan and our sample locations from the late Eocene through Pliocene (Yin et al., 2008b).

Rieser et al. (2005) showed that Qaidam basin sandstones are generally immature with quartz contents that decrease from older to younger strata, suggesting that less recycled sedimentary material contributed to new sediments as the basin evolved. The results of our petrologic study indicate a similar trend, with a significant shift to lower quartz content from the middle-late Eocene (sample 5) to the late Oligocene (sample 6) (Fig. 5). The compositional trajectory displayed by Qaidam basin sandstones is consistent with our detrital zircon results indicating younger Qaidam sediments were isolated from sedimentary sources that were important through much of the Paleogene. These sources were replaced by uplifting and/or advancing deformation belts that define the modern northwestern and southern topographic boundaries of Qaidam basin (e.g., Yin et al., 2002, 2008b). Thus, the character of Qaidam basin sediments changed in concert with the evolution of the basin margins, with exposure of Archean and Proterozoic basement rocks in Altyn Tagh Range uplifts and unroofing of voluminous igneous rocks in the Eastern Kunlun Range driving compositions towards a more mixed provenance (Fig. 5).

An alternative interpretation of the detrital zircon age distribution in sample 5 is that it also represents mixing of Eastern Kunlun and Altyn Tagh sources, with the ~2500 Ma population explained by recycling of Proterozoic and Paleozoic (meta)sedimentary units of the Kunlun basement and the ~1870 Ma population derived from Proterozoic metasedimentary rocks in the Altyn Tagh (Fig. 7B and C). However, there are several problematic aspects to this interpretation:

- (1) During deposition of the Xiaganchaigou Formation, a major depocenter was present in western Qaidam basin north and west of the location of sample 5 (Yin et al., 2008b) which would have prevented significant sediment transport from the Altyn Tagh to distal regions. Additionally, detrital zircon age distributions for samples of the Xiaganchaigou Formation collected at other localities north and west of sample 5 typically exhibit prominent peaks corresponding to the Permian-Triassic ages of the Kunlun terrane (Cheng et al., 2016a; Zhu et al., 2017; Zhou et al., 2018), indicating that sediment was transported from generally south to north across the southern Qaidam margin (either directly from the Eastern Kunlun or recycled from Hoh Xil basin).
- (2) Age distributions in Neogene samples collected near the Altyn Tagh fault (samples 6–8) and from within the Eastern Kunlun Range (sample 9), each of which must have been sourced at least in part from the Kunlun terrane to account for their Permian-Triassic zircon populations, do not include ca. 2500 Ma ages (Fig. 7A). This is consistent with a general lack of these ages in Neogene strata at

Table 2
Two-sample Kolmogorov-Smirnov (K-S) test results.

	P-value	Qiangtang				Hoh Xil Basin				Qaidam Basin				Eastern Kunlun
		Late Cretaceous	Miocene	Miocene	Miocene	Late Eocene	Oligocene	Late Miocene	Pliocene	Inf. Miocene				
D-value		Sample 1	Sample 2	Sample 3	Sample 4	Sample 5	Sample 6	Sample 7	Sample 8	Sample 9				
Qiangtang	Jurassic	Sample 1	–	0.000	0.113	0.008	0.000	0.000	0.000	0.000	0.000			
Hoh Xil Basin	Late Cretaceous	Sample 2	0.301	–	0.004	0.080	0.341	0.002	0.002	0.035	0.049			
	Miocene	Sample 3	0.168	0.243	–	0.596	0.037	0.000	0.000	0.000	0.000			
	Miocene	Sample 4	0.236	0.178	0.107	–	0.497	0.000	0.000	0.000	0.003			
Qaidam Basin	Late Eocene	Sample 5	0.333	0.131	0.195	0.116	–	0.000	0.000	0.001	0.015			
	Oligocene	Sample 6	0.516	0.269	0.477	0.416	0.372	–	0.000	0.031	0.053			
	Late Miocene	Sample 7	0.515	0.272	0.397	0.330	0.296	0.450	–	0.003	0.001			
	Pliocene	Sample 8	0.446	0.202	0.402	0.305	0.269	0.208	0.263	–	0.097			
Eastern Kunlun	inf. Miocene	Sample 9	0.442	0.191	0.332	0.255	0.218	0.192	0.285	0.176	–			

least partly derived from the Kunlun terrane collected elsewhere in western Qaidam basin (Cheng et al., 2016a, 2016b; Zhu et al., 2017; Zhou et al., 2018). This age population is also absent from Paleogene samples with an Eastern Kunlun provenance collected near the Altyn Tagh fault (Cheng et al., 2016b; Zhu et al., 2017), and from modern river sand samples collected from the western part of the Eastern Kunlun Range (Li et al., 2013a, 2013b).

- (3) The age distributions in Neogene samples collected near the Altyn Tagh fault (samples 6–8), which are interpreted to have a mixed Kunlun-Altyn Tagh provenance (also see Cheng et al., 2016b; Zhu et al., 2017), only include rare ca. 1870 Ma ages that this alternative interpretation suggests should be a notable component of Altyn Tagh detritus. Moreover, this age population is largely absent from all Qaidam strata interpreted to have a proximal Altyn Tagh provenance (Cheng et al., 2016a, 2016b; Zhu et al., 2017). The absence of this age population in Altyn Tagh-sourced sediments despite the prominent late Paleoproterozoic peak in Altyn Tagh detrital zircons (Fig. 7C) may be explained by the fact that most of the ~1800–2000 Ma detrital zircon ages were obtained from the Annanba sequence (Gehrels et al., 2003b; Zhang et al., 2011) which is presently only exposed at the far northeastern end of the Altyn Tagh Range and may not have been available as a potential sediment source.
- (4) Ages corresponding to the ca. 1870 Ma and ca. 2500 populations are present in proportions comparable to sample 5 in several samples of the Xiaganchaigou Formation collected from locations away from the Altyn Tagh fault (Cheng et al., 2016a; Zhou et al., 2018). These ages typically only occur in tandem, suggesting that their presence is not a product of source mixing. It could be argued that the presence of these Proterozoic ages in Paleogene strata and their absence from Neogene strata reflects a progressive decrease of detrital contribution from (meta)sedimentary units during Paleogene uplift of the Eastern Kunlun Range rather than a fundamental change in provenance. The shift away from a recycled sedimentary source suggested by petrologic analyses (e.g., Rieser et al., 2005; this study) is consistent with both interpretations and cannot be used to distinguish these models. However, the widespread occurrence of Kunlun-age detrital zircons in Jurassic strata across central and northern Tibet (e.g., Gehrels et al., 2003b; Ding et al., 2013; Cheng et al., 2016b; Yu et al., 2017a; this study) suggests that unroofing of the Kunlun batholith was likely largely accomplished before the Cenozoic.

We therefore prefer the interpretation that sample 5 was recycled from sedimentary sources south of the Eastern Kunlun Range prior to complete hydrologic separation of the Paleogene Qaidam and Hoh Xil basins.

7.1.4. Eastern Kunlun Intermontane basin

The inferred Miocene-age intermontane basin sandstone (sample 9) displays Kunlun detrital zircon age peaks at ~245 Ma and ~430 Ma (Fig. 7A). This is consistent with sedimentological observations indicating that the Neogene strata are generally immature and likely derived from sources within the range proximal to the basin. A smaller peak consists of ages of 900–1090 Ma (Fig. 7A). In the Eastern Kunlun, ages in this range are known from high-grade metamorphic rocks and granitic gneisses corresponding to a Neoproterozoic tectono-thermal event (He et al., 2016a, 2016b), and as inherited/xenocrystic components of Paleozoic and Mesozoic igneous rocks (e.g., Wu et al., 2016; Shao et al., 2017) (Fig. 7B). Exclusive derivation of detritus from proximal Kunlun sources in sample 9 implies that uplift of the central portion of the Eastern Kunlun initiated no later than the early Miocene.

7.2. Kolmogorov-Smirnov (K-S) test

To examine the relationships between the detrital zircon populations in our samples further, we employed the Kolmogorov-Smirnov (K-S) two-sample test to statistically evaluate the similarity between detrital zircon age populations in each pair of samples we analyzed. The K-S test compares the cumulative distribution functions of detrital zircon ages for two samples by measuring the maximum probability difference between them. If this observed difference (D) exceeds a critical value (D_{crit}) dependent on the number of dated zircons for each sample and the desired confidence level of the test results, then the null hypothesis that the sample distributions are drawn from the same population is rejected. K-S test results include D for each analyzed pair and a P -value, where $1 - P$ represents the probability that the two samples are not drawn from the same population. Thus, a P -value > 0.05 indicates that the two compared age distributions are not likely to have been derived from different populations at the 95% confidence level. That is, a $P > 0.05$ for a pair of detrital zircon age distributions suggests that they were derived from similar sources.

The K-S test results (D and P values) for all pairs of samples 1–9 are shown in Table 2. The results indicate that eight of the 36 unique sample pairs exhibit similar age distributions. In Hoh Xil basin, the lower sample from the Miocene Wudaoliang Group (sample 3) is very similar ($P = 0.113$) to the Jurassic sandstone (sample 1) that is interpreted to be a source of sediment for Hoh Xil strata. Interestingly, sample 3 was collected from the northern part of Hoh Xil basin, supporting the interpretation that recycling of older basin strata via uplift in the Fenghuoshan-Nangqian thrust belt was an important process during the Miocene. This is further supported by the similarity identified between the other Wudaoliang sandstone (sample 4) and sample 2 from the late Cretaceous Fenghuoshan Group ($P = 0.080$). The two Wudaoliang sandstones (samples 3 and 4) are also similar ($P = 0.596$).

Sample 5, from the late Eocene Xiaganchaigou Formation in Qaidam basin, is similar to both sample 2 (Fenghuoshan Group) and sample 4

(Wudaoliang Group) with P -values of 0.341 and 0.497, respectively, but is not similar to any of the other Qaidam basin sandstones (samples 6–8). These results substantiate the conclusion that the sampled Xiaganchaigou sandstone was sourced from regions south of the Eastern Kunlun Range. None of the younger Qaidam basin samples have P -values indicative of being drawn from the same population, possibly resulting from one or more of the following: (1) temporal variations of source region, (2) temporal variations in the proportion of sediments derived from two or more source regions, or (3) spatial variation of ages within source regions over time. Sample 9 from the inferred Miocene-age intermontane basin sediments is similar to the late Oligocene and Pliocene Qaidam basin sandstones (samples 6 and 8, $P = 0.053$ and 0.097 , respectively).

7.3. Uplift history of the Eastern Kunlun Range

Existing thermochronologic data for the Eastern Kunlun Range include $^{40}\text{Ar}/^{39}\text{Ar}$, fission-track, and (U-Th)/He results from across the range (Fig. 8). Muscovite, biotite, and K-feldspar $^{40}\text{Ar}/^{39}\text{Ar}$ results reveal a range-wide Mesozoic cooling event (Wang et al., 2005c, 2016, 2017d) that was locally overprinted by a Cenozoic cooling event at ~30–20 Ma (Mock et al., 1999; Liu et al., 2005b). AFT and (U-Th)/He studies have resulted in a wide range of ages for rapid cooling ranging from ~40–0 Ma (Jolivet et al., 2001; Wang et al., 2004b, 2016, 2017d, 2018b; Liu et al., 2005b, 2017b; Yuan et al., 2003, 2006; Clark et al., 2010; Dai et al., 2013; Duvall et al., 2013). Our AFT results are broadly consistent with these results (Fig. 9) and suggest that Cenozoic uplift of the Eastern Kunlun Range was a delayed, far-field response to Indo-Asian collision. The mid-Mesozoic ZFT ages obtained from our study (Fig. 9) suggest that the zircon fission-track systematics were not reset by late Mesozoic or Cenozoic tectonism. That is, the samples that we collected were all situated above the 240 °C isotherm marking the closure temperature of zircon since at least the early Cretaceous. This implies that the total amount of erosion in the Cenozoic must be < 10 km assuming a geothermal gradient of 25 °C/km. Our AFT data together with existing thermochronological studies (Fig. 8) suggest that the range may have been uplifted in an asynchronous fashion. In this interpretation, Paleogene cooling ages correspond to the emergence of early, isolated basement exposures, and Neogene rapid cooling reflects continued development of the Eastern Kunlun Range into a continuous topographic feature. Sedimentation patterns and structural and growth strata relationships identified in seismic sections from Qaidam basin record basin-wide effects of the uplift of the Eastern Kunlun Range by 29–24 Ma (Yin et al., 2008b). Additionally, an analysis of anisotropy of magnetic susceptibility in late Eocene Xiaganchaigou and Miocene Xiayoushashan rocks indicates a Miocene onset of NE-SW strain in western and southwestern Qaidam basin (Yu et al., 2014), suggesting broad-scale deformation along the Eastern Kunlun margin of Qaidam basin at this time.

Heavy mineral analyses for western Qaidam basin strata have resulted in estimates for rapid uplift within the western part of the Eastern Kunlun Range beginning in the early Miocene (Zhu et al., 2017; Li et al., 2018b), generally consistent with timing suggested by the thermochronologic and seismic data. Zhu et al. (2017) suggest that this portion of the Eastern Kunlun may have persisted to some degree as a topographic high after Mesozoic exhumation. Li et al. (2018b) infer that Paleogene sediments were sourced from the vicinity of the western end of the Kunlun fault, which could have reasonably contributed sediment to extensive north-flowing drainage systems originating farther south. In contrast to the rapid Miocene uplift suggested by these studies, Zhou et al. (2018) used heavy mineral analysis and U-Pb detrital zircon geochronology to conclude that portions of the range initially uplifted in the middle Eocene. However, their Xiaganchaigou Formation samples with detrital zircon age distributions similar to our sample 5 from the same unit generally had the highest zircon-tourmaline-rutile (ZTR) index values of their study at 28.0–41.9% (Zhou et al., 2018),

suggesting relatively long sediment transport distances possibly consistent with a source located to the south of the Eastern Kunlun Range.

Kunlun-age zircons are common in Eocene-Pliocene strata across Qaidam basin and have been used to suggest that units in the Eastern Kunlun region were a direct source of sediment throughout the Cenozoic, either as a result of pre-Cenozoic exhumation (e.g., Cheng et al., 2016a; Zhu et al., 2017) or early Cenozoic uplift (e.g., Bush et al., 2016; Zhou et al., 2018). For strata in western Qaidam basin, we suggest that Kunlun-age zircons may also be explained by recycling of Jurassic and successor units in the Hoh Xil region as suggested by our samples from northern Qinagtang and Hoh Xil basin. Similarly, the occurrence of Kunlun-age zircons in Cenozoic strata in northern Qaidam basin may result from recycling of Jurassic sediments along the Altyn Tagh or Qilian margins of the basin (e.g., Cheng et al., 2015; Yu et al., 2017a).

Based on the combined thermochronologic, sedimentation pattern, structural, seismic, and heavy mineral analyses, we broadly estimate uplift of the Eastern Kunlun Range as a prominent, continuous topographic feature at ~30–20 Ma. However, our proposed late Oligocene-early Miocene timing for the onset of widespread uplift does not preclude the earlier presence of smaller-scale structures suggested by Eocene cooling ages. Our AFT sample S-21, collected from the north-eastern flank of the Eastern Kunlun Range, reveals rapid cooling at ~45 Ma, possibly associated with one of these early contractional structures. Such structures may have developed locally by reactivating older structures (e.g., Meyers et al., 1992; Bayona and Thomas, 2003) of the Permian-Triassic Kunlun suture. Such reactivation may have been promoted by stress localization in this region resulting from the development of a forebulge induced by loading of the lithosphere by the Qilian Shan-Nan Shan thrust belt in the north and the Tanggula and Fenghuoshan-Nangqian thrust belts in the south. Paleogene isopach data for Qaidam basin suggest that the range was a structural high relative to its depocenters, generally located along the present-day axis of the basin (Yin et al., 2008b), consistent with this interpretation. The apparent lack of Eocene strata within the range itself (Pan et al., 2004) also implies that the region was a structural high. Stress localization in the forebulge area may have persisted, leading to Neogene uplift of the continuous Eastern Kunlun Range through development of the Kunlun transpressional system, including the left-slip Kunlun fault and the branching thrust systems to the west (Qimen Tagh thrust belt) and east (Bayanhar thrust belt).

Although not the primary focus of the current study, our findings also have bearing on the Mesozoic deformational history of the Eastern Kunlun region. Our provenance interpretations for the Jurassic sandstone collected from the Yanshiping Group of the Qiangtang terrane (sample 1) require exhumation of the Kunlun batholith in the Jurassic. While previous models have argued for a unified Mesozoic Qaidam-Tarim basin in the foreland of a north-directed Kunlun thrust belt (e.g., Ritts and Biffi, 2000), the exposure of the Kunlun batholith to erosion may have also been accomplished by crustal extension. This interpretation is consistent with several studies that have documented middle to late Mesozoic extension in the central and northern Tibetan plateau and adjacent areas (Huo and Tan, 1995; Huang et al., 1996; Sobel, 1999; Vincent and Allen, 1999; Kapp et al., 2000, 2003; Xia et al., 2001; Chen et al., 2003; Horton et al., 2004; Yin et al., 2008b). Our tentative identification of a major normal fault in the Qiangtang terrane juxtaposing Triassic and Cretaceous(?) strata (Fig. 4B) may extend the duration of this widespread extensional event later into the Mesozoic and nearer to the onset of continental collision between India and Asia.

8. Tectonic reconstruction

A comparison of Qaidam and Hoh Xil stratigraphy reveals important differences in their depositional histories (Fig. 2). Qaidam basin experienced essentially continuous non-marine sedimentation in

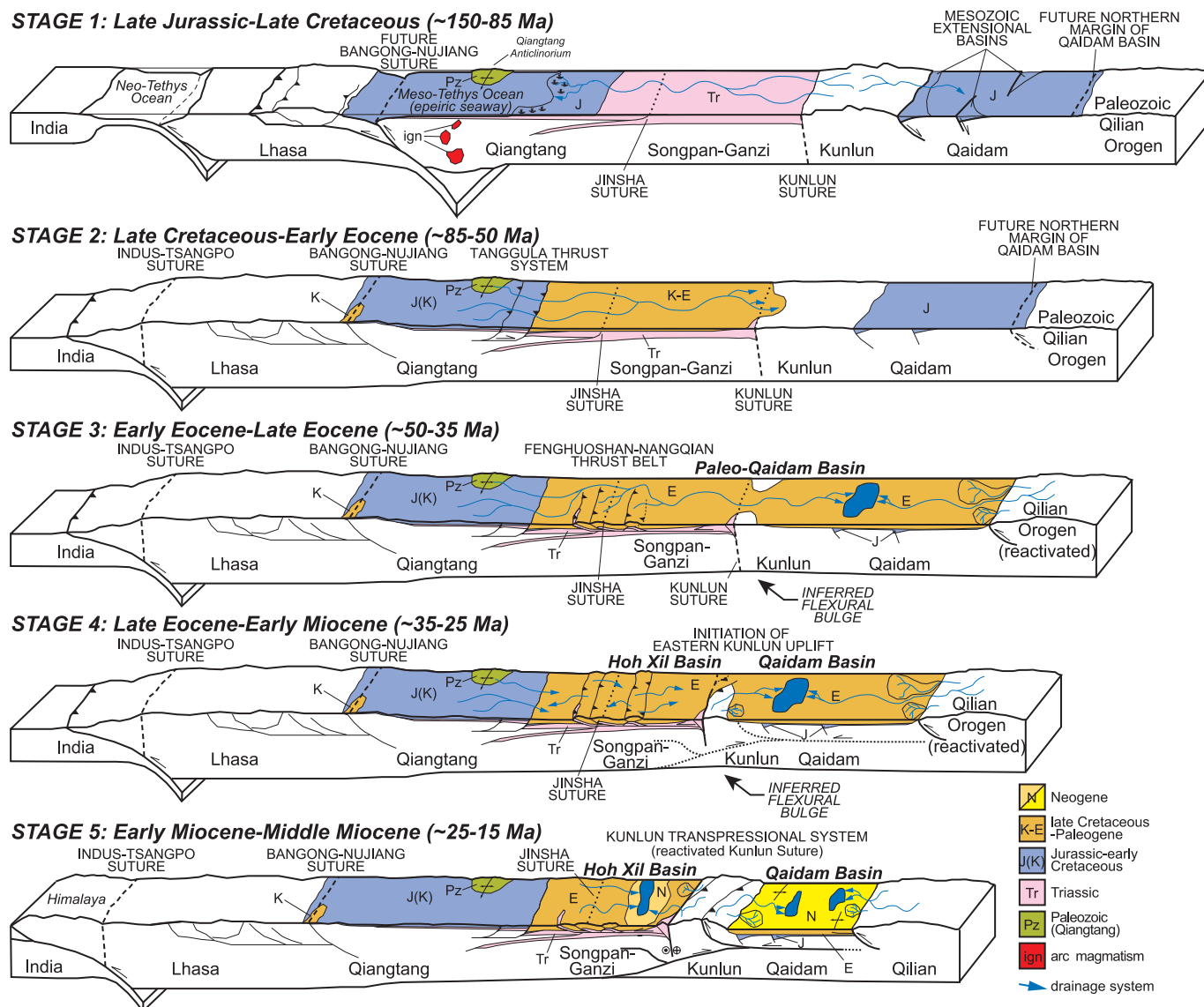


Fig. 10. Block diagrams showing proposed tectonic reconstruction of the central Tibetan plateau and evolution of Cenozoic basins. Stage 1: Unroofing in northern and north-central Tibet exposes the Kunlun batholith to erosion. Sedimentary material is transported to the south across the Songpan-Ganzi terrane and deposited in the Qiangtang terrane as the Jurassic Yanshiping Group. Stage 2: Initiation of tectonic activity in the Tanggula thrust system in the northern Qiangtang terrane. Uplift of the Tanggula range provides sediment source for initial deposition in the foreland Hoh Xil basin. Early Hoh Xil sediments reflect recycling of material from the Yanshiping Group and contribution from Paleozoic units in central Qiangtang. Stage 3: Waning tectonic activity in the Tanggula thrust system is replaced by initiation of uplift in the Fenghuoshan-Nangqian thrust belt within Hoh Xil basin, contemporaneous with reactivation of the Qilian Shan. These uplifting regions define the southern and northern boundaries of the Paleo-Qaidam basin, respectively. Tectonic loading in these belts results in the development of a flexural bulge within the basin near the Kunlun suture. Sediments derived from the Qiangtang terrane and from recycling of late Cretaceous-early Paleogene material within the Fenghuoshan-Nangqian thrust belt is transported northward and deposited across the Paleo-Qaidam basin, including within the southern Qaidam basin. Stage 4: Ongoing deformation in the Fenghuoshan-Nangqian thrust belt significantly alters drainage and depositional patterns in southern Paleo-Qaidam basin. Initiation of localized uplift in the Eastern Kunlun Range begins to partition the Paleo-Qaidam basin. Stage 5: Rapid uplift of the Eastern Kunlun Range completely separates the Hoh Xil and Qaidam basins, resulting in a large lake environment in Hoh Xil basin and continuous deposition in Qaidam basin with sediment derived from the bounding Eastern Kunlun, Altyn Tagh, and Qilian Shan regions.

dominantly fluvial and lacustrine environments from the Paleocene-early Eocene through the Holocene. This long uninterrupted history contrasts strikingly with the evolution of Hoh Xil basin, which experienced a distinct two-stage development (e.g., Wu et al., 2008; Staisch et al., 2014, 2016; Li et al., 2018a). From the late Cretaceous to early Oligocene, deposition in Hoh Xil basin was dominantly in non-marine fluvial and lacustrine environments, largely similar to those existing contemporaneously in Qaidam basin. However, the Oligocene was a time of widespread non-deposition in Hoh Xil basin, with a continuous Oligocene to Miocene section identified in only one marginal basin locality (Liu et al., 2005a; Wang et al., 2008a). Sedimentation resumed

in the Miocene, characterized by lacustrine carbonate and fine-grained clastic deposits. These Miocene strata, unconformably overlying deformed Paleogene strata, are only gently warped and appear to have been deposited on an extensive erosional surface (Wang et al., 2002; Wu et al., 2008).

The Oligocene depositional hiatus in Hoh Xil basin can be attributed to deformation and uplift of the late Cretaceous-Eocene basin sediments at this time (e.g., Liu and Wang, 2001; Wang et al., 2002; Staisch et al., 2016). Detailed investigation of the spatial distribution of the late Cretaceous-Eocene sequence in the central portion of Hoh Xil basin has shown that the thickness and extent of strata of the Fenghuoshan and

Yaxicuo Groups vary with age such that the locus of sedimentation shifted to the north and east from the late Cretaceous to late Eocene (Li et al., 2012). This shift has been interpreted to indicate that deformation in the northern Qiangtang terrane initiated in the late Cretaceous along the Tanggula thrust system before jumping north to the Fenghuoshan thrust belt in the early Eocene at ca. 48 Ma (Li et al., 2018a). Pre-Miocene northeast-southwest crustal shortening across central Tibet in the Fenghuoshan area has been estimated to be ~24–40% (Coward et al., 1988; Wang et al., 2002; Staisch et al., 2016). Similar ages and shortening estimates are inferred for thrusts located along strike in the western Hoh Xil basin (Li et al., 2018a). Farther east in the Yushu-Nangqian area, thrusting initiated at > 51 Ma and accommodated ~45% shortening (Horton et al., 2002; Spurlin et al., 2005). These results suggest that initiation of thrusting in the composite Fenghuoshan-Nangqian thrust belt may have been an early response to the collision of India with Asia, possibly driven by intra-plateau continental subduction (e.g., Spurlin et al., 2005).

The record of Cenozoic deformation in Qaidam basin is more complicated than that in Hoh Xil basin. Paleocene to early Eocene thrusting, approximately coeval with initiation of the Fenghuoshan-Nangqian thrust belt, has been documented along the northern margin of Qaidam basin in association with the southern Qilian Shan-Nan Shan thrust belt (Yin et al., 2002, 2008a, 2008b). Along with deformation at the western margin of Qaidam basin, this phase of crustal shortening has been linked to motion along the Altyn Tagh fault (Yin et al., 2002, 2008a). However, this early deformation does not appear to be widespread across Qaidam basin; rather, interpretation of subsurface data indicates that significant deformation both propagated eastward across the basin and initiated much later along its southern margin at 29–24 Ma (Yin et al., 2008a, 2008b). Initiation of widespread uplift of the Eastern Kunlun Range in the late Oligocene, becoming increasingly more rapid, is also broadly supported by low-temperature thermochronological results (e.g., Mock et al., 1999; Jolivet et al., 2001; Wang et al., 2004b; Liu et al., 2005b; Yuan et al., 2006; this study). The diachronous onset of deformation along the margins of Qaidam basin is further suggested by anisotropy of magnetic susceptibility of Qaidam sediments indicating that compressive strain in the Eocene was restricted to the northern margin of the basin, while in the Miocene compressive strain dominantly affected the southwestern part of the basin (Yu et al., 2014).

The stratigraphic, sedimentologic, and geochronologic data for Hoh Xil and Qaidam basins are useful in evaluating and distinguishing between the *independent* and *contiguous* models of basin development and developing a consistent tectonic reconstruction for northern and central Tibet since the Jurassic. Based on the data presented, we propose that the contiguous development model applies to the Cenozoic basins of the central and northern Tibetan plateau, and that Hoh Xil and Qaidam basins originally comprised a single, large *Paleo-Qaidam* basin. The proposed basin evolution and tectonic reconstruction is outlined below and shown in Fig. 10.

8.1. Stage 1 (late Jurassic–Late Cretaceous, ~150–85 Ma)

In the mid-Mesozoic, the Eastern Kunlun region experienced a phase of unroofing, potentially as part of widespread extension documented across central and northern Tibet in the Jurassic and Cretaceous, which resulted in exposure of the Kunlun batholith to erosion. Materials removed from the Kunlun batholith were transported southwards via large river systems incising into and flowing across the deformed flysch of the Songpan-Ganzi terrane and the northern Qiangtang terrane to a shallow marine environment on the northern epeiric margin of the actively-closing ocean basin between the Lhasa and Qiangtang terrane (e.g., Dewey et al., 1988; Murphy et al., 1997), consistent with paleocurrent data (Leeder et al., 1988). This sediment, the precursor of the Yanshiping Group, included detrital zircons with ages corresponding to both the Kunlun batholith and Songpan-Ganzi strata (Fig. 7A, B, and E).

We suggest this model, invoking unroofing of the Kunlun region in the mid-Mesozoic to supply Kunlun-age zircons rather than derivation from the Songpan-Ganzi terrane exclusively, because it additionally provides a possible explanation for abundant Permian-age zircons identified in a Jurassic conglomeratic sandstone from the Yumen area north of the Tibetan plateau (Gehrels et al., 2003b) that are otherwise more difficult to explain by sourcing from the Altyn Tagh-Qilian Shan region (see Fig. 7C and D). This inference is also consistent with detrital zircon ages documented for Jurassic strata in Qaidam basin, which exhibit clear Kunlun age peaks (Cheng et al., 2015, 2016b; Yu et al., 2017a). Additional material deposited in the Yanshiping Group sediments may have come from local (southern Qiangtang terrane) sources, accounting for the middle-late Jurassic and Grenville ages. Based on our tentatively identified Cretaceous unit and its normal-fault relationship with Triassic rocks, extension-driven erosion and deposition may have continued in the Qiangtang terrane until the onset of continental collision between India and Asia.

8.2. Stage 2 (Late Cretaceous–Early Eocene, ~85–50 Ma)

Uplift and deformation of the Jurassic strata in the Qiangtang terrane along the Tanggula thrust system (Li et al., 2012) led to erosion and mobilization of detrital material from the Yanshiping Group and related units. The elevated topography resulting from the Tanggula thrusts formed the southern margin of the Hoh Xil foreland basin, where sediment shed northward from the uplifted regions was deposited as the Fenghuoshan Group (Li et al., 2012, 2018a), consistent with paleocurrent indicators (Leeder et al., 1988; Wang et al., 2002; Cyr et al., 2005; Li et al., 2012) and an inferred sedimentary source (Wang et al., 2002). Continued deposition into the Paleocene contemporaneous with northward in-sequence development of thrusts and subsequent waning tectonic activity in the Tanggula thrust belt led to northward expansion of deposition in the Hoh Xil basin towards the Kunlun region.

8.3. Stage 3 (Early Eocene–Late Eocene, ~50–35 Ma)

Within the basin north of the Tanggula Range, the thin-skinned Fenghuoshan-Nangqian thrust belt initiated in the early to middle Eocene (Coward et al., 1988; Leeder et al., 1988; Horton et al., 2002; Spurlin et al., 2005; Staisch et al., 2016). Reactivation of the Qilian Shan-Nan Shan thrust belt along the northern margin of the Tibetan plateau also occurred at about this time (Yin et al., 2008a; Bush et al., 2016). The two thrust belts were separated by > 500 km and the intervening topographic low, the Paleo-Qaidam basin, became the locus of sedimentary deposition for much of the Paleogene. Detritus was recycled from Fenghuoshan Group strata in the inverted portion of Hoh Xil basin into Paleo-Qaidam basin, consistent with paleocurrent indicators (Wang et al., 2002). Additionally, fluvial transport systems were extensive enough to transport some material at least as far north as the present modern southern margin of Qaidam basin to be deposited as part of the Xiaganchaigou Formation, as suggested by a detrital zircon age distribution that indicates a major direct or recycled Songpan-Ganzi contribution and is derived from a statistically indistinguishable source as some Fenghuoshan and Yaxicuo Group strata (Table 2). Sedimentary material derived from the uplifting Qilian Shan-Nan Shan belt appears to have been restricted to the northern margin of Paleo-Qaidam basin (e.g., Bush et al., 2016). Syn-sedimentation deformation in the thin-skinned Fenghuoshan-Nangqian thrust belt evolved throughout the Eocene along and within the southern Paleo-Qaidam basin (Liu et al., 2001; Liu and Wang, 2001; Wang et al., 2002; Zhu et al., 2006b). The absence of Eocene sedimentary units in the Eastern Kunlun Range, located near the middle of the paleobasin, suggests that thrust loading associated with the two bounding and opposed fold-and-thrust belts may have resulted in the development of a flexural bulge across the center of Paleo-Qaidam basin with localized

structural highs possibly exposed in this zone.

8.4. Stage 4 (Late Eocene–Early Miocene, ~35–25 Ma)

Continuing deformation in the Fenghuoshan-Nangqian belt likely restricted *syn*-tectonic deposition in the southern Paleo-Qaidam basin to relatively localized basins (Liu et al., 2001; Zhu et al., 2006b). Compressive stresses resulting from the ongoing collision of India with Asia also continued to be transferred farther north across Paleo-Qaidam basin to the Qilian orogenic belt. As indicated by the low-temperature thermochronologic data discussed above, collisional stresses continued to induce strain localization within the inferred flexural forebulge across the center of the basin, reactivating the Permian-Triassic Kunlun suture resulting in uplift of the Eastern Kunlun on a regional scale. Progressive uplift of the range partitioned the Paleo-Qaidam basin, creating Hoh Xil basin to the south and Qaidam basin to the north. North-flowing fluvial transport systems in Hoh Xil basin were severely modified, the basin transitioned from a depositional to a dominantly erosional phase, and a widespread peneplanation surface was produced (Wang et al., 2002). Qaidam basin, now cut off from source regions south of the Eastern Kunlun Range, received sediment from the newly-uplifted range, as well as from the Qilian orogenic belt to the north and the Altyn Tagh Range to the west, topographic highs since the Paleocene and Oligocene, respectively (Yin et al., 2002, 2008b).

8.5. Stage 5 (Early Miocene–Middle Miocene, ~25–15 Ma)

After cessation of deformation in the Fenghuoshan-Nangqian thrust belt at ca. 27 Ma (Staisch et al., 2016), continued and increasingly rapid uplift of the Eastern Kunlun Range into the Miocene imparted a new tectonic load onto the northern margin of Hoh Xil basin, the majority of which had become internally-drained, hydrologically-isolated, and the site of establishment of several large lakes (Wu et al., 2008). Renewed sedimentation in Hoh Xil basin at this time was characterized by lacustrine carbonates of the Wudaoliang Group (Liu and Wang, 2001; Wu et al., 2008), which thicken towards the Eastern Kunlun Range (Liu et al., 2001; Zhu et al., 2006b). Miocene and younger sediments in Qaidam basin became dominated by material sourced from the Eastern Kunlun Range to the south, as suggested by the prevalence of Kunlun-age zircons in these units where examined away from the northern and northwestern basin margins (Fig. 7A–B; Cheng et al., 2016b; Zhou et al., 2018). This is consistent with petrographic results that indicate Qaidam sediments became less quartz-rich by the late Oligocene (Rieser et al., 2005; this study) (Fig. 5), suggesting that the basin had become isolated from recycled sedimentary sources that were important through much of the Paleogene (i.e., Triassic Songpan-Ganzi flysch and Jurassic Yanshiping Group strata recycled through Fenghuoshan Group strata). Western (Altyn Tagh Range) and northern (Qilian orogen) sources also contributed detritus to the basin, with their influence most apparent in sediments deposited adjacent to their respective margins (Bush et al., 2016; Cheng et al., 2016a; Wang et al., 2017b; Zhu et al., 2017). The diversion of the evolutionary histories of the Hoh Xil and Qaidam basins throughout the Neogene is also expressed by an increase in the surface elevation of Hoh Xil basin relative to Qaidam basin (e.g., Staisch et al., 2016; Li et al., 2018a) resulting from mantle melting-induced magmatic inflation (Chen et al., 2018a).

9. Conclusions

Our integrated study of the sedimentary basins of central and northern Tibet has led to the following conclusions and interpretations. Our sandstone petrology study indicates that sediments deposited in Hoh Xil basin were derived from a craton-interior provenance setting in the Eocene, but that Miocene strata were sourced from a recycled-orogen provenance setting. In contrast, the western Qaidam basin received sediments from recycled-orogen sources throughout the

Cenozoic. These results are consistent with existing sedimentologic studies suggesting that Hoh Xil basin experienced two distinct stages during its evolution: a Paleogene fluvial/alluvial stage and a Neogene lacustrine stage. We interpret this transition to be a tectonically controlled. The western Qaidam basin experienced a continuous development history during which sedimentary composition evolved in response to basin margin deformation.

The results of our U-Pb detrital zircon geochronology indicate that Jurassic strata in the basement of Hoh Xil basin exhibit two prominent age clusters at 230–290 Ma and 430–470 Ma. Cenozoic strata of Hoh Xil basin have similar age clusters at 210–300 Ma and 390–480 Ma for the Eocene strata, and at 220–310 Ma and 400–500 Ma for the early Miocene strata. When combined with our petrologic analysis and available paleocurrent data, these results suggest that Cenozoic sediments were recycled from the Jurassic rocks below that were themselves originally sourced from the Kunlun batholith. In Qaidam basin, Cenozoic strata have the following age clusters: 210–290 Ma and 370–480 Ma in the Eocene, 220–280 Ma and 350–500 Ma in the Oligocene, 250–290 Ma and 395–510 Ma in the Miocene, and 225–290 Ma and 375–480 Ma in the Pliocene. Proterozoic detrital zircon ages, though less abundant than the above Phanerozoic ages, were particularly useful for provenance interpretation. Specifically, we found that the distinctive age peaks of ~1870 Ma and ~2500 Ma, attributed to the Songpan-Ganzi terrane south of the Eastern Kunlun Range, were present in all analyzed samples except those collected from Neogene units in Qaidam basin. The absence of these Proterozoic ages suggests the emergence of a topographic barrier between the Hoh Xil and Qaidam basins near the beginning of the Neogene.

Our fission track thermochronological data from the Eastern Kunlun Range, which show that rapid cooling did not start until ~30–20 Ma, are consistent with the *contiguous* basin formation model in which the Hoh Xil and Qaidam basins were not partitioned until the Oligocene. Although the Hoh Xil and Qaidam basins were interconnected in a sedimentological sense, the current extent of the Eastern Kunlun Range marks the location of a broad structural arch in the center of the Paleo-Qaidam basin as indicated by the Paleogene isopach patterns in southern Qaidam and the absence of Eocene strata in the Eastern Kunlun Range. We interpret this structural high to be a flexural bulge induced by thrust loading of the Qilian Shan and Fenghuoshan thrust belts along the northern and southern margins of the Paleogene Paleo-Qaidam basin.

Supplementary data to this article can be found online at <https://doi.org/10.1016/j.tecto.2018.12.015>.

Acknowledgements

This project is partially funded by the Tectonics Program of the US National Science Foundation awarded to An Yin.

References

- Allègre, C.J., Courtillot, V., Tapponnier, P., Hirn, A., Mattauer, M., Coulon, C., Jaeger, J.J., Achache, J., Schärer, U., Marcoux, J., Burg, J.P., Girardeau, J., Armijo, R., Gariépy, C., Göpel, C., Li, T., Xiao, X., Chang, C., Li, G., Lin, B., Teng, J., Wang, N., Chen, G., Han, T., Wang, X., Den, W., Sheng, H., Cao, Y., Zhou, J., Qiu, H., Bao, P., Wang, S., Wang, B., Zhou, Y., Xu, R., 1984. Structure and evolution of the Himalaya-Tibet orogenic belt. *Nature* 307, 17–22. <https://doi.org/10.1038/307017a0>.
- An, W., Hu, X., Garzanti, E., BouDagher-Fadel, M.K., Wang, J., Sun, G., 2014. Xigaze forearc basin revisited (South Tibet): provenance changes and origin of the Xigaze Ophiolite. *Bull. Geol. Soc. Am.* 126, 1595–1613. <https://doi.org/10.1130/B31020.1>.
- Arnaud, N., Tapponnier, P., Roger, F., Brunel, M., Scharer, U., Chen, W., Xu, Z., 2003. Evidence for Mesozoic shear along the western Kunlun and Altyn-Tagh fault, northern Tibet (China). *J. Geophys. Res. Solid Earth* 108, 1–27. <https://doi.org/10.1029/2001JB000904>.
- Bally, A.W., Chou, I.M., Clayton, R., Eugster, H.P., Kidwell, S., Meckel, L.D., Ryder, R.T., Watts, A.B., Wilson, A.A., 1986. Notes on Sedimentary Basins in China - Report of the American Sedimentary Basins Delegation to the People's Republic of China. U.S. Geological Survey Open-File Report 86-327. pp. 108.
- Bayona, G., Thomas, W.A., 2003. Distinguishing fault reactivation from flexural deformation in the distal stratigraphy of the Peripheral Blountian foreland basin,

- southern Appalachians, USA. *Basin Res.* 15, 503–526. <https://doi.org/10.1046/j.1365-2117.2003.00217.x>.
- Bernet, M., Garver, J.I., 2005. Fission-track analysis of detrital zircon. *Rev. Mineral. Geochem.* 58, 205–238.
- Bian, Q.T., Zhu, S.X., Pospelov, I.I., Semikhatov, M.A., Sun, S.F., Chen, D.Z., Na, C., 2005. Discovery of the Jiawengmen stromatolite assemblage in the Southern Belt of Eastern Kunlun, NW China and its significance. *Acta Geol. Sin. - English Ed.* 79, 471–480.
- Bruguier, O., Lancelot, J.R., Malavieille, J., 1997. U–Pb dating on single detrital zircon grains from the Triassic Songpan–Ganze flysch (Central China): provenance and tectonic correlations. *Earth Planet. Sci. Lett.* 152, 217–231. [https://doi.org/10.1016/S0012-821X\(97\)00138-6](https://doi.org/10.1016/S0012-821X(97)00138-6).
- Burchfiel, B.C., Chen, Z., 2012. Tectonics of the southeastern Tibetan Plateau and its adjacent foreland. *Geol. Soc. Am. Mem.* 210.
- Burchfiel, B.C., Chen, Z., Liu, Y., Royden, L.H., 1995. Tectonics of the Longmen Shan and Adjacent Regions, Central China. *Int. Geol. Rev.* 37, 661–735. <https://doi.org/10.1080/00206819509465424>.
- Burchfiel, B.C., Deng, Q., Molnar, P., Royden, L., Wang, Y., Zhang, P., Zhang, W., 1989a. Intracrustal detachment within zones of continental deformation. *Geology* 17, 448–452.
- Burchfiel, B.C., Molnar, P., Zhao, Z., Liang, K., Wang, S., Huang, M., Sutter, J., 1989b. Geology of the Ulugh Muztagh area, northern Tibet. *Earth Planet. Sci. Lett.* 94, 57–70. <https://doi.org/10.1016/j.elsevier.1989.09.0083-6>.
- Bush, M.A., Saylor, J.E., Horton, B.K., Nie, J., 2016. Growth of the Qaidam Basin during Cenozoic exhumation in the northern Tibetan Plateau: Inferences from depositional patterns and multiproxy detrital provenance signatures. *Lithosphere* 8, 58–82. <https://doi.org/10.1130/L449.1>.
- Cao, K., Xu, J.F., Chen, J.L., Huang, X.X., Ren, J.B., Zhao, X.D., Liu, Z.X., 2016. Double-layer structure of the crust beneath the Zhongdian arc, SW China: U–Pb geochronology and Hf isotope evidence. *J. Asian Earth Sci.* 115, 455–467. <https://doi.org/10.1016/j.jseas.2015.10.024>.
- Chang, C.-F., Zheng, S.-L., 1973. Tectonic features of the Mount Jolmo Lungma region in southern Tibet, China. *Sci. Geol. Sin.* 1, 1–12.
- Chang, H., Li, L., Qiang, X., Garzzone, C.N., Pullen, A., An, Z., 2015. Magnetostratigraphy of Cenozoic deposits in the western Qaidam Basin and its implication for the surface uplift of the northeastern margin of the Tibetan Plateau. *Earth Planet. Sci. Lett.* 430, 271–283. <https://doi.org/10.1016/j.epsl.2015.08.029>.
- Chen, J.L., Xu, J.F., Ren, J.B., Huang, X.X., Wang, B.D., 2014. Geochronology and geochemical characteristics of Late Triassic porphyritic rocks from the Zhongdian arc, eastern Tibet, and their tectonic and metallogenic implications. *Gondwana Res.* 26, 492–504. <https://doi.org/10.1016/j.gr.2013.07.022>.
- Chen, J.L., Yin, A., Xu, J.F., Dong, Y.H., Kang, Z.Q., 2018a. Late Cenozoic magmatic inflation, crustal thickening, and > 2 km of surface uplift in Central Tibet. *Geology* 46, 19–22. <https://doi.org/10.1130/G39699.1>.
- Chen, K., Bowler, J.M., 1986. Late Pleistocene evolution of salt lakes in the Qaidam basin, Qinghai province, China. *Palaeogeogr. Palaeoclimatol. Palaeoecol.* 54, 87–104. [https://doi.org/10.1016/0031-0182\(86\)90119-7](https://doi.org/10.1016/0031-0182(86)90119-7).
- Chen, N., Gong, S., Sun, M., Li, X., Xia, X., Wang, Q., Wu, F., Xu, P., 2009. Precambrian evolution of the Quanji Block, northeastern margin of Tibet: Insights from zircon U–Pb and Lu–Hf isotope compositions. *J. Asian Earth Sci.* 35, 367–376. <https://doi.org/10.1016/j.jseas.2008.10.004>.
- Chen, N., Li, X., Wang, X., Chen, Q., Wang, Q., Wan, Y., 2006. Zircon SHRIMP U–Pb age of Neoproterozoic metagranite in the North Kunlun unit on the southern margin of the Qaidam block in China. *Geol. Bull. China* 25, 1311–1314 (in Chinese with English abstract).
- Chen, N., Liao, F., Wang, L., Santosh, M., Sun, M., Wang, Q., Mustafa, H.A., 2013. Late Paleoproterozoic multiple metamorphic events in the Quanji Massif: Links with Tarim and North China Cratons and implications for assembly of the Columbia supercontinent. *Precambrian Res.* 228, 102–116. <https://doi.org/10.1016/j.precamres.2013.01.013>.
- Chen, N., Sun, M., He, L., Zhang, K., Wang, G., 2002. Precise timing of the Early Paleozoic metamorphism and thrust deformation in the Eastern Kunlun Orogen. *Chin. Sci. Bull.* 47, 1130–1133. <https://doi.org/10.1360/02tb9253>.
- Chen, N., Sun, M., Zhang, K., Zhu, Y., 2001. ⁴⁰Ar–³⁹Ar and U–Pb ages of metadiorite from the East Kunlun Orogenic Belt: evidence for Early–Paleozoic magmatic zone and excess argon in amphibole minerals. *Chin. Sci. Bull.* 46, 330–333. <https://doi.org/10.1007/BF03187197>.
- Chen, N., Zhang, L., Sun, M., Wang, Q., Kusky, T.M., 2012. U–Pb and Hf isotopic compositions of detrital zircons from the paragneisses of the Quanji Massif, NW China: implications for its early tectonic evolution history. *J. Asian Earth Sci.* 54–55, 110–130. <https://doi.org/10.1016/j.jseas.2012.04.006>.
- Chen, Q., Sun, M., Zhao, G., Yang, F., Long, X., Li, J., Wang, J., Yu, Y., 2017. Origin of the mafic microgranular enclaves (MMEs) and their host granitoids from the Tagong pluton in Songpan–Ganze terrane: an igneous response to the closure of the Paleo-Tethys ocean. *Lithos* 290–291, 1–17. <https://doi.org/10.1016/j.lithos.2017.07.019>.
- Chen, X., Xu, R., Schertl, H.-P., Zheng, Y., 2018b. Eclogite-facies metamorphism in impure marble from north Qaidam orogenic belt: geodynamic implications for early Paleozoic continental-arc collision. *Lithos* 310–311, 201–224. <https://doi.org/10.1016/j.lithos.2018.04.005>.
- Chen, X., Yin, A., Gehrels, G.E., Cowgill, E.S., Grove, M., Harrison, T.M., Wang, X.-F., 2003. Two phases of Mesozoic north-south extension in the eastern Altyn Tagh range, northern Tibetan Plateau. *Tectonics* 22, 1053. <https://doi.org/10.1029/2001TC001336>.
- Cheng, F., Fu, S., Jolivet, M., Zhang, C., Guo, Z., 2016a. Source to sink relation between the Eastern Kunlun Range and the Qaidam Basin, northern Tibetan Plateau, during the Cenozoic. *Geol. Soc. Am. Bull.* 128, 258–283. <https://doi.org/10.1130/B31260.1>.
- Cheng, F., Guo, Z., Jenkins, H.S., Fu, S., Cheng, X., 2015. Initial rupture and displacement on the Altyn Tagh fault, northern Tibetan Plateau: constraints based on residual Mesozoic to Cenozoic strata in the western Qaidam Basin. *Geosphere* 11, 921–942. <https://doi.org/10.1130/GES01070.1>.
- Cheng, F., Jolivet, M., Fu, S., Zhang, C., Zhang, Q., Guo, Z., 2016b. Large-scale displacement along the Altyn Tagh Fault (North Tibet) since its Eocene initiation: insight from detrital zircon U–Pb geochronology and subsurface data. *Tectonophysics* 677–678, 261–279. <https://doi.org/10.1016/j.tecto.2016.04.023>.
- Cheng, F., Jolivet, M., Fu, S., Zhang, Q., Guan, S., Yu, X., Guo, Z., 2014. Northward growth of the Qimen Tagh Range: a new model accounting for the Late Neogene strike-slip deformation of the SW Qaidam Basin. *Tectonophysics* 632, 32–47. <https://doi.org/10.1016/j.tecto.2014.05.034>.
- Chung, S.L., Chu, M.F., Zhang, Y., Xie, Y., Lo, C.H., Lee, T.Y., Lan, C.Y., Li, X., Zhang, Q., Wang, Y., 2005. Tibetan tectonic evolution inferred from spatial and temporal variations in post-collisional magmatism. *Earth Sci. Rev.* 68, 173–196. <https://doi.org/10.1016/j.earscirev.2004.05.001>.
- Chung, S.L., Liu, D., Ji, J., Chu, M.F., Lee, H.Y., Wen, D.J., Lo, C.H., Lee, T.Y., Qian, Q., Zhang, Q., 2003. Adakites from continental collision zones: melting of thickened lower crust beneath southern Tibet. *Geology* 31, 1021–1024. <https://doi.org/10.1130/G19796.1>.
- Chung, S.L., Lo, C.H., Lee, T.Y., Zhang, Y., Xie, Y., Li, X., Wang, K.L., Wang, P.L., 1998. Diachronous uplift of the Tibetan plateau starting 40 Myr ago. *Nature* 394, 769–773. <https://doi.org/10.1038/29511>.
- Clark, M.K., Farley, K.A., Zheng, D., Wang, Z., Duvall, A.R., 2010. Early Cenozoic faulting of the northern Tibetan Plateau margin from apatite (U–Th)/He ages. *Earth Planet. Sci. Lett.* 296, 78–88. <https://doi.org/10.1016/j.epsl.2010.04.051>.
- Copeland, P., Harrison, T.M., Pan, Y., Kidd, W.S.F., Roden, M., Zhang, Y., 1995. Thermal evolution of the Gangdese Batholith, southern Tibet: a history of episodic unroofing. *Tectonics* 14, 223–236.
- Coulon, C., Maluski, H., Bollinger, C., Wang, S., 1986. Mesozoic and cenozoic volcanic rocks from central and southern Tibet: ³⁹Ar–⁴⁰Ar dating, petrological characteristics and geodynamical significance. *Earth Planet. Sci. Lett.* 79, 281–302. [https://doi.org/10.1016/0012-821X\(86\)90186-X](https://doi.org/10.1016/0012-821X(86)90186-X).
- Coward, M.P., Kidd, W.S.F., Pan, Y., Shackleton, R.M., Zhang, H., 1988. The structure of the 1985 Tibet Geotraverse, Lhasa to Golmud. *Philos. Trans. R. Soc. London, Ser. A* 327, 307–336.
- Cowgill, E., Yin, A., Harrison, T.M., Wang, X.-F., 2003. Reconstruction of the Altyn Tagh fault based on U–Pb geochronology: role of back thrusts, mantle sutures, and heterogeneous crustal strength in forming the Tibetan Plateau. *J. Geophys. Res. Solid Earth* 108. <https://doi.org/10.1029/2002JB002080>.
- Cyr, A.J., Currie, B.S., Rowley, D.B., 2005. Geochemical evaluation of Fenghuoshan Group lacustrine carbonates, North-Central Tibet: implications for the paleoaltimetry of the Eocene Tibetan Plateau. *J. Geol.* 113, 517–533. <https://doi.org/10.1086/431907>.
- Dai, J., Wang, C., Hourigan, J., Santosh, M., 2013. Multi-stage tectono-magmatic events of the Eastern Kunlun Range, northern Tibet: insights from U–Pb geochronology and (U–Th)/He thermochronology. *Tectonophysics* 599, 97–106. <https://doi.org/10.1016/j.tecto.2013.04.005>.
- Dai, J., Zhao, X., Wang, C., Zhu, L., Li, Y., Finn, D., 2012. The vast proto-Tibetan Plateau: new constraints from Paleogene Hoh Xil Basin. *Gondwana Res.* 22, 434–446. <https://doi.org/10.1016/j.gr.2011.08.019>.
- Debon, F., Lefort, P., Sheppard, S.M.F., Sonet, J., 1986. The four plutonic belts of the Transhimalaya Himalaya: a chemical, mineralogical, isotopic, and chronological synthesis along a Tibet–Nepal section. *J. Petrol.* 27, 219–250. <https://doi.org/10.1093/petrology/27.1.219>.
- DeCelles, P.G., Gehrels, G.E., Najman, Y., Martin, A.J., Carter, A., Garzanti, E., 2004. Detrital geochronology and geochemistry of Cretaceous–Early Miocene strata of Nepal: implications for timing and diachroneity of initial Himalayan orogenesis. *Earth Planet. Sci. Lett.* 227, 313–330. <https://doi.org/10.1016/j.epsl.2004.08.019>.
- Delville, N., Arnaud, N., Montel, J.-M., Roger, F., Brunel, M., Tapponnier, P., Sobel, E.R., 2001. Paleozoic to Cenozoic deformation along the Altyn Tagh fault in the Altun Shan Massif area, eastern Qilian Shan, northeastern Tibet, China. *Geol. Soc. Am. Mem.* 194, 269–292.
- Dewey, J.F., Shackleton, R.M., Chang, C., Sun, Y., 1988. The tectonic evolution of the Tibetan Plateau. *Philos. Trans. R. Soc. London, Ser. A* 327, 379–413.
- Dickinson, W.R., Beard, L.S., Brakenridge, G.R., Erjavec, J.L., Ferguson, R.C., Inman, K.F., Knepp, R.A., Lindberg, F.A., Ryberg, P.T., 1983. Provenance of North American Phanerozoic sandstones in relation to tectonic setting. *Geol. Soc. Am. Bull.* 222–235. [https://doi.org/10.1130/0016-7606\(1983\)94<222>](https://doi.org/10.1130/0016-7606(1983)94<222>).
- Ding, L., Kapp, P., Yue, Y., Lai, Q., 2007. Postcollisional calc-alkaline lavas and xenoliths from the southern Qiangtang terrane, Central Tibet. *Earth Planet. Sci. Lett.* 254, 28–38. <https://doi.org/10.1016/j.epsl.2006.11.019>.
- Ding, L., Kapp, P., Zhong, D., Deng, W., 2003. Cenozoic volcanism in Tibet: evidence for a transition from oceanic to continental subduction. *J. Petrol.* 44, 1833–1865. <https://doi.org/10.1093/petrology/egg061>.
- Ding, L., Yang, D., Cai, F.L., Pullen, A., Kapp, P., Gehrels, G.E., Zhang, L.Y., Zhang, Q.H., Lai, Q.Z., Yue, Y.H., Shi, R.D., 2013. Provenance analysis of the Mesozoic Hoh-Xil–Songpan–Ganzi turbidites in northern Tibet: Implications for the tectonic evolution of the eastern Paleo-Tethys Ocean. *Tectonics* 32, 34–48. <https://doi.org/10.1002/tect.20013>.
- Dong, C.Y., Li, C., Wan, Y.S., Wang, W., Wu, Y.W., Xie, H.Q., Liu, D.Y., 2011. Detrital zircon age model of Ordovician Wenquan quartzite south of Lungmuco-Shuanghu Suture in the Qiangtang area, Tibet: constraint on tectonic affinity and source regions. *Chin. J. Earth Sci.* 54, 1034–1042. <https://doi.org/10.1007/s11430-010-4166-x>.
- Dong, G., Mo, X., Zhao, Z., Guo, T., Wang, L., Chen, T., 2005. Geochronologic constraints

- on the magmatic underplating of the Gangdise belt in the India-Eurasia collision: evidence of SHRIMP II zircon U-Pb dating. *Acta Geol. Sin.* 79, 787–794.
- Dürr, S.B., 1996. Provenance of Xigaze fore-arc basin clastic rocks (Cretaceous, south Tibet). *Bull. Geol. Soc. Am.* 108, 669–684. [https://doi.org/10.1130/0016-7606\(1996\)108<0669:POXFAB>2.3.CO;2](https://doi.org/10.1130/0016-7606(1996)108<0669:POXFAB>2.3.CO;2).
- Duvall, A.R., Clark, M.K., Kirby, E., Farley, K.A., Craddock, W.H., Li, C., Yuan, D.Y., 2013. Low-temperature thermochronometry along the Kunlun and Haiyuan Faults, NE Tibetan Plateau: evidence for kinematic change during late-stage orogenesis. *Tectonics* 32, 1190–1211. <https://doi.org/10.1002/tect.20072>.
- Einsele, G., Liu, B., Dürr, S., Frisch, W., Liu, G., Luterbacher, H.P., Ratschbacher, L., Ricken, W., Wendt, J., Wetzel, A., Yu, G., Zheng, H., 1994. The Xigaze forearc basin: evolution and facies architecture (Cretaceous, Tibet). *Sediment. Geol.* 90, 1–32. [https://doi.org/10.1016/0037-0738\(94\)90014-0](https://doi.org/10.1016/0037-0738(94)90014-0).
- Enkelmann, E., Weislogel, A., Ratschbacher, L., Eide, E., Renno, A., Wooden, J., 2007. How was the Triassic Songpan-Ganzi basin filled? A provenance study. *Tectonics* 26. <https://doi.org/10.1029/2006TC002078>.
- Fan, J.J., Li, C., Xie, C.M., Wang, M., Chen, J.W., 2015. Petrology and U-Pb zircon geochronology of bimodal volcanic rocks from the Maierze Group, northern Tibet: constraints on the timing of closure of the Banggong-Nujiang Ocean. *Lithos* 227, 148–160. <https://doi.org/10.1016/j.lithos.2015.03.021>.
- Fang, X., Zhang, W., Meng, Q., Gao, J., Wang, X., King, J., Song, C., Dai, S., Miao, Y., 2007. High-resolution magnetostratigraphy of the Neogene Huaitoutala section in the eastern Qaidam Basin on the NE Tibetan Plateau, Qinghai Province, China and its implication on tectonic uplift of the NE Tibetan Plateau. *Earth Planet. Sci. Lett.* 258, 293–306. <https://doi.org/10.1016/j.epsl.2007.03.042>.
- Gansu BGMR (Bureau of Geology and Mineral Resources), 1989. *Regional Geology of Gansu Province*. Geological Publishing House, Beijing, pp. 690 (in Chinese with English summary).
- Gehrels, G., Kapp, P., Decelles, P., Pullen, A., Blakey, R., Weislogel, A., Ding, L., Guynn, J., Martin, A., McQuarrie, N., Yin, A., 2011. Detrital zircon geochronology of pre-Tertiary strata in the Tibetan-Himalayan orogen. *Tectonics* 30. <https://doi.org/10.1029/2011TC002868>.
- Gehrels, G.E., Yin, A., Wang, X.-F., 2003a. Magmatic history of the northeastern Tibetan Plateau. *J. Geophys. Res. Solid Earth* 108, 1–14. <https://doi.org/10.1029/2002JB001876>.
- Gehrels, G.E., Yin, A., Wang, X.-F., 2003b. Detrital-zircon geochronology of the northeastern Tibetan plateau. *Geol. Soc. Am. Bull.* 115, 881–896. [https://doi.org/10.1130/0016-7606\(2003\)115<0881](https://doi.org/10.1130/0016-7606(2003)115<0881).
- Gleadow, A.J.W., 1981. Fission-track dating methods: what are the real alternatives? *Nucl. Tracks* 5, 3–14. [https://doi.org/10.1016/0191-278X\(81\)900021-4](https://doi.org/10.1016/0191-278X(81)900021-4).
- Gong, S., Chen, N., Wang, Q., Kusky, T.M., Wang, L., Zhang, L., Ba, J., Liao, F., 2012. Early Paleoproterozoic magmatism in the Quanji Massif, northeastern margin of the Qinghai-Tibet Plateau and its tectonic significance: LA-ICPMS U-Pb zircon geochronology and geochemistry. *Gondwana Res.* 21, 152–166. <https://doi.org/10.1016/j.gr.2011.07.011>.
- Gu, X.X., 1994. Geochemical characteristics of the Triassic Tethys-turbidites in northwestern Sichuan, China: implications for provenance and interpretation of the tectonic setting. *Geochim. Cosmochim. Acta* 58, 4615–4631. [https://doi.org/10.1016/0016-7037\(94\)90195-3](https://doi.org/10.1016/0016-7037(94)90195-3).
- Guo, Z., Wilson, M., Liu, J., Mao, Q., 2006. Post-collisional, potassic and ultrapotassic magmatism of the Northern Tibetan Plateau: constraints on characteristics of the mantle source, geodynamic setting and uplift mechanisms. *J. Petrol.* 47, 1177–1220. <https://doi.org/10.1093/ptrology/egl007>.
- Guynn, J.H., Kapp, P., Pullen, A., Heizler, M., Gehrels, G., Ding, L., 2006. Tibetan basement rocks near Amdo reveal “missing” mesozoic tectonism along the Banggong suture, Central Tibet. *Geology* 34, 505–508. <https://doi.org/10.1130/G22453.1>.
- Hacker, B.R., Gnos, E., Ratschbacher, L., Grove, M., McWilliams, M., Sobolev, S.V., Wan, J., Wu, Z., 2000. Hot and dry deep crustal xenoliths from Tibet. *Science* 287, 2463–2466. <https://doi.org/10.1126/science.287.5462.2463>.
- Hanson, A.D., Ritts, B.D., Zinniker, D., Moldovan, J.M., Biffi, U., 2001. Upper Oligocene lacustrine source rocks and petroleum systems of the Northern Qaidam Basin, Northwest China. *Am. Assoc. Pet. Geol. Bull.* 85, 601. <https://doi.org/10.1130/8626C95B-173B-11D7-8645000102C1865D>.
- Hao, L.L., Wang, Q., Wyman, D.A., Ou, Q., Dan, W., Jiang, Z.Q., Wu, F.Y., Yang, J.H., Long, X.P., Li, J., 2016. Underplating of basaltic magmas and crustal growth in a continental arc: evidence from Late Mesozoic intermediate-felsic intrusive rocks in southern Qiangtang, Central Tibet. *Lithos* 245, 223–242. <https://doi.org/10.1016/j.lithos.2015.09.015>.
- Harris, N.B.W., Xu, R., Lewis, C.L., Hawkesworth, C.J., Zhang, Y., 1988. Isotope geochemistry of the 1985 Tibet Geotraverse, Lhasa to Golmud. *Philos. Trans. R. Soc. London, Ser. A* 327, 263–285.
- Harrison, T.M., Yin, A., Grove, M., Lovera, O.M., Ryerson, F.J., Zhou, X., 2000. The Zedong window: a record of superposed Tertiary convergence in southeastern Tibet. *J. Geophys. Res. Solid Earth* 105, 19211–19230.
- He, D., Dong, Y., Liu, X., Yang, Z., Sun, S., Cheng, B., Li, W., 2016a. Tectono-thermal events in East Kunlun, Northern Tibetan Plateau: evidence from zircon U-Pb geochronology. *Gondwana Res.* 30, 179–190. <https://doi.org/10.1016/j.gr.2015.08.002>.
- He, D., Dong, Y., Zhang, F., Yang, Z., Sun, S., Cheng, B., Zhou, B., Liu, X., 2016b. The 1.0 Ga S-type granite in the East Kunlun Orogen, Northern Tibetan Plateau: Implications for the Meso- to Neoproterozoic tectonic evolution. *J. Asian Earth Sci.* 130, 46–59. <https://doi.org/10.1016/j.jseas.2016.07.019>.
- Honegger, K., Dietrich, V., Frank, W., Gansser, A., Thöni, M., Trommsdorff, V., 1982. Magmatism and metamorphism in the Ladakh Himalayas (the Indus-Tsangpo suture zone). *Earth Planet. Sci. Lett.* 60, 253–292. [https://doi.org/10.1016/0012-821X\(82\)90007-3](https://doi.org/10.1016/0012-821X(82)90007-3).
- Horton, B.K., Dupont-Nivet, G., Zhou, J., Waanders, G.L., Butler, R.F., Wang, J., 2004. Mesozoic-Cenozoic evolution of the Xining-Minhe and Dangchang basins, north-eastern Tibetan Plateau: magnetostratigraphic and biostratigraphic results. *J. Geophys. Res. Solid Earth* 109, 1–15. <https://doi.org/10.1029/2003JB002913>.
- Horton, B.K., Yin, A., Spurlin, M.S., Zhou, J., Wang, J., 2002. Paleocene-Eocene syn-contractual sedimentation in narrow, lacustrine-dominated basins of east-Central Tibet. *Bull. Geol. Soc. Am.* 114, 771–786. [https://doi.org/10.1130/0016-7606\(2002\)114<0771:PESSIN>2.0.CO;2](https://doi.org/10.1130/0016-7606(2002)114<0771:PESSIN>2.0.CO;2).
- Hou, Z.Q., Zheng, Y.C., Zeng, L., Sen, Gao, L.E., Huang, K.X., Li, W., Li, Q.Y., Fu, Q., Liang, W., Sun, Q.Z., 2012. Eocene-Oligocene granitoids in southern Tibet: constraints on crustal anatexis and tectonic evolution of the Himalayan orogen. *Earth Planet. Sci. Lett.* 349–350, 38–52. <https://doi.org/10.1016/j.epsl.2012.06.030>.
- Hu, P., Zhai, Q., Jahn, B., Wang, J., Li, C., Lee, H., Tang, S., 2015. Early Ordovician granites from the South Qiangtang terrane, northern Tibet: implications for the early Paleozoic tectonic evolution along the Gondwanan proto-Tethyan margin. *Lithos* 220–223, 318–338. <https://doi.org/10.1016/j.lithos.2014.12.020>.
- Huang, H., Huang, Q., Ma, Y., 1996. *Geology of Qaidam Basin and its Petroleum Prediction*. Geological Publishing House, Beijing, pp. 257 (in Chinese).
- Huang, T.K., Chen, B.W., 1987. *The Evolution of the Tethys in China and Adjacent Regions*. Geological Publishing House, Beijing, pp. 109 (in Chinese).
- Huo, G.M. (Ed.), 1990. *Petroleum Geology of China: Oil Fields in Qianghai and Xizang*. Vol. 14. Press, Chinese Petroleum Industry, pp. 483 (in Chinese).
- Huo, Y.L., Tan, S.D., 1995. *Exploration Case History and Petroleum Geology in Jiuquan Continental Basin*. Chinese Petroleum Industry Press, Beijing, pp. 211 (in Chinese).
- Hurfurd, A.J., Green, P.F., 1983. The zeta age calibration of fission-track dating. *Chem. Geol.* 41, 285–317. [https://doi.org/10.1016/S0009-2541\(83\)80026-6](https://doi.org/10.1016/S0009-2541(83)80026-6).
- Ingersoll, R.V., Bullard, T.F., Ford, R.L., Grimm, J.P., Pickle, J.D., Sares, S.W., 1984. The effect of grain size on detrital modes: a test of the Gazzi-Dickinson point-counting method. *J. Sediment. Res.* 54, 103–116. <https://doi.org/10.1306/212F878D-2B24-11D7-8648000102C1865D>.
- Ingersoll, R.V., Graham, S.A., Dickinson, W.R., 1995. Remnant ocean basins. In: Busby, C.J., Ingersoll, R.V. (Eds.), *Tectonics of Sedimentary Basins*. MA, Blackwell Science, Cambridge, pp. 363–391.
- Ji, J., Zhang, K., Clift, P.D., Zhuang, G., Song, B., Ke, X., Xu, Y., 2017. High-resolution magnetostratigraphic study of the Paleogene-Neogene strata in the Northern Qaidam Basin: implications for the growth of the Northeastern Tibetan Plateau. *Gondwana Res.* 46, 141–155. <https://doi.org/10.1016/j.gr.2017.02.015>.
- Jiang, D., Liu, J., Ding, L., 2008a. Geochemistry and petrogenesis of Cenozoic potassic volcanic rocks in the Hoh Xil area, northern Tibet plateau. *Acta Petrol. Sin.* 24, 279–290 (in Chinese with English abstract).
- Jiang, R.-B., Chen, X.-H., Dang, Y.-Q., Yin, A., Wang, L.-Q., Jiang, W.-M., Wan, J.-L., Li, L., Wang, X.-F., 2008b. Apatite fission track evidence for two phases Mesozoic-Cenozoic thrust faulting in eastern Qaidam basin. *Chin. J. Geophys.* 51, 116–124 (in Chinese with English abstract).
- Jiang, Y.H., Jiang, S.Y., Ling, H.F., Dai, B.Z., 2006. Low-degree melting of a metasomatized lithospheric mantle for the origin of Cenozoic Yulong monzogranite-porphyr, east Tibet: geochemical and Sr-Nd-Pb-Hf isotopic constraints. *Earth Planet. Sci. Lett.* 241, 617–633. <https://doi.org/10.1016/j.epsl.2005.11.023>.
- Jin, C., Liu, Q., Liang, W., Roberts, A.P., Sun, J., Hu, P., Zhao, X., Su, Y., Jiang, Z., Liu, Z., Duan, Z., Yang, H., Yuan, S., 2018. Magnetostratigraphy of the Fenghuoshan Group in the Hoh Xil Basin and its tectonic implications for India-Eurasia collision and Tibetan Plateau deformation. *Earth Planet. Sci. Lett.* 486, 41–53. <https://doi.org/10.1016/j.epsl.2018.01.010>.
- Jin, L., Zhou, H., Wang, J., Zhu, Y., Lin, Q., 2015. LA-ICP-MS U-Pb dating of the detrital zircons from clastic rocks of Naij Tal Group in East Kunlun and its geological implications. *Geol. Bull. China* 34, 1848–1859 (in Chinese with English abstract).
- Jolivet, M., Brunel, M., Seward, D., Xu, Z., Yang, J., Malavieille, J., Roger, F., Leyreloup, A., Arnaud, N., Wu, C., 2003. Neogene extension and volcanism in the Kunlun Fault Zone, northern Tibet: new constraints on the age of the Kunlun Fault. *Tectonics* 22, 1052. <https://doi.org/10.1029/2002TC001428>.
- Jolivet, M., Brunel, M., Seward, D., Xu, Z., Yang, J., Roger, F., Tapponnier, P., Malavieille, J., Arnaud, N., Wu, C., 2001. Mesozoic and Cenozoic tectonics of the northern edge of the Tibetan plateau: fission-track constraints. *Tectonophysics* 343, 111–134. [https://doi.org/10.1016/S0040-1951\(01\)00196-2](https://doi.org/10.1016/S0040-1951(01)00196-2).
- Jolivet, M., Roger, F., Xu, Z.Q., Paquette, J.L., Cao, H., 2015. Mesozoic-Cenozoic evolution of the Danba dome (Songpan Garze, East Tibet) as inferred from LA-ICPMS U-Pb and fission-track data. *J. Asian Earth Sci.* 102, 180–204. <https://doi.org/10.1016/j.jseas.2015.02.009>.
- Kapp, J.L.D., Harrison, T.M., Kapp, P., Grove, M., Lovera, O.M., Lin, D., 2005b. Nyainqentanglha Shan: a window into the tectonic, thermal, and geochemical evolution of the Lhasa block, southern Tibet. *J. Geophys. Res. Solid Earth* 110, 1–23. <https://doi.org/10.1029/2004JB003330>.
- Kapp, P., DeCelles, P.G., Gehrels, G.E., Heizler, M., Ding, L., 2007a. Geological records of the Lhasa-Qiangtang and Indo-Asian collisions in the Nima area of Central Tibet. *Bull. Geol. Soc. Am.* 119, 917–932. <https://doi.org/10.1130/B26033.1>.
- Kapp, P., DeCelles, P.G., Leier, A.L., Fabijanic, J.M., He, S., Pullen, A., Gehrels, G.E., Ding, L., 2007b. The Gangdese retroarc thrust belt revealed. *GSA Today* 17, 4–9. <https://doi.org/10.1130/GSAT01707A.1>.
- Kapp, P., Yin, A., Harrison, T.M., Ding, L., 2005a. Cretaceous-Tertiary shortening, basin development, and volcanism in Central Tibet. *Bull. Geol. Soc. Am.* 117, 865–878. <https://doi.org/10.1130/B25595.1>.
- Kapp, P., Yin, A., Manning, C., Murphy, M., Harrison, M., Lin, D., Deng, X., Wu, C., 2000. Blueschist-bearing metamorphic core complexes in the Qiangtang block reveal deep crustal structure of northern Tibet. *Geology* 28, 19–22. [https://doi.org/10.1130/0091-7613\(2000\)28<19:BMCCIT>2.0.CO;2](https://doi.org/10.1130/0091-7613(2000)28<19:BMCCIT>2.0.CO;2).
- Kapp, P., Yin, A., Manning, C.E., Harrison, T.M., Taylor, M.H., Ding, L., 2003. Tectonic evolution of the early Mesozoic blueschist-bearing Qiangtang metamorphic belt,

- Central Tibet. *Tectonics* 22, 1043. <https://doi.org/10.1029/2002TC001383>.
- Ketchum, R.A., 2005. Forward and inverse modeling of low-temperature thermochronometry data. *Rev. Mineral. Geochem.* 58, 275–314. <https://doi.org/10.2138/rmg.2005.58.11>.
- Ketchum, R.A., Carter, A., Donelick, R.A., Barbarand, J., Hurford, A.J., 2007. Improved modeling of fission-track annealing in apatite. *Am. Mineral.* 92, 799–810. <https://doi.org/10.2138/am.2007.2281>.
- Lee, K.Y., 1984. Geology of the Chaidamu Basin, Qinghai Province, Northwest China. U.S. Geological Survey Open-File Report 84–413. pp. 42.
- Leeder, M.R., Smith, A.B., Yin, J., 1988. Sedimentology, palaeoecology and palaeoenvironmental evolution of the 1985 Lhasa to Golmud Geotraverse. *Philos. Trans. R. Soc. London, Ser. A* 327, 107–143.
- Lehmkuhl, F., Haselein, F., 2000. Quaternary palaeoenvironmental change on the Tibetan Plateau and adjacent areas (Western China and Western Mongolia). *Quat. Int.* 65–66, 121–145. [https://doi.org/10.1016/S1040-6182\(99\)00040-3](https://doi.org/10.1016/S1040-6182(99)00040-3).
- Leier, A.L., Kapp, P., Gehrels, G.E., Decelles, P.G., 2007. Detrital zircon geochronology of Carboniferous–Cretaceous strata in the Lhasa terrane, southern Tibet. *Basin Res.* 19, 361–378. <https://doi.org/10.1111/j.1365-2117.2007.00330.x>.
- Li, J., Batten, D.J., 2004. Early Cretaceous palynofloras from the Tanggula Mountains of the northern Qinghai-Xizang (Tibet) Plateau, China. *Cretac. Res.* 25, 531–542. <https://doi.org/10.1016/j.cretres.2004.04.005>.
- Li, C.Y., Liu, Y., Zhu, B.C., Feng, Y.M., Wu, H.C., 1978. Structural Evolution of Qingling and Qilian Shan. Scientific Papers in Geology and International Exchange. Beijing, Geological Publishing House, pp. 174–197 (in Chinese).
- Li, G.M., Li, J.X., Zhao, J.X., Qin, K.Z., Cao, M.J., Evans, N.J., 2015a. Petrogenesis and tectonic setting of Triassic granitoids in the Qiangtang terrane, Central Tibet: evidence from U–Pb ages, petrochemistry and Sr–Nd–Hf isotopes. *J. Asian Earth Sci.* 105, 443–455. <https://doi.org/10.1016/j.jseas.2015.02.017>.
- Li, G.M., Qin, K.Z., Li, J.X., Evans, N.J., Zhao, J.X., Cao, M.J., Zhang, X.N., 2017a. Cretaceous magmatism and metallogeny in the Bangong–Nujiang metallogenic belt, Central Tibet: evidence from petrogeochemistry, zircon U–Pb ages, and Hf–O isotopic compositions. *Gondwana Res.* 41, 110–127. <https://doi.org/10.1016/j.gr.2015.09.006>.
- Li, J., Bai, D., Wang, X., 2004. Ages of volcanic rocks and planation surface in the Canmei Mountain area, northern Tibet. *Geol. Bull. China* 23, 670–675 (in Chinese with English abstract).
- Li, J., Peng, J., Batten, D.J., 2015b. Palynomorph assemblages from the Fenghuoshan Group, southern Qinghai, China: their age and palaeoenvironmental significance. *Chin. Sci. Bull.* 60, 470–476. <https://doi.org/10.1007/s11434-014-0677-8>.
- Li, J.X., Qin, K.Z., Li, G.M., Richards, J.P., Zhao, J.X., Cao, M.J., 2014. Geochronology, geochemistry, and zircon Hf isotopic compositions of Mesozoic intermediate-felsic intrusions in Central Tibet: Petrogenetic and tectonic implications. *Lithos* 198–199, 77–91. <https://doi.org/10.1016/j.lithos.2014.03.025>.
- Li, J.X., Qin, K.Z., Li, G.M., Xiao, B., Zhao, J.X., Cao, M.J., Chen, L., 2013a. Petrogenesis of ore-bearing porphyries from the Duolong porphyry Cu–Au deposit, Central Tibet: evidence from U–Pb geochronology, petrochemistry and Sr–Nd–Hf–O isotope characteristics. *Lithos* 160–161, 216–227. <https://doi.org/10.1016/j.lithos.2012.12.015>.
- Li, L., Garzzone, C.N., Pullen, A., Zhang, P., Li, Y., 2018a. Late Cretaceous–Cenozoic basin evolution and topographic growth of the Hoh Xil Basin, central Tibetan Plateau. *Bull. Geol. Soc. Am.* 130, 499–521. <https://doi.org/10.1130/B31769.1>.
- Li, L., Wu, C., Yu, X., 2018b. Cenozoic evolution of the Altyn Tagh and East Kunlun fault zones inferred from detrital garnet, tourmaline and rutile in southwestern Qaidam Basin (Northern Tibetan Plateau). *Basin Res.* 30, 35–58. <https://doi.org/10.1111/bre.12241>.
- Li, S., Ding, L., Guilmette, C., Fu, J., Xu, Q., Yue, Y., Henrique-Pinto, R., 2017b. The subduction-accretion history of the Bangong–Nujiang Ocean: constraints from provenance and geochronology of the Mesozoic strata near Gaize, Central Tibet. *Tectonophysics* 702, 42–60. <https://doi.org/10.1016/j.tecto.2017.02.023>.
- Li, S., Guilmette, C., Ding, L., Xu, Q., Fu, J., Yue, Y.H., 2017c. Provenance of Mesozoic clastic rocks within the Bangong–Nujiang suture zone, Central Tibet: implications for the age of the initial Lhasa–Qiangtang collision. *J. Asian Earth Sci.* 147, 469–484. <https://doi.org/10.1016/j.jseas.2017.08.019>.
- Li, W., Neubauer, F., Liu, Y., Genser, J., Ren, S., Han, G., Liang, C., 2013b. Paleozoic evolution of the Qimantagh magmatic arcs, Eastern Kunlun Mountains: constraints from zircon dating of granitoids and modern river sands. *J. Asian Earth Sci.* 77, 183–202. <https://doi.org/10.1016/j.jseas.2013.08.030>.
- Li, Y., Wang, C., Zhao, X., Yin, A., Ma, C., 2012. Cenozoic thrust system, basin evolution, and uplift of the Tanggula Range in the Tuotuohe region, Central Tibet. *Gondwana Res.* 22, 482–492. <https://doi.org/10.1016/j.gr.2011.11.017>.
- Liu, C., Mo, X., Luo, Z., Yu, X., Chen, H., Li, S., Zhao, X., 2004. Mixing events between the crust- and mantle-derived magmas in Eastern Kunlun: evidence from zircon SHRIMP II chronology. *Chin. Sci. Bull.* 49, 828–834. <https://doi.org/10.1007/BF02889756>.
- Liu, D., Li, H., Sun, Z., Pan, J., Wang, M., Wang, H., Chevalier, M.-L., 2017b. AFT dating constrains the Cenozoic uplift of the Qimen Tagh Mountains, Northeast Tibetan Plateau, comparison with LA-ICPMS Zircon U–Pb ages. *Gondwana Res.* 41, 438–450. <https://doi.org/10.1016/j.gr.2015.08.008>.
- Liu, D., Shi, R., Ding, L., Huang, Q., Zhang, X., Yue, Y., Zhang, L., 2017a. Zircon U–Pb age and Hf isotopic compositions of Mesozoic granitoids in southern Qiangtang, Tibet: implications for the subduction of the Bangong–Nujiang Tethyan Ocean. *Gondwana Res.* 41, 157–172. <https://doi.org/10.1016/j.gr.2015.04.007>.
- Liu, Z., Wang, C., 2001. Facies analysis and depositional systems of Cenozoic sediments in the Hoh Xil basin, Northern Tibet. *Sediment. Geol.* 140, 251–270. [https://doi.org/10.1016/S0037-0738\(00\)00188-3](https://doi.org/10.1016/S0037-0738(00)00188-3).
- Liu, Y., Genser, J., Neubauer, F., Jin, W., Ge, X., Handler, R., Takasu, A., 2005b. ⁴⁰Ar/³⁹Ar mineral ages from basement rocks in the Eastern Kunlun Mountains, NW China, and their tectonic implications. *Tectonophysics* 398, 199–224. <https://doi.org/10.1016/j.tecto.2005.02.007>.
- Liu, Y., Li, C., Xie, C., Fan, J., Wu, H., Jiang, Q., Li, X., 2016. Cambrian granitic gneiss within the central Qiangtang terrane, Tibetan Plateau: implications for the early Palaeozoic tectonic evolution of the Gondwanan margin. *Int. Geol. Rev.* 58, 1043–1063. <https://doi.org/10.1080/00206814.2016.1141329>.
- Liu, Z., Wang, C., Jin, W., Yi, H., Zheng, H., Zhao, X., Li, Y., 2005a. Oligo-Miocene depositional environment of the Tuotuohe basin, central Tibetan plateau. *Acta Sedimentol. Sin.* 23, 210–217 (in Chinese with English abstract).
- Liu, Z., Wang, C., Yi, H., 2001. Evolution and mass accumulation of the Cenozoic Hoh Xil basin, northern Tibet. *J. Sediment. Res.* 71, 971–984. <https://doi.org/10.1306/030901710971>.
- Liu, Z., Zhao, X., Wang, C., Liu, S., Yi, H., 2003. Magnetostratigraphy of Tertiary sediments from the Hoh Xil basin: implications for the Cenozoic tectonic history of the Tibetan plateau. *Geophys. J. Int.* 154, 233–252.
- Liu, Z.Q., 1988. Geologic Map of the Qinghai-Xizang Plateau (1:1,500,000). Chengdu Institute of Geology and Mineral Resources. Chinese Academy of Geological Sciences, Beijing, Geological Publishing House (compiler).
- Long, X., Wilde, S.A., Wang, Q., Yuan, C., Wang, X.C., Li, J., Jiang, Z., Dan, W., 2015. Partial melting of thickened continental crust in Central Tibet: evidence from geochemistry and geochronology of Eocene adakitic rhyolites in the northern Qiangtang Terrane. *Earth Planet. Sci. Lett.* 414, 30–44. <https://doi.org/10.1016/j.epsl.2015.01.007>.
- Lu, H., Xiong, S., 2009. Magnetostratigraphy of the Dahonggou section, northern Qaidam Basin and its bearing on Cenozoic tectonic evolution of the Qilian Shan and Altyn Tagh Fault. *Earth Planet. Sci. Lett.* 288, 539–550. <https://doi.org/10.1016/j.epsl.2009.10.016>.
- Lu, L., Zhang, K.J., Yan, L.L., Jin, X., Zhang, Y.X., 2017. Was late Triassic Tanggula granitoid (Central Tibet, western China) a product of melting of underthrust Songpan-Ganzi flysch sediments? *Tectonics* 36, 902–928. <https://doi.org/10.1002/2016TC004384>.
- Lu, S., Li, H., Zhang, C., Niu, G., 2008. Geological and geochronological evidence for the Precambrian evolution of the Tarim Craton and surrounding continental fragments. *Precambrian Res.* 160, 94–107. <https://doi.org/10.1016/j.precamres.2007.04.025>.
- Lu, S.N., Li, H.K., Wang, H.C., Chen, Z.H., Zheng, J.K., Xiang, Z.Q., 2009. Detrital zircon population of Proterozoic meta-sedimentary strata in the Qinling-Qilian-Kunlun Orogen. *Acta Petrol. Sin.* 25, 2195–2208 (in Chinese with English abstract).
- Ludwig, K.R., 2012. *Isoplot 3.75*. Berkeley Geochronology Center, Special Publication 5. pp. 75.
- Meng, Q.R., Fang, X., 2008. Cenozoic tectonic development of the Qaidam Basin in the northeastern Tibetan Plateau. *Geol. Soc. Am. Spec. Pap.* 444, 1–24. [https://doi.org/10.1130/2008.2444\(01\)](https://doi.org/10.1130/2008.2444(01)).
- Métivier, F., Gaudemer, Y., Tapponnier, P., Meyer, B., 1998. Northeastward growth of the Tibet plateau deduced from balanced reconstruction of two depositional areas: the Qaidam and Hexi Corridor basins, China. *Tectonics* 17, 823–842.
- Meyers, J.H., Suttner, L.J., Furer, L.C., May, M.T., Soreghan, M.J., 1992. Intrabasinal tectonic control on fluvial sandstone bodies in the Cloverly Formation (Early Cretaceous), west-Central Wyoming, USA. *Basin Res.* 4, 315–335. <https://doi.org/10.1111/j.1365-2117.1992.tb00051.x>.
- Miao, Y., Wu, F., Chang, H., Fang, X., Deng, T., Sun, J., Jin, C., 2016. A Late-Eocene palynological record from the Hoh Xil Basin, northern Tibetan Plateau, and its implications for stratigraphic age, paleoclimate and paleoelevation. *Gondwana Res.* 31, 241–252. <https://doi.org/10.1016/j.gr.2015.01.007>.
- Miller, C., Schuster, R., Klötzli, U., Frank, W., Purtscheller, F., 1999. Post-collisional potassic and ultrapotassic magmatism in SW Tibet: Geochemical and Sr–Nd–Pb–O isotopic constraints for mantle source characteristics and petrogenesis. *J. Petrol.* 40, 1399–1424. <https://doi.org/10.1093/ptro/40.9.1399>.
- Mischke, S., Herzschuh, U., Sun, N.D., Qiao, Z.Z., Sun, Z.C., 2006a. A large Middle Pleistocene freshwater to oligohaline lake in the contemporary hyperarid Qaidam Basin (China). *Episodes* 29, 34–38.
- Mischke, S., Herzschuh, U., Sun, Z., Qiao, Z., Sun, N., Zander, A.M., 2006b. Middle Pleistocene Ostracoda from a large freshwater lake in the presently dry Qaidam Basin (NW China). *J. Micropalaeontol.* 25, 57–64. <https://doi.org/10.1144/jm.25.1.57>.
- Mo, X., Dong, G., Zhao, Z., Guo, T., Wang, L., Chen, T., 2005. Timing of magma mixing in the Gangdise magmatic belt during the India-Asia collision: zircon SHRIMP U–Pb dating. *Acta Geol. Sin. - English Ed.* 79, 66–76.
- Mo, X., Hou, Z., Niu, Y., Dong, G., Qu, X., Zhao, Z., Yang, Z., 2007. Mantle contributions to crustal thickening during continental collision: evidence from Cenozoic igneous rocks in southern Tibet. *Lithos* 96, 225–242. <https://doi.org/10.1016/j.lithos.2006.10.005>.
- Mo, X., Zhao, Z., Deng, J., Flower, M., Yu, X., Lui, Z., Li, Y., Zhou, S., Dong, G., Zhu, D., Wang, L., 2006. Petrology and geochemistry of postcollisional volcanic rocks from the Tibetan plateau: implications for lithosphere heterogeneity and collision-induced asthenosphere flow. *Geol. Soc. Am. Spec. Pap.* 409, 507–530.
- Mock, C., Arnaud, N.O., Cantagrel, J.M., 1999. An early unroofing in northeastern Tibet? Constraints from ⁴⁰Ar/³⁹Ar thermochronology on granitoids from the eastern Kunlun range (Qianghai, NW China). *Earth Planet. Sci. Lett.* 171, 107–122. [https://doi.org/10.1016/S0012-821X\(99\)00133-8](https://doi.org/10.1016/S0012-821X(99)00133-8).
- Murphy, M.A., Yin, A., Harrison, T.M., Dürer, S.B., Ryerson, F.J., Kidd, W.S.F., 1997. Did the Indo-Asian collision alone create the Tibetan plateau? *Geology* 25, 719–722. [https://doi.org/10.1130/0091-7613\(1997\)025<0719:DTIACA>2.3.CO;2](https://doi.org/10.1130/0091-7613(1997)025<0719:DTIACA>2.3.CO;2).
- Nie, S., Yin, A., Rowley, D.B., Jin, Y., 1994. Exhumation of the Dabie Shan ultra-high-pressure rocks and accumulation of the Songpan-Ganzi flysch sequence, Central China. *Geology* 22, 999–1002. [https://doi.org/10.1130/0091-7613\(1995\)023<0764](https://doi.org/10.1130/0091-7613(1995)023<0764).
- Orme, D.A., Carrapa, B., Kapp, P., 2015. Sedimentology, provenance and geochronology of the upper Cretaceous–lower Eocene western Xigaze forearc basin, southern Tibet.

- Basin Res. 27, 387–411. <https://doi.org/10.1111/bre.12080>.
- Ou, Q., Wang, Q., Wyman, D.A., Zhang, H.X., Yang, J.H., Zeng, J.P., Hao, L.L., Chen, Y.W., Liang, H., Qi, Y., 2017. Eocene adakitic porphyries in the central-northern Qiangtang Block, Central Tibet: partial melting of thickened lower crust and implications for initial surface uplifting of the plateau. *J. Geophys. Res. Solid Earth* 122, 1025–1053. <https://doi.org/10.1002/2016JB013259>.
- Pan, G., Mo, X., Hou, Z., Zhu, D., Wang, L., Li, G., Zhao, Z., Geng, Q., Liao, Z., 2006. Spatial-temporal framework of the Gangdese orogenic belt and its evolution. *Acta Petrol. Sin.* 22, 521–533 (in Chinese with English abstract).
- Pan, G.T., Ding, J., Yao, D., Wang, L., 2004. Geological Map of Qinghai-Xiang (Tibet) Plateau and Adjacent Areas (1:1,500,000). Chengdu Institute of Geology and Mineral Resources. China Geological Survey, Chengdu Cartographic Publishing House, Chengdu, China.
- Pang, X.Q., Li, Y.X., Jiang, Z.X., 2004. Key geological controls on migration and accumulation for hydrocarbons derived from mature source rocks in Qaidam Basin. *J. Pet. Sci. Eng.* 41, 79–95. [https://doi.org/10.1016/S0920-4105\(03\)00145-1](https://doi.org/10.1016/S0920-4105(03)00145-1).
- Pei, L., Li, R., Pei, X., Liu, J., Li, Z., Liu, C., Chen, Y., Liu, Z., Chen, G., Hu, N., Gao, F., 2017. Sediment source analysis for the Maerzheng Formation sandstone in Gerizhuotuo area, southern margin of the East Kunlun region: evidence for detrital zircon U-Pb geochronology. *Acta Geol. Sin.* 91, 1326–1344 (in Chinese with English abstract).
- Peng, H., Li, C., Xie, C., Wang, M., Jiang, Q., Chen, J., 2014. Riwanchaka Group in central Qiangtang Basin, the Tibetan Plateau: evidence from detrital zircons. *Geol. Bull. China* 33, 1715–1727 (in Chinese with English abstract).
- Pullen, A., Kapp, P., Gehrels, G.E., Ding, L., Zhang, Q., 2011. Metamorphic rocks in Central Tibet: Lateral variations and implications for crustal structure. *Bull. Geol. Soc. Am.* 123, 585–600. <https://doi.org/10.1130/B30154.1>.
- Pullen, A., Kapp, P., Gehrels, G.E., Vervoort, J.D., Ding, L., 2008. Triassic continental subduction in Central Tibet and Mediterranean-style closure of the Paleo-Tethys Ocean. *Geology* 36, 351–354. <https://doi.org/10.1130/G24435A.1>.
- Qinghai BGMR (Bureau of Geology and Mineral Resources), 1991. Regional Geology of Qinghai Province. Geological Publishing House, Beijing, pp. 662 (in Chinese with English summary).
- Qiu, N., 2002. Tectono-thermal evolution of the Qaidam Basin, China: evidence from R₀ and apatite fission track data. *Pet. Geosci.* 8, 279–285. <https://doi.org/10.1144/petgeo.8.3.279>.
- Quidelleur, X., Grove, M., Lovera, O.M., Harrison, T.M., Yin, A., Ryerson, F.J., 1997. Thermal evolution and slip history of the Renbu Zedong Thrust, southeastern Tibet. *J. Geophys. Res.* 102, 2659–2680. <https://doi.org/10.1029/96JD02483>.
- Reid, A., Wilson, C.J.L., Shun, L., Pearson, N., Belousova, E., 2007. Mesozoic evolution of the Yidun Arc, SW China: U/Pb geochronology and Hf isotopic signature. *Ore Geol. Rev.* 31, 88–106. <https://doi.org/10.1016/j.oregeorev.2004.11.003>.
- Rieser, A.B., Liu, Y., Genser, J., Neubauer, F., Handler, R., Friedl, G., Ge, X.H., 2006a. ⁴⁰Ar/³⁹Ar ages of detrital white mica constrain the Cenozoic development of the intracontinental Qaidam Basin, China. *Bull. Geol. Soc. Am.* 118, 1522–1534. <https://doi.org/10.1130/B25962.1>.
- Rieser, A.B., Liu, Y., Genser, J., Neubauer, F., Handler, R., Ge, X.H., 2006b. Uniform Permian ⁴⁰Ar/³⁹Ar detrital mica ages in the eastern Qaidam Basin (NW China): where is the source? *Terra Nova* 18, 79–87. <https://doi.org/10.1111/j.1365-3121.2005.00666.x>.
- Rieser, A.B., Neubauer, F., Liu, Y., Ge, X., 2005. Sandstone provenance of north-western sectors of the intracontinental Cenozoic Qaidam basin, western China: Tectonic vs. climatic control. *Sediment. Geol.* 177, 1–18. <https://doi.org/10.1016/j.sedgeo.2005.01.012>.
- Ritts, B.D., Biffi, U., 2000. Magnitude of post-Middle Jurassic (Bajocian) displacement on the Central Altyn Tagh fault system, Northwest China. *Bull. Geol. Soc. Am.* 112, 61–74. [https://doi.org/10.1130/0016-7606\(2000\)112<61:MOPJBD>2.0.CO;2](https://doi.org/10.1130/0016-7606(2000)112<61:MOPJBD>2.0.CO;2).
- Ritts, B.D., Biffi, U., 2001. Mesozoic northeast Qaidam basin; response to contractional reactivation of the Qilian Shan, and implication for the extent of Mesozoic intracontinental deformation in Central Asia. *Geol. Soc. Am. Mem.* 194, 293–316.
- Ritts, B.D., Hanson, A.D., Zinniker, D., Moldovan, J.M., 1999. Lower-Middle Jurassic nonmarine source rocks and petroleum systems of the northern Qaidam Basin, Northwest China. *Am. Assoc. Pet. Geol. Bull.* 83, 1980.
- Robinson, A.C., Ducea, M., Lapen, T.J., 2012. Detrital zircon and isotopic constraints on the crustal architecture and tectonic evolution of the northeastern Pamir. *Tectonics* 31, 1–16. <https://doi.org/10.1029/2011TC003013>.
- Robinson, D.M., Dupont-Nivet, G., Gehrels, G.E., Zhang, Y., 2003. The Tula uplift, northwestern China: evidence for regional tectonism of the northern Tibetan Plateau during late Mesozoic-early Cenozoic time. *Bull. Geol. Soc. Am.* 115, 35–47. [https://doi.org/10.1130/0016-7606\(2003\)115<0035:TTUNCE>2.0.CO;2](https://doi.org/10.1130/0016-7606(2003)115<0035:TTUNCE>2.0.CO;2).
- Roger, F., Arnaud, N., Gilder, S., Tapponnier, P., Jolivet, M., Brunel, M., Malavieille, J., Xu, Z., Yang, J., 2003. Geochronological and geochemical constraints on Mesozoic suturing in east Central Tibet. *Tectonics* 22, <https://doi.org/10.1029/2002TC001466>.
- Roger, F., Malavieille, J., Leloup, P.H., Calassou, S., Xu, Z., 2004. Timing of granite emplacement and cooling in the Songpan-Garzê Fold Belt (eastern Tibetan Plateau) with tectonic implications. *J. Asian Earth Sci.* 22, 465–481. [https://doi.org/10.1016/S1367-9120\(03\)00089-0](https://doi.org/10.1016/S1367-9120(03)00089-0).
- Roger, F., Tapponnier, P., Arnaud, N., Schärer, U., Brunel, M., Zhiqin, X., Jingsui, Y., 2000. An Eocene magmatic belt across Central Tibet: mantle subduction triggered by the Indian collision? *Terra Nova* 12, 102–108. <https://doi.org/10.1111/j.1365-3121.2000.00282.x>.
- Rubatto, D., 2002. Zircon trace element geochemistry: partitioning with garnet and the link between U-Pb ages and metamorphism. *Chem. Geol.* 184, 123–138. [https://doi.org/10.1016/S0009-2541\(01\)00355-2](https://doi.org/10.1016/S0009-2541(01)00355-2).
- Schärer, U., Xu, R.-H., Allègre, C.J., 1984. U-Pb geochronology of Gangdese (Transhimalaya) plutonism in the Lhasa-Xigaze region, Tibet. *Earth Planet. Sci. Lett.* 69, 311–320. [https://doi.org/10.1016/0012-821X\(84\)90190-0](https://doi.org/10.1016/0012-821X(84)90190-0).
- Sengör, A.M.C., Natal'in, B.A., 1996. Paleotectonics of Asia: fragments of a synthesis. In: Yin, A., Harrison, T.M. (Eds.), *The tectonic evolution of Asia*. New York, Cambridge University Press, pp. 486–640.
- Sha, J., Smith, P.L., Fürsich, F.T., 2002. Jurassic *Ostreoida* (Bivalvia) from China (Tanggula Mountains, Qinghai-Xizang Plateau) and their paleobiogeographic context. *J. Paleontol.* 76, 431–446.
- Shao, F., Niu, Y., Liu, Y., Chen, S., Kong, J., Duan, M., 2017. Petrogenesis of Triassic granitoids in the East Kunlun Orogenic Belt, northern Tibetan Plateau and their tectonic implications. *Lithos* 282–283, 33–44. <https://doi.org/10.1016/j.lithos.2017.03.002>.
- She, Z., Ma, C., Mason, R., Li, J., Wang, G., Lei, Y., 2006. Provenance of the Triassic Songpan-Ganzi flysch, West China. *Chem. Geol.* 231, 159–175. <https://doi.org/10.1016/j.chemgeo.2006.01.001>.
- Smith, A.B., Xu, J., 1988. Palaeontology of the 1985 Tibet traverse, Lhasa to Golmud. *Philos. Trans. R. Soc. London, Ser. A* 327, 53–105.
- Sobel, E.R., 1999. Basin analysis of the Jurassic–Lower Cretaceous southwest Tarim basin, Northwest China. *Geol. Soc. Am. Bull.* 111, 709–724.
- Sobel, E.R., Arnaud, N., Jolivet, M., Ritts, B.D., Brunel, M., 2001. Jurassic to Cenozoic exhumation history of the Altyn Tagh range, Northwest China, constrained by ⁴⁰Ar/³⁹Ar and apatite fission track thermochronology. *Geol. Soc. Am. Mem.* 194, 247–267.
- Song, B., Zhang, K., Zhang, L., Ji, J., Hong, H., Wei, Y., Xu, Y., Algeo, T.J., Wang, C., 2018. Qaidam Basin paleosols reflect climate and weathering intensity on the northeastern Tibetan Plateau during the Early Eocene Climatic Optimum. *Palaeogeogr. Palaeoclimatol. Palaeoecol.* <https://doi.org/10.1016/j.palaeo.2018.03.027>. (in press).
- Song, S., Niu, Y., Su, L., Zhang, C., Zhang, L., 2014. Continental orogenesis from ocean subduction, continent collision/subduction, to orogen collapse, and orogen recycling: the example of the North Qaidam UHPM belt, NW China. *Earth Sci. Rev.* 129, 59–84. <https://doi.org/10.1016/j.earscirev.2013.11.010>.
- Song, S., Zhang, L., Niu, Y., Su, L., Jian, P., Liu, D., 2005. Geochronology of diamond-bearing zircons from garnet peridotite in the North Qaidam UHPM belt, Northern Tibetan Plateau: a record of complex histories from oceanic lithosphere subduction to continental collision. *Earth Planet. Sci. Lett.* 234, 99–118. <https://doi.org/10.1016/j.epsl.2005.02.036>.
- Song, S., Zhang, L., Niu, Y., Su, L., Song, B., Liu, D., 2006. Evolution from oceanic subduction to continental collision: a case study from the Northern Tibetan Plateau based on geochemical and geochronological data. *J. Petrol.* 47, 435–455. <https://doi.org/10.1093/petrology/egi080>.
- Song, T., Wang, X., 1993. Structural styles and stratigraphic patterns of syndepositional faults in a contractional setting; examples from Qaidam Basin, northwestern China. *Am. Assoc. Pet. Geol. Bull.* 77, 102–117.
- Spurlin, M.S., Yin, A., Horton, B.K., Zhou, J., Wang, J., 2005. Structural evolution of the Yushu-Nangqian region and its relationship to syn-collisional igneous activity, East-Central Tibet. *Bull. Geol. Soc. Am.* 117, 1293–1317. <https://doi.org/10.1130/B25572.1>.
- Stacey, J.S., Kramers, J.D., 1975. Approximation of terrestrial lead isotope evolution by a two-stage model. *Earth Planet. Sci. Lett.* 26, 207–221. [https://doi.org/10.1016/0012-821X\(75\)90088-6](https://doi.org/10.1016/0012-821X(75)90088-6).
- Staisch, L.M., Niemi, N.A., Clark, M.K., Chang, H., 2016. Eocene to Late Oligocene history of crustal shortening within the Hoh Xil Basin and implications for the uplift history of the northern Tibetan Plateau. *Tectonics* 35, 862–895. <https://doi.org/10.1002/2015TC003972>.
- Staisch, L.M., Niemi, N.A., Hong, C., Clark, M.K., Rowley, D.B., Currie, B., 2014. A Cretaceous-Eocene depositional age for the Fenghuoshan Group, Hoh Xil Basin: Implications for the tectonic evolution of the northern Tibet Plateau. *Tectonics* 33, 281–301. <https://doi.org/10.1002/2013TC003367>.
- Sun, Z., Feng, X., Li, D., Yang, F., Qu, Y., Wang, H., 1999. Cenozoic ostracoda and palaeoenvironments of the northeastern Tarim Basin, western China. *Palaeogeogr. Palaeoclimatol. Palaeoecol.* 148, 37–50. [https://doi.org/10.1016/S0031-0182\(98\)00174-6](https://doi.org/10.1016/S0031-0182(98)00174-6).
- Sun, Z., Yang, Z., Pei, J., Ge, X., Wang, X., Yang, T., Li, W., Yuan, S., 2005. Magnetostratigraphy of Paleogene sediments from northern Qaidam Basin, China: implications for tectonic uplift and block rotation in northern Tibetan plateau. *Earth Planet. Sci. Lett.* 237, 635–646. <https://doi.org/10.1016/j.epsl.2005.07.007>.
- Tang, Y., Zhang, Y., Tong, L., 2018. Mesozoic-Cenozoic evolution of the Zoige depression in the Songpan-Ganzi flysch basin, eastern Tibetan Plateau: constraints from detrital zircon U-Pb ages and fission-track ages of the Triassic sedimentary sequence. *J. Asian Earth Sci.* 151, 285–300. <https://doi.org/10.1016/j.jseaes.2017.10.021>.
- Tapponnier, P., Xu, Z., Roger, F., Meyer, B., Arnaud, N., Wittlinger, G., Yang, J., 2001. Oblique stepwise rise and growth of the Tibet Plateau. *Science* 294, 1671–1677. <https://doi.org/10.1126/science.105978>.
- Taylor, M., Yin, A., 2009. Active structures of the Himalayan-Tibetan orogen and their relationships to earthquake distribution, contemporary strain field, and Cenozoic volcanism. *Geosphere* 5, 199–214. <https://doi.org/10.1130/GES00217.1>.
- Turner, S., Arnaud, N., Liu, J., Rogers, N., Hawkesworth, C., Harris, N., Kelley, S., Van Calsteren, P., Deng, W., 1996. Post-collision, shoshonitic volcanism on the Tibetan plateau: implications for convective thinning of the lithosphere and the source of ocean island basalts. *J. Petrol.* 37, 45–71. <https://doi.org/10.1093/petrology/37.1.45>.
- Turner, S., Hawkesworth, C., Liu, J., Rogers, N., Kelley, S., van Calsteren, P., 1993. Timing of Tibetan uplift constrained by analysis of volcanic rocks. *Nature* 364, 50–54.
- Vermeesch, P., Resentini, A., Garzanti, E., 2016. An R package for statistical provenance analysis. *Sediment. Geol.* 336, 14–25. <https://doi.org/10.1016/j.sedgeo.2016.01>.

- 009.
- Vincent, S.J., Allen, M.B., 1999. Evolution of the Minle and Chaoshui Basins, China: implications for Mesozoic strike-slip basin formation in Central Asia. *Bull. Geol. Soc. Am.* 111, 725–742. [https://doi.org/10.1130/0016-7606\(1999\)111<0725:EOTMAC>2.3.CO;2](https://doi.org/10.1130/0016-7606(1999)111<0725:EOTMAC>2.3.CO;2).
- Volkmer, J.E., Kapp, P., Guynn, J.H., Lai, Q., 2007. Cretaceous-Tertiary structural evolution of the north Central Lhasa terrane, Tibet. *Tectonics* 26, 1–18. <https://doi.org/10.1029/2005TC001832>.
- Wallis, S., Tsujimori, T., Aoya, M., Kawakami, T., Terada, K., Suzuki, K., Hyodo, H., 2003. Cenozoic and Mesozoic metamorphism in the Longmenshan orogen: implications for geodynamic models of eastern Tibet. *Geology* 31, 745–748. <https://doi.org/10.1130/G19562.1>.
- Wang, C., Liu, L., Yang, W.-Q., Zhu, X.-H., Cao, Y.-T., Kang, L., Chen, S.-F., Li, R.-S., He, S.-P., 2013b. Provenance and ages of the Altyn Complex in Altyn Tagh: implications for the Early Neoproterozoic evolution of northwestern China. *Precambrian Res.* 230, 193–208. <https://doi.org/10.1016/j.precamres.2013.02.003>.
- Wang, C., Zhao, X., Liu, Z., Lippert, P.C., Graham, S.A., Coe, R.S., Yi, H., Zhu, L., Liu, S., Li, Y., 2008a. Constraints on the early uplift history of the Tibetan Plateau. *Proc. Natl. Acad. Sci.* 105, 4987–4992. <https://doi.org/10.1073/pnas.0703595105>.
- Wang, C.S., Liu, Z.F., Yi, H.S., Liu, S., Zhao, X.X., 2002. Tertiary crustal shortenings and peneplanation in the Hoh Xil region: implications for the tectonic history of the northern Tibetan Plateau. *J. Asian Earth Sci.* 20, 211–223. [https://doi.org/10.1016/S1367-9120\(01\)00051-7](https://doi.org/10.1016/S1367-9120(01)00051-7).
- Wang, E., Xu, F.Y., Zhou, J.X., Wan, J., Burchfiel, B.C., 2006. Eastward migration of the Qaidam basin and its implications for Cenozoic evolution of the Altyn Tagh fault and associated river systems. *Bull. Geol. Soc. Am.* 118, 349–365. <https://doi.org/10.1130/B25778.1>.
- Wang, F., Feng, H., Shi, W., Zhang, W., Wu, L., Yang, L., Wang, Y., Zhang, Z., Zhu, R., 2016. Relief history and denudation evolution of the northern Tibet margin: constraints from $^{40}\text{Ar}/^{39}\text{Ar}$ and (U-Th)/He dating and implications for far-field effect of rising plateau. *Tectonophysics* 675, 196–208. <https://doi.org/10.1016/j.tecto.2016.03.001>.
- Wang, F., Lo, C.H., Li, Q., Yeh, M.W., Wan, J., Zheng, D., Wang, E., 2004b. Onset timing of significant unroofing around Qaidam basin, northern Tibet, China: constraints from $^{40}\text{Ar}/^{39}\text{Ar}$ and FT thermochronology on granitoids. *J. Asian Earth Sci.* 24, 59–69. <https://doi.org/10.1016/j.jseaeas.2003.07.004>.
- Wang, F., Shi, W., Zhang, W., Wu, L., Yang, L., Wang, Y., Zhu, R., 2017d. Differential growth of the northern Tibetan margin: evidence for oblique stepwise rise of the Tibetan Plateau. *Sci. Rep.* 7, 1–9. <https://doi.org/10.1038/srep41164>.
- Wang, G., Wang, Q., Jian, P., Zhu, Y., 2004a. Zircon SHRIMP ages of Precambrian metamorphic basement rocks and their tectonic significance in the eastern Kunlun Mountains, Qinghai Province, China. *Earth Sci. Front.* 11, 481–490 (in Chinese with English abstract).
- Wang, G., Wei, Q., Jia, C., Zhang, K., Li, D., Zhu, Y., Xiang, S., 2007a. Some ideas of Precambrian geology in the East Kunlun, China. *Geol. Bull. China* 26, 929–937. (in Chinese with English abstract). [10.15931/j.cnki.1006-1096.2011.06.017](https://doi.org/10.15931/j.cnki.1006-1096.2011.06.017).
- Wang, J.G., Hu, X., Garzanti, E., An, W., Liu, X.C., 2017a. The birth of the Xigaze forearc basin in southern Tibet. *Earth Planet. Sci. Lett.* 465, 38–47. <https://doi.org/10.1016/j.epsl.2017.02.036>.
- Wang, J.H., Yin, A., Harrison, T.M., Grove, M., Zhang, Y.Q., Xie, G.H., 2001. A tectonic model for Cenozoic igneous activities in the eastern Indo-Asian collision zone. *Earth Planet. Sci. Lett.* 188, 123–133. [https://doi.org/10.1016/S0012-821X\(01\)00315-6](https://doi.org/10.1016/S0012-821X(01)00315-6).
- Wang, L.Q., Pan, G.T., Ding, J., Yao, D.S., 2013a. Geological Map of the Tibetan Plateau at a Scale of 1:1.5 M with Explanations. Geological Publishing House, Beijing, pp. 288 (compilers).
- Wang, Q., Coward, M.P., 1990. The Chaidam Basin (NW China): formation and hydrocarbon potential. *J. Pet. Geol.* 13, 93–112. <https://doi.org/10.1111/j.1747-5457.1990.tb00255.x>.
- Wang, Q., McDermott, F., Xu, J.F., Bellon, H., Zhu, Y.T., 2005a. Cenozoic K-rich adakitic volcanic rocks in the Hohxil area, northern Tibet: lower-crustal melting in an intra-continental setting. *Geology* 33, 465–468. <https://doi.org/10.1130/G21522.1>.
- Wang, Q., Wyman, D.A., Xu, J., Dong, Y., Vasconcelos, P.M., Pearson, N.J., Wan, Y., Dong, H., Li, C., Yu, Y., Zhu, T., Feng, X., Zhang, Q., Zi, F., Chu, Z., 2008b. Eocene melting of subducting continental crust and early uplifting of Central Tibet: evidence from central-western Qiangtang high-K calc-alkaline andesites, dacites and rhyolites. *Earth Planet. Sci. Lett.* 272, 158–171. <https://doi.org/10.1016/j.epsl.2008.04.034>.
- Wang, S., Li, Z., Qiangba, X., 1983. Unpublished Geologic Map (scale 1:1,000,000) and Geologic Report of the Xigaze Area. Xizang Bureau of Geology and Mineral Resources, pp. 568.
- Wang, W., Zheng, W., Zhang, P., Li, Q., Kirby, E., Yuan, D., Zheng, D., Liu, C., Wang, Z., Zhang, H., Pang, J., 2017b. Expansion of the Tibetan Plateau during the Neogene. *Nat. Commun.* 8, 1–12. <https://doi.org/10.1038/ncomms15887>.
- Wang, X., Qiu, Z., Li, Q., Wang, B., Qiu, Z., Downs, W.R., Xie, G., Xie, J., Deng, T., Takeuchi, G.T., Tseng, Z.J., Chang, M., Liu, J., Wang, Y., Biasatti, D., Sun, Z., Fang, X., Meng, Q., 2007b. Vertebrate paleontology, biostratigraphy, geochronology, and paleoenvironment of Qaidam Basin in northern Tibetan Plateau. *Palaeogeogr. Palaeoclimatol. Palaeoecol.* 254, 363–385. <https://doi.org/10.1016/j.palaeo.2007.06.007>.
- Wang, X., Wang, S., Wang, C., Tang, W., 2018a. Permo-Triassic arc-like granitoids along the northern Lancangjiang zone, eastern Tibet: age, geochemistry, Sr–Nd–Hf isotopes, and tectonic implications. *Lithos* 308–309, 278–293. <https://doi.org/10.1016/j.lithos.2018.03.008>.
- Wang, Y., Mosbrugger, V., Zhang, H., 2005b. Early to Middle Jurassic vegetation and climatic events in the Qaidam Basin, Northwest China. *Palaeogeogr. Palaeoclimatol. Palaeoecol.* 224, 200–216. <https://doi.org/10.1016/j.palaeo.2005.03.035>.
- Wang, Y., Zhang, X., Wang, E., Zhang, J., Li, Q., Sun, G., 2005c. $^{40}\text{Ar}/^{39}\text{Ar}$ thermochronological evidence for formation and Mesozoic evolution of the northern-central segment of the Altyn Tagh fault system in the northern Tibetan Plateau. *Bull. Geol. Soc. Am.* 117, 1336–1346. <https://doi.org/10.1130/B25685.1>.
- Wang, Y., Zheng, J., Zheng, Y., 2018b. Mesozoic-Cenozoic exhumation history of the Qimen Tagh Range, northeastern margins of the Tibetan Plateau: evidence from apatite fission track analysis. *Gondwana Res.* 58, 16–26. <https://doi.org/10.1016/j.gr.2018.01.014>.
- Wang, Z., Wang, J., Fu, X., Feng, X., Wang, D., Song, C., Chen, W., Zeng, S., Yu, F., 2017c. Provenance and tectonic setting of the Quemoco sandstones in the North Qiangtang Basin, North Tibet: evidence from geochemistry and detrital zircon geochronology. *Geol. J.* 1465–1481. <https://doi.org/10.1002/gj.2967>.
- Weislogel, A.L., 2008. Tectonostratigraphic and geochronologic constraints on evolution of the northeast Paleotethys from the Songpan-Ganzi complex, Central China. *Tectonophysics* 451, 331–345. <https://doi.org/10.1016/j.tecto.2007.11.053>.
- Weislogel, A.L., Graham, S.A., Chang, E.Z., Wooden, J.L., Gehrels, G.E., 2010. Detrital zircon provenance from three turbidite depocenters of the Middle-Upper Triassic Songpan-Ganzi complex, Central China: record of collisional tectonics, erosional exhumation, and sediment production. *Bull. Geol. Soc. Am.* 122, 2041–2062. <https://doi.org/10.1130/B26606.1>.
- Weislogel, A.L., Graham, S.A., Chang, E.Z., Wooden, J.L., Gehrels, G.E., Yang, H., 2006. Detrital zircon provenance of the Late Triassic Songpan-Ganzi complex: sedimentary record of collision of the North and South China blocks. *Geology* 34, 97–100. <https://doi.org/10.1130/G21929.1>.
- Williams, H., Turner, S., Kelley, S., Harris, N., 2001. Age and composition of dikes in Southern Tibet: new constraints on the timing of east-west extension and its relationship to postcollisional volcanism. *Geology* 29, 339–342. [https://doi.org/10.1130/0091-7613\(2001\)029<0339:AACODI>2.0.CO;2](https://doi.org/10.1130/0091-7613(2001)029<0339:AACODI>2.0.CO;2).
- Wu, C., Yin, A., Zuza, A.V., Zhang, J., Liu, W., Ding, L., 2016. Pre-Cenozoic geologic history of the central and northern Tibetan Plateau and the role of Wilson cycles in constructing the Tethyan orogenic system. *Lithosphere* 8, 254–292. <https://doi.org/10.1130/L494.1>.
- Wu, C., Zuza, A.V., Yin, A., Liu, C., Reith, R.C., Zhang, J., Liu, W., Zhou, Z., 2017b. Geochronology and geochemistry of Neoproterozoic granitoids in the central Qilian Shan of northern Tibet: reconstructing the amalgamation processes and tectonic history of Asia. *Lithosphere* (L640), 1. <https://doi.org/10.1130/L640.1>.
- Wu, F.Y., Ji, W.Q., Liu, C.Z., Chung, S.L., 2010. Detrital zircon U–Pb and Hf isotopic data from the Xigaze fore-arc basin: constraints on Transhimalayan magmatic evolution in southern Tibet. *Chem. Geol.* 271, 13–25. <https://doi.org/10.1016/j.chemgeo.2009.12.007>.
- Wu, L., Xiao, A., Wang, L., Shen, Z., Zhou, S., Chen, Y., Wang, L., Liu, D., Guan, J., 2011. Late Jurassic–Early Cretaceous Northern Qaidam Basin, NW China: implications for the earliest Cretaceous intracontinental tectonism. *Cretac. Res.* 32, 552–564. <https://doi.org/10.1016/j.cretres.2011.04.002>.
- Wu, L., Xiao, A., Yang, S., Wang, L., Mao, L., Wang, L., Dong, Y., Xu, B., 2012. Two-stage evolution of the Altyn Tagh Fault during the Cenozoic: new insight from provenance analysis of a geological section in NW Qaidam Basin, NW China. *Terra Nova* 24, 387–395. <https://doi.org/10.1111/j.1365-3121.2012.01077.x>.
- Wu, T., Xiao, L., Wilde, S.A., Ma, C.Q., Zhou, J.X., 2017a. A mixed source for the Late Triassic Garzè–Daocheng granitic belt and its implications for the tectonic evolution of the Yidun arc belt, eastern Tibetan Plateau. *Lithos* 288–289, 214–230. <https://doi.org/10.1016/j.lithos.2017.07.002>.
- Wu, Z., Barosh, P.J., Wu, Z., Hu, D., Zhao, X., Ye, P., 2008. Vast early Miocene lakes of the central Tibetan plateau. *Bull. Geol. Soc. Am.* 120, 1326–1337. <https://doi.org/10.1130/B26043.1>.
- Wu, Z., Wu, Z., Hu, D., Peng, H., Zhang, Y., 2009. Carbon and isotope changes and palaeoclimate cycles recorded by lacustrine deposits of Miocene Wudaoliang Group in northern Tibetan Plateau. *Geol. China* 36, 966–975 (in Chinese with English abstract).
- Xia, W., Zhang, N., Yuan, X., Fan, L., Zhang, B., 2001. Cenozoic Qaidam Basin, China: a stronger tectonic inverted, extensional rifted basin. *Am. Assoc. Pet. Geol. Bull.* 85, 715. <https://doi.org/10.1306/8626C98D-173B-11D7-8645000102C1865D>.
- Xu, B., Griffin, W.L., Xiong, Q., Hou, Z.Q., O'Reilly, S.Y., Guo, Z., Pearson, N.J., Gréau, Y., Yang, Z.M., Zheng, Y.C., 2017. Ultrapotassic rocks and xenoliths from South Tibet: contrasting styles of interaction between lithospheric mantle and asthenosphere during continental collision. *Geology* 45, 51–54. <https://doi.org/10.1130/G38466.1>.
- Xu, C., 1985. Chaidamu Basin. Stratigraphic Correlation Between Sedimentary Basins of the ESCAP Region, Volume X - ESCAP Atlas of Stratigraphy IV: People's Republic of China. Mineral Resources Development Series No. 52 United Nations, New York, pp. 70–74.
- Xu, R., 1990. Geochronological study of granitoids and metamorphic rocks in Xizang. In: Liu, G. (Ed.), *Metamorphic and Igneous Rocks in Xizang*. Geological Press, Beijing, pp. 287–302 (in Chinese).
- Xu, R., Schärer, U., Allègre, C.J., 1985. Magmatism and metamorphism in the Lhasa block (Tibet): a geochronological study. *J. Geol.* 93, 41–57.
- Yang, F., 1988. Distribution of the brackish-salt water ostracod in northwestern Qinghai Plateau and its geological significance. In: Hanai, T. (Ed.), *Evolutionary Biology of Ostracoda*. Proceedings of 9th International Symposium on Ostracoda, New York, Elsevierpp. 519–530.
- Yang, F., Ma, Z., Xu, T., Ye, S., 1992. A Tertiary paleomagnetic stratigraphic profile in Qaidam basin. *Acta Pet. Sin.* 13, 97–101 (in Chinese with English abstract).
- Yang, F., Sun, Z., Cao, C., Ma, Z., Zhang, Y., 1997. Quaternary fossil ostracod zones and magnetostratigraphic profile in the Qaidam basin. *Acta Micropaleont. Sin.* 14, 378–390 (in Chinese with English abstract).
- Yang, J., Xu, Z., Zhang, J., Song, S., Wu, C., Shi, R., Li, H., Brunel, M., 2002. Early Palaeozoic North Qaidam UHP metamorphic belt on the north-eastern Tibetan Plateau and a paired subduction model. *Terra Nova* 14, 397–404. <https://doi.org/10.1130/B25685.1>.

- 1046/j.1365-3121.2002.00438.x.
- Yang, J.H., Du, Y.S., Cawood, P.A., Xu, Y.J., 2009. Silurian collisional suturing onto the southern margin of the North China craton: detrital zircon geochronology constraints from the Qilian Orogen. *Sediment. Geol.* 220, 95–104. <https://doi.org/10.1016/j.sedgeo.2009.07.001>.
- Yang, L.Q., Deng, J., Dilek, Y., Meng, J.Y., Gao, X., Santosh, M., Wang, D., Yan, H., 2016. Melt source and evolution of I-type granitoids in the SE Tibetan Plateau: Late Cretaceous magmatism and mineralization driven by collision-induced transtensional tectonics. *Lithos* 245, 258–273. <https://doi.org/10.1016/j.lithos.2015.10.005>.
- Yang, Y., Ritts, B., Zou, C., Xu, T., Zhang, B., Xi, P., 2003. Upper Triassic-Middle Jurassic stratigraphy and sedimentology in the NE Qaidam Basin, NW China: petroleum geological significance of new outcrop and subsurface data. *J. Pet. Geol.* 26, 429–450. <https://doi.org/10.1111/j.1747-5457.2003.tb00037.x>.
- Yang, Z., Hou, Z., Xu, J., Bian, X., Wang, G., Yang, Z., Tian, S., Liu, Y., Wang, Z., 2014. Geology and origin of the post-collisional Narigongma porphyry Cu-Mo deposit, southern Qinghai, Tibet. *Gondwana Res.* 26, 536–556. <https://doi.org/10.1016/j.gr.2013.07.012>.
- Yang, Z., Li, X., 2006. SHRIMP U-Pb dating of zircons from low-grade metamorphic rocks in the Rola Kangri junction zone, northern Tibet, China. *Geol. Bull. China* 25, 118–123 (in Chinese with English abstract).
- Yi, H., Wang, C., Shi, Z., Lin, J., Zhu, L., 2008. Early uplift history of the Tibetan Plateau: records from paleocurrents and paleodrainage in the Hoh Xil Basin. *Acta Geol. Sin.* 82, 206–213. <https://doi.org/10.1111/j.1755-6724.2008.tb00339.x>.
- Yin, A., 2010. Cenozoic tectonic evolution of Asia: a preliminary synthesis. *Tectonophysics* 488, 293–325. <https://doi.org/10.1016/j.tecto.2009.06.002>.
- Yin, A., Dang, Y., Zhang, M., McRivette, M.W., Burgess, W.P., Chen, X., 2007a. Cenozoic tectonic evolution of Qaidam basin and its surrounding regions (part 2): wedge tectonics in southern Qaidam basin and the Eastern Kunlun Range. *Geol. Soc. Am. Spec. Pap.* 433, 369–390.
- Yin, A., Dang, Y.Q., Wang, L.C., Jiang, W.M., Zhou, S.P., Chen, X.H., Gehrels, G.E., McRivette, M.W., 2008a. Cenozoic tectonic evolution of Qaidam basin and its surrounding regions (part 1): the southern Qilian Shan-Nan Shan thrust belt and northern Qaidam basin. *Geol. Soc. Am. Bull.* 120, 813–846. <https://doi.org/10.1130/B26180.1>.
- Yin, A., Dang, Y.Q., Zhang, M., Chen, X.H., McRivette, M.W., 2008b. Cenozoic tectonic evolution of the Qaidam basin and its surrounding regions (part 3): Structural geology, sedimentation, and regional tectonic reconstruction. *Geol. Soc. Am. Bull.* 120, 847–876. <https://doi.org/10.1130/B26232.1>.
- Yin, A., Harrison, T.M., 2000. Geologic evolution of the Himalayan-Tibetan orogen. *Annu. Rev. Earth Planet. Sci.* 28, 211–280. <https://doi.org/10.1080/01947641003598252>.
- Yin, A., Harrison, T.M., Murphy, M.A., Grove, M., Nie, S., Ryerson, F.J., Feng, W.X., Le, C.Z., 1999. Tertiary deformation history of southeastern and southwestern Tibet during the Indo-Asian collision. *Bull. Geol. Soc. Am.* 111, 1644–1664. [https://doi.org/10.1130/0016-7606\(1999\)111<1644:TDHOSA>2.3.CO;2](https://doi.org/10.1130/0016-7606(1999)111<1644:TDHOSA>2.3.CO;2).
- Yin, A., Harrison, T.M., Ryerson, F.J., Wenji, C., Kidd, W.S.F., Copeland, P., 1994. Tertiary structural evolution of the Gangdese thrust system, southeastern Tibet. *J. Geophys. Res.* 99, 18175–18201. <https://doi.org/10.1029/94JB00504>.
- Yin, A., Manning, C.E., Lovera, O., Menold, C.A., Chen, X., Gehrels, G.E., 2007b. Early paleozoic tectonic and thermomechanical evolution of ultrahigh-pressure (UHP) metamorphic rocks in the northern Tibetan Plateau, Northwest China. *Int. Geol. Rev.* 49, 681–716. <https://doi.org/10.2747/0020-6814.49.8.681>.
- Yin, A., Nie, S., 1993. An indentation model for the North and South China collision and the development of the Tan-Lu and Honam fault systems, eastern Asia. *Tectonics* 12, 801–813.
- Yin, A., Nie, S., 1996. A Phanerozoic palinspastic reconstruction of China and its neighboring regions. In: Yin, A., Harrison, T.M. (Eds.), *The tectonic evolution of Asia*. Cambridge University Press, New York, pp. 442–485.
- Yin, A., Rumlhart, P.E., Butler, R., Cowgill, E., Harrison, T.M., Foster, D.A., Ingersoll, R.V., Zhang, Q., Zhou, X.Q., Wang, X.F., Hanson, A., Raza, A., 2002. Tectonic history of the Altyn Tagh fault system in northern Tibet inferred from Cenozoic sedimentation. *Geol. Soc. Am. Bull.* 114, 1257–1295. [https://doi.org/10.1130/0016-7606\(2002\)114<1257:THOTAT>2.0.CO;2](https://doi.org/10.1130/0016-7606(2002)114<1257:THOTAT>2.0.CO;2).
- Yin, J., Xu, J., Liu, C., Li, H., 1988. The Tibetan plateau: regional stratigraphic context and previous work. *Philos. Trans. R. Soc. London, Ser. A* 327.
- Yu, L., Xiao, A., Wu, L., Tian, Y., Rittner, M., Lou, Q., Pan, X., 2017a. Provenance evolution of the Jurassic northern Qaidam Basin (West China) and its geological implications: evidence from detrital zircon geochronology. *Int. J. Earth Sci.* 106, 2713–2726. <https://doi.org/10.1007/s00531-017-1455-z>.
- Yu, S., Zhang, J., Del Real, P.G., Zhao, X., Hou, K., Gong, J., Li, Y., 2013a. The Grenvillian orogeny in the Altyn-Qilian-North Qaidam mountain belts of northern Tibet Plateau: constraints from geochemical and zircon U-Pb age and Hf isotopic study of magmatic rocks. *J. Asian Earth Sci.* 73, 372–395. <https://doi.org/10.1016/j.jseas.2013.04.042>.
- Yu, S., Zhang, J., Li, H., Hou, K., Mattinson, C.G., Gong, J., 2013b. Geochemistry, zircon U-Pb geochronology and Lu-Hf isotopic composition of eclogites and their host gneisses in the Dulan area, Northern Qaidam UHP terrane: new evidence for deep continental subduction. *Gondwana Res.* 23, 901–919. <https://doi.org/10.1016/j.gr.2012.07.018>.
- Yu, S., Zhang, J., Li, S., Sun, D., Li, Y., Liu, X., Guo, L., Suo, Y., Peng, Y., Zhao, X., 2017b. Paleoproterozoic granulite-facies metamorphism and anatexis in the Oulongbuluke Block, NW China: respond to assembly of the Columbia supercontinent. *Precambrian Res.* 291, 42–62. <https://doi.org/10.1016/j.precamres.2017.01.016>.
- Yu, X., Fu, S., Wang, Z., Li, Q., Guo, Z., 2017c. The discovery of early Paleoproterozoic high-Na trondhjemite in the northeastern Qaidam basin: evidence from the drilling core samples. *Precambrian Res.* 298, 615–628. <https://doi.org/10.1016/j.precamres.2017.04.002>.
- Yu, X., Guo, Z., Zhang, Q., Cheng, X., Du, W., Wang, Z., Bian, Q., 2017d. Denan Depression controlled by northeast-directed Olongbuluk Thrust Zone in northeastern Qaidam basin: implications for growth of northern Tibetan Plateau. *Tectonophysics* 717, 116–126. <https://doi.org/10.1016/j.tecto.2017.06.017>.
- Yu, X., Huang, B., Guan, S., Fu, S., Cheng, F., Cheng, X., Zhang, T., Guo, Z., 2014. Anisotropy of magnetic susceptibility of Eocene and Miocene sediments in the Qaidam Basin, Northwest China: implication for Cenozoic tectonic transition and depocenter migration. *Geochim. Geophys. Geosyst.* 15, 2095–2108. <https://doi.org/10.1002/2015GC005918>. Received.
- Yuan, W., Dong, J., Shicheng, W., Carter, A., 2006. Apatite fission track evidence for Neogene uplift in the eastern Kunlun Mountains, Northern Qinghai-Tibet Plateau, China. *J. Asian Earth Sci.* 27, 847–856. <https://doi.org/10.1016/j.jseas.2005.09.002>.
- Yuan, W.M., Zhang, X.T., Dong, J.Q., Tang, Y.H., Yu, F.S., Wang, S.C., 2003. A new vision of the intracontinental evolution of the eastern Kunlun Mountains, Northern Qinghai-Tibet Plateau, China. *Radiat. Meas.* 36, 357–362. [https://doi.org/10.1016/S1350-4487\(03\)00151-3](https://doi.org/10.1016/S1350-4487(03)00151-3).
- Zhang, J., Li, H., Meng, F., Xiang, Z., Yu, S., Li, J., 2011. Polyphase tectonothermal events recorded in “metamorphic basement” from the Altyn Tagh, the southeastern margin of the Tarim basin, western China: Constraint from U-Pb zircon geochronology. *Acta Petrol. Sin.* 27, 23–46 (in Chinese with English abstract).
- Zhang, J.X., Li, J.P., Yu, S.Y., Meng, F.C., Mattinson, C.G., Yang, H.J., Ker, C.M., 2012b. Provenance of eclogitic metasediments in the north Qilian HP/LT metamorphic terrane, western China: geodynamic implications for early Paleozoic subduction-erosion. *Tectonophysics* 570–571, 78–101. <https://doi.org/10.1016/j.tecto.2012.08.018>.
- Zhang, J.X., Yang, J.S., Mattinson, C.G., Xu, Z.Q., Meng, F.C., Shi, R.D., 2005. Two contrasting eclogite cooling histories, North Qaidam HP/UHP terrane, western China: petrological and isotopic constraints. *Lithos* 84, 51–76. <https://doi.org/10.1016/j.lithos.2005.02.002>.
- Zhang, J.Y., Yin, A., Liu, W.C., Wu, F.Y., Lin, D., Grove, M., 2012a. Coupled U-Pb dating and Hf isotopic analysis of detrital zircon of modern river sand from the Yalu river (Yarlung Tsangpo) drainage system in southern Tibet: constraints on the transport processes and evolution of Himalayan rivers. *Bull. Geol. Soc. Am.* 124, 1449–1473. <https://doi.org/10.1130/B30592.1>.
- Zhang, K.J., Zhang, Y.X., Li, B., Zhong, L.F., 2007. Nd isotopes of siliciclastic rocks from Tibet, western China: constraints on provenance and pre-Cenozoic tectonic evolution. *Earth Planet. Sci. Lett.* 256, 604–616. <https://doi.org/10.1016/j.epsl.2007.02.014>.
- Zhang, K.J., Zhang, Y.X., Li, B., Zhu, Y.T., Wei, R.Z., 2006a. The blueschist-bearing Qiangtang metamorphic belt (northern Tibet, China) as an in situ suture zone: evidence from geochemical comparison with the Jinsa suture. *Geology* 34, 493–496. <https://doi.org/10.1130/G22404.1>.
- Zhang, K.-J., Zhang, Y.-X., Xia, B.-D., He, Y.-B., 2006b. Temporal variations of Mesozoic sandstone compositions in the Qiangtang Block, Northern Tibet (China): implications for provenance and tectonic setting. *J. Sediment. Res.* 76, 1035–1048. <https://doi.org/10.2110/jsr.2006.089>.
- Zhang, L., Chen, R.-X., Zheng, Y.-F., Hu, Z., Xu, L., 2017. Whole-rock and zircon geochemical distinction between oceanic- and continental-type eclogites in the North Qaidam orogen, northern Tibet. *Gondwana Res.* 44, 67–88. <https://doi.org/10.1016/j.jgr.2016.10.021>.
- Zhang, L., Wang, Q., Chen, N., Sun, M., Santosh, M., Ba, J., 2014b. Geochemistry and detrital zircon U-Pb and Hf isotopes of the paragneiss suite from the Quanji massif, SE Tarim Craton: implications for Paleoproterozoic tectonics in NW China. *J. Asian Earth Sci.* 95, 33–50. <https://doi.org/10.1016/j.jseas.2014.05.014>.
- Zhang, L.Y., Ding, L., Pullen, A., Xu, Q., Liu, D.L., Cai, F.L., Yue, Y.H., Lai, Q.Z., Shi, R.D., Ducea, M.N., Kapp, P., Chapman, A., 2014a. Age and geochemistry of western Hoh-Xil-Songpan-Ganzi granitoids, northern Tibet: implications for the Mesozoic closure of the Paleo-Tethys ocean. *Lithos* 190–191, 328–348. <https://doi.org/10.1016/j.lithos.2013.12.019>.
- Zhang, Y., Zheng, J., 1994. *Geologic Overview in Kokshili, Qinghai and Adjacent Areas*. Seismological Publishing House, Beijing, pp. 177 (in Chinese).
- Zhong, J.H., Wen, Z.F., Guo, Z.Q., Wang, H.Q., Gao, J.B., 2004. Paleogene and early Neogene lacustrine reefs in the western Qaidam Basin, China. *Acta Geol. Sin. - English Ed.* 78, 736–743.
- Zhou, D., Graham, S.A., 1996. The Songpan-Ganzi complex of the West Qinling Shan as a Triassic remnant ocean basin. In: Yin, A., Harrison, T.M. (Eds.), *The Tectonic Evolution of Asia*. Cambridge University Press, New York, pp. 281–299.
- Zhou, H., Chen, L., Lei, C., 2018. Cenozoic uplift of the Qimantage Mountains, north-eastern Tibet: constraints from provenance analysis of Cenozoic sediments in Qaidam Basin. *Geol. J.* 1–20. <https://doi.org/10.1002/gj.3095>.
- Zhou, J., Xu, F., Wang, T., Cao, A., Yin, C., 2006. Cenozoic deformation history of the Qaidam Basin, NW China: results from cross-section restoration and implications for Qinghai-Tibet Plateau tectonics. *Earth Planet. Sci. Lett.* 243, 195–210. <https://doi.org/10.1016/j.epsl.2005.11.033>.
- Zhou, K., Yin, H., Lin, J., 2007. Petrology and sedimentary environments of the lacustrine carbonate rocks from the Miocene Wudaoliang Group in the Hoh Xil basin, Qinghai. *Sediment. Geol. Tethyan Geol.* 27, 25–31 (in Chinese with English abstract).
- Zhu, D.C., Li, S.M., Cawood, P.A., Wang, Q., Zhao, Z.D., Liu, S.A., Wang, L.Q., 2016. Assembly of the Lhasa and Qiangtang terranes in Central Tibet by divergent double subduction. *Lithos* 245, 7–17. <https://doi.org/10.1016/j.lithos.2015.06.023>.
- Zhu, L., Wang, C., Zheng, H., Xiang, F., Yi, H., Liu, D., 2006b. Tectonic and sedimentary evolution of basins in the northeast of Qinghai-Tibet Plateau and their implication for the northward growth of the Plateau. *Palaeogeogr. Palaeoclimatol. Palaeoecol.* 241, 49–60. <https://doi.org/10.1016/j.palaeo.2006.06.019>.
- Zhu, W., Wu, C., Wang, J., Zhou, T., Li, J., Zhang, C., Li, L., 2017. Heavy mineral compositions and zircon U-Pb ages of Cenozoic sandstones in the SW Qaidam basin,

- northern Tibetan Plateau: Implications for provenance and tectonic setting. *J. Asian Earth Sci.* 146, 233–250. <https://doi.org/10.1016/j.jseas.2017.05.023>.
- Zhu, Y., Lin, Q., Jia, C., Wang, G., 2006a. SHRIMP zircon U-Pb age and significance of Early Paleozoic volcanic rocks in East Kunlun orogenic belt, Qinghai Province, China. *Sci. China Ser. D Earth Sci.* 49, 88–96. <https://doi.org/10.1007/s11430-004-5317-8>.
- Zhuang, G., Hourigan, J.K., Ritts, B.D., Kent-Corson, M.L., 2011. Cenozoic multiple-phase tectonic evolution of the northern Tibetan Plateau: constraints from sedimentary records from Qaidam basin, Hexi corridor, and Subei basin, Northwest China. *Am. J. Sci.* 311, 116–152. <https://doi.org/10.2475/02.2011.02>.
- Zuza, A.V., Wu, C., Reith, R.C., Yin, A., Li, J., Zhang, J., Zhang, Y., Wu, L., Liu, W., 2018. Tectonic evolution of the Qilian Shan: an early Paleozoic orogen reactivated in the Cenozoic. *Bull. Geol. Soc. Am.* 130, 881–925. <https://doi.org/10.1130/B31721.1>.
- Zuza, A.V., Yin, A., 2017. Balkatach hypothesis: a new model for the evolution of the Pacific, Tethyan, and Paleo-Asian oceanic domains. *Geosphere* 13, 1664–1712. <https://doi.org/10.1130/GES01463.1>.